Atmospheric Pressure Chemical Vapour Deposition of the nitrides and oxynitrides of Vanadium, Titanium and Chromium.

Submitted for the degree of
Doctor of Philosophy in May 1999

By

Gareth Steven Elwin

University College London
Department of Chemistry

Abstract

A study has been made into the atmospheric pressure chemical vapour deposition of nitrides and oxynitrides of vanadium, titanium and chromium. Vanadium tetrachloride, vanadium oxychloride, chromyl chloride and titanium tetrachloride have been used as precursors with ammonia, at different flow conditions and temperatures. Vanadium nitride, vanadium oxynitride, chromium oxynitride, titanium/vanadium nitride and titanium/chromium oxynitride have been deposited as thin films on glass.

The APCVD reaction of VCl_4 and ammonia leads to films with general composition VN_xO_y. By raising the ammonia concentration so that it is in excess (0.42 dm^3 min^{-1} VCl_4 with 1.0 dm^3 min^{-1} NH_3 at 500 °C) a film has been deposited with the composition $VN_{0.8}O_{0.2}$. Further investigation discovered similar elemental compositions could be reached by deposition at 350 °C (0.42 dm^3 min^{-1} VCl_4 with 0.5 dm^3 min^{-1} NH_3), followed by annealing at 650 °C, and cooled under a flow of ammonia. Only films formed below 400 °C were found to contain carbon or chlorine (<5 %). The reaction of $VOCl_3$ and ammonia also lead to films of composition VN_xO_y the oxygen to nitrogen ratios depending on the deposition conditons. The reaction of $VOCl_3$ (0.42 dm^3 min^{-1}) and ammonia (0.2 dm^3 min^{-1}) at 500 °C lead to a film of composition $VN_{0.47}O_{1.06}$. The reaction of $VOCl_3$ (0.42 dm^3 min^{-1}) and ammonia (0.5 dm^3 min^{-1}) at 650 °C lead to a film of composition $VN_{0.63}O_{0.41}$. The reaction of chromyl chloride with excess ammonia led to the formation of chromium oxide (Cr_2O_3) films.

Mixed metal films were prepared from the reactions of vanadium tetrachloride, titanium tetrachloride and ammonia to prepare $V_xTi_yN_z$ and chromyl chloride, titanium tetrachloride and ammonia to form $TiCr_xO_yN_z$. Both reactions produced the intended mixed coating but it was found that the vanadium / titanium nitride contained around 10 % vanadium whatever the conditions used. Oxygen contamination affected the films to a lesser extent than the single metal films. The reaction of VCl_4 (0.33 dm^3 min^{-1}) and $TiCl_4$ (0.1 dm^3 min^{-1}) with NH_3 (0.5 dm^3 min^{-1}), at 550 °C lead to a film of composition $Ti_{0.75}V_{0.1}NO_{0.15}$. Chromium / titanium oxynitride films contained minimal titanium (<10 %), but in contrast to the chromyl chloride / ammonia reaction nitrogen incorporation was good. The reaction of CrO_2Cl_2 (0.25 dm^3 min^{-1}) and $TiCl_4$ (0.1 dm^3 min^{-1}) with NH_3 (0.5 dm^3 min^{-1}), at 600 °C lead to a film of composition $CrTi_{0.1}N_{0.5}O_{0.75}$.

All films have been investigated for their use as heat control mirrors, with vanadium / titanium nitride films and vanadium oxynitride films providing results of interest to the solar control industry. A film prepared by the reaction of $VOCl_3$ (0.42 dm^3 min^{-1}) and NH_3 (0.8 dm^3 min^{-1}) at 500 °C for 30 seconds resulted in a film with nearly 65% IR reflectance, good visual transmission and an attractive lustre. A film deposited from VCl_4 (0.33 dm^3 min^{-1}), $TiCl_4$ (0.1 dm^3 min^{-1}) and NH_3 (0.6 dm^3 min^{-1}) at 550 °C for 30 seconds produced a film of equivalent heat mirror quality. Films deposited from CrO_2Cl_2 and NH_3 were found not to confer heat control mirror qualities.

Table of Contents

List of Illustrations

Acknowledgements

I would like to thank my supervisor Dr. Ivan Parkin for help, assistance and encouragement throughout this project. In addition I would like to thank Dr. Kevin Sanderson and Dr. David Sheel from Pilkington Glass for their financial help and assistance.

My thanks go to Dave Morfett and Dave Knapp for their technical expertise in the construction of the reaction rig.

I would like to thank all my friends, my lab colleagues (Leigh, Arjumen, Vanessa, Mark and Louise) and Tim, Carol and Craig for their support and encouragement.

Chapter 1

Introduction.

1.1 Aims and objectives

The aim of this research was to produce some novel thin films of nitrides and oxynitrides that could be used as wavelength selective transparent films, particularly for use in solar-control coatings on windows.

The first objective was to design and construct an atmospheric pressure chemical vapour deposition reactor. The rig was designed to lay thin films on glass and consisted of a furnace capable of heating the substrate up to 650 °C, and two bubblers for introduction of precursors.

The next objective was the selection of precursors of early transition metal halides and oxyhalides for deposition studies. These groups of materials were chosen because they have the potential to react with ammonia to produce thin films of nitrides and oxynitrides via Atmospheric Pressure Chemical Vapour Deposition (APCVD). The substrate used for the coatings was glass precoated in siclon (a silicon-oxide based layer to prevent diffusion from the glass to the coating). Each of the experiments was studied by varying the deposition temperature, concentrations and flow rates of carrier gases, deposition times and the effects of annealing.

The final objective was to investigate the physical, chemical and optical properties of the thin films by a range of analytical techniques. The techniques used were XRD, XPS-depth profiling, 4-probe resistance measurements, electronprobe, SEM, reflectance / transmission in the visible and near-IR regions and visual assessment of film quality.

1.2 The structure and properties of titanium and vanadium nitrides and oxynitrides.

The early transition metal nitrides are well known for their almost unique combination of properties. They are materials with extreme hardness, high melting points, chemical durability and interesting optical properties[1]. Titanium nitride, for example, is a stable compound, resistant to attack from both acids and bases and oxidises in O_2, NO, N_2O, or CO_2 atmospheres at temperatures above 1200 °C[2]. TiN has a melting point at 2930 °C and is an extremely hard material with a microhardness of 2000 kgf / mm^2 ranking it close to diamond. Titanium nitride is a brown-yellow powder but after pressing and sintering can be polished to a golden-yellow mirror. Pure TiN has a NaCl type cubic crystal-structure (Fm3m), with a bulk lattice parameter of 4.213 Å. It is an interstitial material with nitrogen atoms occupying vacancies within a close packed metal lattice. The material is non-stoichiometric and can be obtained with composition from $TiN_{0.42}$ (a = 4.210 Å) – $TiN_{1.16}$ (a = 4.213 Å) all with the NaCl structure type. The electrical resistivity, 21.7 μΩ/ cm of $TiN_{1.0}$ make it a better conductor of electricity than titanium metal[2-4].

The properties of vanadium nitride (VN) relate closely to those of TiN. Both materials adopt the same crystal-structure (Fm3m, NaCl type cubic). The microhardness of $VN_{1.0}$ is slightly lower than $TiN_{1.0}$ at 1500 kgf /mm^2 and the electrical resistivity a little higher at 85 μΩ/ cm[5]. Pure $VN_{1.0}$ is brown in colour and resistant to most chemical attack. The melting point of $VN_{1.0}$ is 2350 °C and its lattice parameter is 4.139 Å. A range of stoichiometries are known for the VN phase from $VN_{1.0}$ to $VN_{0.7}$[6]. Notably, as with TiN, all of these non-stoichiometric materials have the NaCl cubic structure[4,5].

Vanadium oxide ($VO_{0.9}$) also has the same structure as TiN (Fm3m, NaCl type cubic). The lattice parameter is 4.12 Å[4]. The oxygen in $VO_{0.9}$, occupies similar interstitial positions to nitrogen in the VN metal lattice. A material exists with both oxygen and nitrogen mixed in the metal lattice. This material is known as vanadium oxynitride. It has a formula VO_xN_y. The lattice parameter is located between 4.12 and 4.139 Å, depending on the degree of nitridation. This material is similar to VN in appearance and in terms of its chemical properties.

Mixed metal nitrides of the form Ti_xV_yN are known. The four materials with the Fm3m (225) space group are VN (a = 4.139 Å). $VO_{0.9}$ (a = 4.12 Å), TiN (a = 4.241 Å) and $TiO_{1.04}$(a = 4.194 Å).

In the preparation of mixed metal nitrides, it is easy to control the chosen metal but as oxygen is often a contaminant in nitrogen gas and is also present from the air, it can be very difficult to exclude oxygen completely when preparing nitride films. The majority of nitride films that have been reported in the literature are heavily contaminated with oxygen[1].

There are a number of routes by which VN and TiN materials can be coated as thin films on to various substrates.

1.3 Thin films.

A thin film is a solid layer on a surface having properties independent from those of the bulk (substrate). The term 'thin film' is usually applied to layers several micrometers, or less, thick, although they can be just a few atomic layers thick[7]. The properties of thin layers often differ from the properties of the bulk forms of the same materials. This is not only because of the thickness involved but is also due to stresses induced by differing thermal coefficients between the film and the substrate[8]. In many cases thin film properties are affected by the properties of the underlying substrate material[7]. Often small amounts of oxygen or carbon impurities may become incorporated during deposition, affecting the properties of the thin films further. There are many ways of forming thin films. The two major methods are called Physical Vapour Deposition (PVD) and Chemical Vapour Deposition (CVD). Each of these deposition techniques can be subdivided further depending on the specific conditions used. These differences affect the purity and conformality of the final film and thus its properties. Some of the deposition conditions in common use are described in section 1.31.

1.31 Introduction to CVD and other deposition methods.

Chemical Vapour Deposition (CVD) is a technique in which a thin film can be produced from the reaction of pyrolysed gaseous precursor materials[9]. The CVD process can be summarised as a collection of several steps, not always in this order: (1) initial transport of reactive species to the reaction site, (2) gas phase reaction, (3) chemisorption, (4) surface nucleation, (5) reaction and desorption of by-products, (6) growth of film.

Chemical Vapour Deposition has many sub-techniques associated with it. With each one slightly different conditions are used to give the required film.

Low Pressure Chemical Vapour Deposition (LPCVD)[10-13] is probably the most common CVD process. It means simply the use of a vacuum to aid the flow of the precursor materials to the substrate, so no process gases are required. Contamination of the film from unclean process gases is eliminated in LPCVD, although contamination can arise through side-reactions, or through use of impure precursors. This route offers good conformality, step coverage and a final film stoichiometry that is relatively easy to control, making it ideal for the semiconductor industry[14]. The reactor walls in LPCVD tend to also get coated with a thick and adhesive coating rather than the thin, particulate, non-adhered coating found on the walls of an Atmospheric Pressure Chemical Vapour Deposition reactor, meaning less particulate incorporation and pinhole defects in the film.

Plasma Enhanced CVD (PECVD)[15] features the basic LPCVD set up with the addition of a glow discharge sustained simultaneously to the CVD reaction[14]. Radio frequencies allow a high electron or positive ion density that in turn aids decomposition of the gaseous molecules into their component species. This means that the reaction can occur at much lower temperatures, allowing coating of temperature sensitive substrates. The disadvantage of this process is the need for low-pressure conditions and extra contamination that can be generated by the use of a plasma[14].

Laser Enhanced CVD (LECVD)[16] is another method that follows the basic LPCVD set up. It uses a beam of monochromatic photons to enhance and control the reactions at the substrate. The LECVD process can proceed via two mechanisms, pyrolytic and photolytic[9,14]. Pyrolytic effectively uses the laser source to heat the substrate so reactions occur via decomposition on the substrate. This means the substrate must have a higher melting point than the temperatures required for gas decomposition. The photolytic process uses energetic photons to directly dissociate the gas phase molecules. This allows the deposition temperature to be lowered. Good deposition rates have been observed by photolytic LECVD using substrate temperatures as low as 50 °C[8,14].

Metallorganic CVD (MOCVD)[17-25] and Organometallic Vapour Phase Epitaxy (OMVPE) describes subsections of LPCVD that are distinguished by the chemical nature of the precursors. An example of MOCVD is the reaction of Group III metalorganic compounds such as Me_3Ga with a Group V hydride such as AsH_3. This reaction has allowed the formation of epitaxial semiconducting films of GaAs. Organometallic compounds are used, as they tend to be volatile at low temperatures, although carbon contamination from the organic side chains can be problematic.

Aerosol Assisted CVD (AACVD)[26] is a technique that can be coupled with other CVD methods such as APCVD. An aerosol precursor delivery system can be used to overcome the problems with conventional precursor delivery, which is often limited by low volatility and thermal stability of the precursors[27]. This system involves the precursor being dissolved into a solvent, which can then be passed through an aerosol generator. The tiny micron sized droplets are transported effectively in a carrier gas to the preheated zone where the precursor decomposes and the solvent evaporates. The precursor goes on to the heated substrate surface, and eventually forms a coating.

APCVD[28-33] varies from most of the methods mentioned above, in that, the reaction chamber is at, or near, atmospheric pressure. APCVD has the advantages of providing fast growth rates, requires no vacuum and can be readily used with dual source precursors. Unfortunately, APCVD does require precursors that are fairly volatile liquids or low-melting solids and a relatively high substrate temperature is required to initiate deposition.

CVD is one of two major techniques known for depositing a thin film onto a substrate. Physical Vapour Deposition (PVD) is an older and until recently a more popular method for laying thin films. PVD techniques vary from CVD in that they involve mainly solid sources, though molten sources are also used. PVD techniques are carried out at reduced pressures. PVD can be subdivided into two major techniques; sputtering[29,34] and evaporation[35]. Both these techniques originated in the nineteenth century as methods to form metal films and mirrors[14]. Evaporation involves removing atoms from a source by thermal means; the film is then able to form on the cooler substrate. Sputtering uses the impact of gaseous ions as the method for obtaining source atoms.

Molecular Beam Epitaxy (MBE) is an example of a PVD technique for forming simple lattice matched crystalline films. It involves the use of a highly controlled evaporation of precursors in an ultrahigh vacuum (*ca.* 10^{-10} torr)[8]. One or more evaporated beams react at a substrate surface to yield epitaxial films usually of very precise heterostructures. This technique is very slow (1 μm / hour) but can form very precise films down to a single monolayer.

Evaporation was the most widely used technique for thin film formation until the 1960's when sputtering took over[8]. PVD has the advantage of forming pure films with low contamination and is still used for the formation of very high quality films. PVD is unsuitable for the formation of large-scale heat mirrors, as it is carried out under vacuum and the growth rates (usually around 1μm / hour) are often too slow for large-scale industrial processes. The equipment used for PVD is often very expensive.

1.32 The history of CVD

The earliest example of CVD deposition is the prehistoric pyrolytic carbon deposition from the incomplete oxidation of firewood in cave art[9]. In the late nineteenth century, the earliest patents on the CVD process were issued to John Howarth for the preparation of carbon black as a pigment[9].

The next major industrial process to profit from the use of CVD was for improvements to the early carbon electric light filaments by Sawyer and Mann in 1880[9]. Shortly after this in 1890, Mond carried out the first metal preparation of nickel from nickel carbonyl[9]. From this period until the 1930's a number of other CVD processes were used for the preparation of refractory metals. This period also saw the first preparation of silicon from the hydrogen reduction of silicon tetrachloride (Pring and Fielding 1909, Hoelbling 1927)[9]. The semiconductor industry has benefited the most from improvements in the CVD technique in the last 50 years[9]. Other examples of industries that have benefited from the CVD process are optical films, decorative films and wear-resistant coatings[36].

The earliest example of CVD being used to deposit heat-control mirrors on glass come from the 1970's when the thin film properties of silver and titanium nitride films were investigated[9,40].

In the next section the processes involved in growing a film by CVD are discussed.

1.4 Nucleation and growth of CVD films.

Nucleation is defined as the aggregation of a condensed species to form clusters of atoms possessing a specific volume[37]. The energy needed to create a unit area is always positive, so a larger surface area also means increasing the energy of the system[38]. The free energy of the system can be defined as the combination of the surface energy equal to $4\pi r^2\gamma$ (where r is the radius of the particle and γ is the specific surface area), which is always increasing for a growing nucleus and the volume energy which decreases for a growing nucleus due to the negative free energy of formation ΔG_v[14,37,38].

Hence:

$$\Delta G = 4\pi r^2\gamma + 4/3\ \pi r^3\Delta G_v \qquad \text{(Equ. 1.4a)}$$

The term ΔG_v, the volumetric free energy term is given by:

$\Delta G_v = -kT/V \times \log S$ (where S is supersaturation $S = P/P_{eq}$)

(P = Pressure, P_{eq} = Equilibrium pressure) (Equ. 1.4b)

A graph of the free energy in the system vs the number of atoms in the nucleus is given by the graph in figure 1.4a.

Fig.1.4a Graph of system free energy vs. number of atoms.

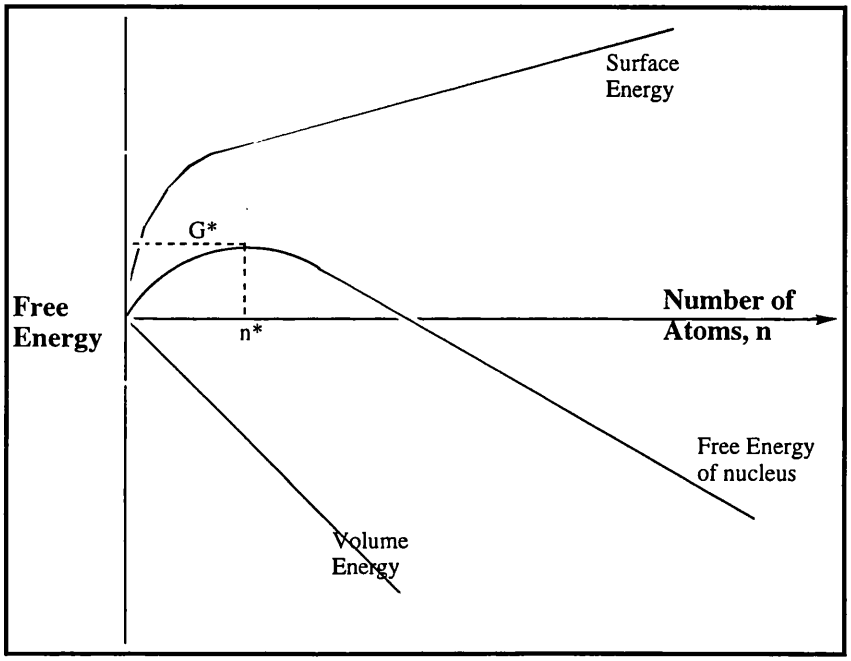

The free energy of the system, as can be seen from fig. 1.4a, increases until a critical radius is achieved with n* atoms and an energy of G*. The size of the nucleus at this point can be calculated by setting d (ΔG) / dr = 0. This gives:

$$r^* = -\frac{2\gamma}{\Delta G_v} = \frac{2\gamma V}{kT \log (P/P_{eq})} \quad \text{(Equ. 1.4c)}$$

When the radius of the nucleus is below r* there is a high likelihood that the particle will disintegrate back into the gas phase, while above r* the nucleus is likely to grow, as it will reduce the overall free energy of the system[38].

The theory detailed above describes homogeneous nucleation in a supersaturated system to give spherical nuclei. Nucleation on a substrate is slightly different as nuclei form in the shape of a water droplet on the substrate surface (fig. 1.4b).

Fig. 1.4b Theory of nucleation

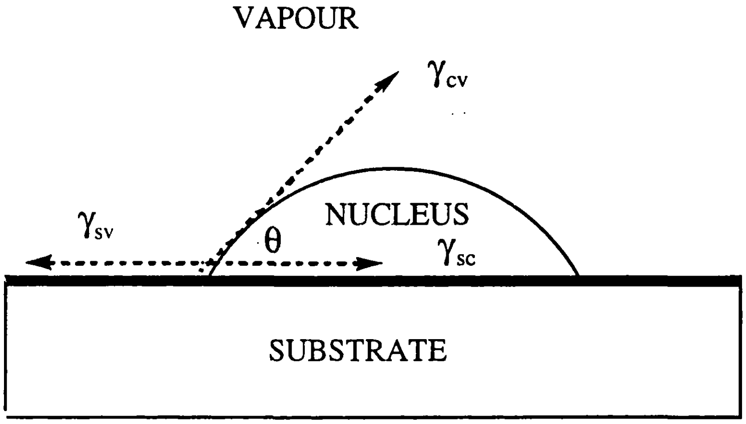

The angle that the top of the nuclei makes with the substrate is determined by:

$$\gamma_{cv} \cos\theta = \gamma_{sv} - \gamma_{sc} \qquad \text{(Equ. 1.4d)}$$

Where γ is the surface free energy and the subscripts c, v and s refer to the condensation nucleus, the vapour and the substrate respectively[37].

The heterogeneous surface lowers the critical nucleus size acting as a catalyst for nucleation. As the angle θ, tends towards zero, in the limiting case complete wetting occurs and nucleation is favoured, as the free energy is negative[37]. As the angle goes the other way towards 180° the substrate becomes less involved and the nucleation process becomes more like the homogeneous nucleation process.

The growth of films on any substrate can be explained by one of three growth mechanisms[8,39,40]. The first of these mechanisms is known as the Volmer-Weber growth mechanism. This approach involves nucleation followed by threedimensional island growth. This growth mode tends to occur when the film atoms are more strongly bound to each other than to the substrate surface. A second approach is the Franck-van der Merve method, in which the growth proceeds in a layer by layer fashion, where one layer is complete before growth of the next layer begins. This occurs when film atoms are more strongly bound to the substrate than to each other. The final approach is known as the Stranski-Kastanov growth mechanism and is an intermediate between the two methods already discussed. This occurs when after the growth of one or two monolayers, subsequent layer growth becomes energetically unfavourable and islands form. These methods of growth are displayed graphically in figure 1.4c[8,39,40].

Figure 1.4c Approaches to nucleation and growth.

Volmer-Weber

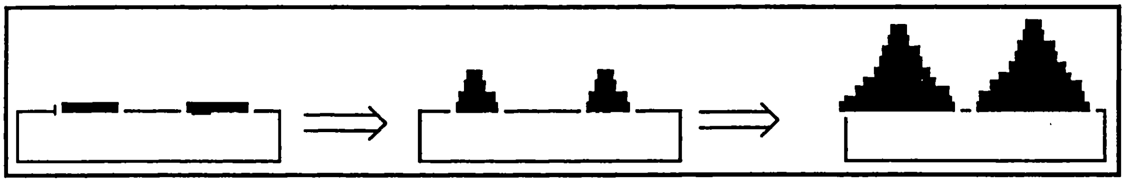

Stranski-Kastanov

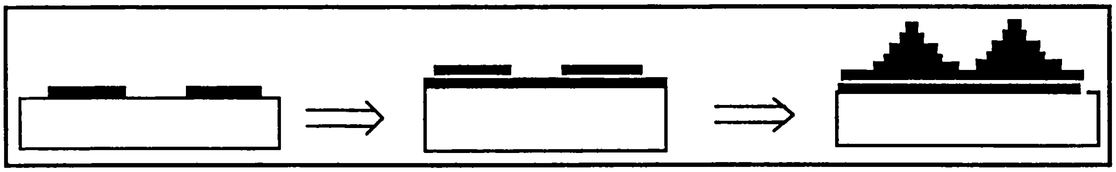

Franck-van der Merwe

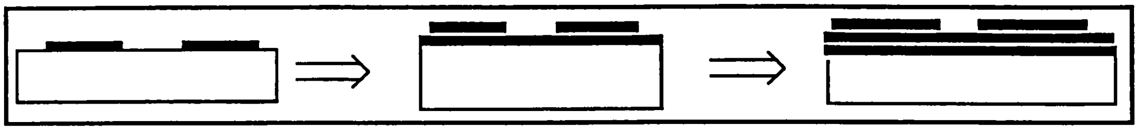

The most common of these growth mechanisms is the "Volmer-Weber" method. A defining characteristic of "Volmer-Weber" films is that the atoms or molecules making up the film are more strongly bound to themselves than to the substrate.

The Volmer-Weber growth mechanism can be summarised as a combination of several steps. Initially for growth to proceed, nucleation must have occurred. In this theory, clusters are formed by collisions of precursors on the substrate surface, and in the vapour phase if supersaturation is sufficiently high[37]. The nuclei that form on the film are statistically distributed across the substrate surface. Once nucleation has occurred the next stage is growth. Initially the nuclei develop with an increase in free energy, until a critical size is reached, after which growth continues with a decrease in free energy[37]. The nuclei grow by the accommodation of adsorbed particles to form small islands or crystallites. The final stage of the growth process is coalescence. Coalescence is the agglomeration of islands to form larger crystals and eventually a continuous film[38]. Surface diffusion and nucleation processes occurring on the substrate surface affect the growth type and microstructure of a film. These are strongly influenced by the temperature, pressure and gas phase composition in the reactor. Amorphous films are often formed at lower substrate temperatures (and high growth rates), as surface diffusion is slow, relative to the arrival of precursors. At higher substrate temperatures (and slower growth rates), surface diffusion is fast compared to the incoming precursors so the growth often replicates the substrate lattice[8,38-40].

1.41 Physical processes and boundary layers

The physical processes behind the CVD reaction can be linked with one of two regimes, the mass transport limited or the surface reaction limited reaction rate.

In the gas phase mass-transport rate limited process, the speed with which the film grows on the substrate is limited only by the rate at which the reactants can be delivered to the substrate.

A surface rate limited process occurs when the rate of decomposition of the reactants or surface chemical reactions, determine the growth rate of the film. A reaction can be forced to follow the surface reaction limited regime by increasing the precursor flow rates or reducing the pressure.

The surface reaction rate limited regime may be affected further by a number of other factors occuring in the CVD reactor[9]. A reactor can operate by the molecular flow regime or the continuous flow regime. The molecular flow regime is linked to reactors where the gas mean free path (λ_{mfp}) is long (such as in a vacuum), compared to the reactor dimensions, thus this type of regime is typically found in LPCVD or vacuum-based reactors. A continuous flow regime is found where the gas mean free path is much smaller than the reactor dimensions, thus it is typically found in APCVD reactors. The Knudsen number (Kn), calculated by the ratio of the gas mean free path (λ_{mfp}) to the characteristic reactor dimension (D_p), is used in CVD reactions to determine the type of gas flow (equ. 1.41a)[8,9].

$$K_n = \lambda_{mfp} / D_p \qquad \text{(equ.1.41a)}$$

In an APCVD reactor such as the one described in this thesis, the Knudsen number is less than 1, ($K_n << 1$), because high vapour pressure in the reactor make the gas mean free path low, compared to the relatively high chamber diameter (~10 cm). For continuum flow reactors ($K_n << 1$) boundary layers, which affect the surface reaction occur. This can happen in three ways. In the first, the gaseous material entering the reactor chamber, as a result of its 'viscosity', clings to the surfaces, while away from the surfaces the gas moves at a faster rate. This results in a parabolic velocity gradient, zero at the walls to the high velocity of the free stream. A thermal boundary layer is observed where gas entering the reactor close to the hot surfaces heats up, while gas further away from the surfaces hasn't enough time to heat to the same level. This results in a boundary layer for temperature, with the temperature of the gas varying from the inlet temperature to the temperature of the walls and substrate. In the third type of boundary layer, a concentration boundary layer can be observed where chemical reactions at the walls and substrate result in the removal of the reactants and the formation of products and by-products. If this reaction is sufficiently rapid and gas transport through the boundary layer slow, a concentration gradient occurs where the reactant concentration at the walls is nearly zero and increases with distance away from the walls. The thickness of this concentration boundary layer will increase along the reactor[8,9].

The result of the boundary layer phenomena described, is the existance of a 'stagnant' layer that hangs over the substrate[9]. The degree to which this forms will determine how far the film deposition proceeds along the substrate, or whether a reaction occurs at all.

1.5 The CVD of nitrides and oxynitrides

Nitrides and oxynitrides of transition metals can be made using the CVD and PVD processes described in section 1.31, although the purity of the product and cost of the film production varies considerably. By far the most work of any thin nitride film has been carried out on titanium nitride. It has been deposited by APCVD, LPCVD, LECVD, and PVD (both evaporation and sputtered). It has been deposited from both single and dual source precursors, on a variety of different substrates including glass, solar cells, steel and plastics[24]. Titanium nitride has been deposited at temperatures as low as 200 – 400 °C from $Ti(NR_2)_4$ [59], or from

$Ti(NR_2)_4$ and ammonia[41]. It has been coated in a mid-temperature range of 400 – 700 °C from reaction of $TiCl_4$ and NH_3[1,42-47]. It has been coated at high substrate temperatures above 800° C from $TiCl_4$ and N_2/H_2[41]. Laser enhanced CVD depositions of TiN can be achieved at lower temperatures even with $TiCl_4$ and N_2/H_2 as precursors[41] but it is more expensive than conventional methods. The most inexpensive method of forming TiN is by APCVD and is perhaps the only viable technique for large-scale industrial work because of the cost and speed requirements. APCVD of TiN films can be split into two subdivisions dependent on whether the reactor is a cold wall or hot wall type[38].

All precursors selected for use in APCVD are volatile liquids, or low melting solids with high volatility once in the liquid state. From there, a single source or dual source precursor system can be selected. Each of these have their relative merits, and required chemistry.

A single source precursor has the bonds required in the final film present in the precursor. On the introduction of heat at the substrate surface, the precursor can break apart to leave the required film product while other components will be removed safely by the exhaust as waste gases. An example of a single source precursor for a well investigated system is the CVD of $Ti(NR_2)_4$ (where R= Et[24] or Me[48]) to give titanium nitride. In this example the organic ligands are removed to leave the Ti-N, as shown by the illustration in figure 1.5a.

Fig. 1.5a Structural diagram of Ti $(NR_2)_4$

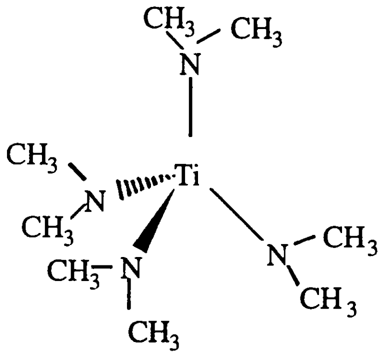

$$Ti(NR_2)_4 \xrightarrow{150\text{-}400^{\circ}C} TiN + 3\ {\bullet}NR_2 + 2{\bullet}R \qquad \text{(Equ. 1.5a)}$$

The advantages of the single source system are that lower temperatures can be employed and prereaction prior to the coater is reduced. A disadvantage is that products are often highly contaminated due to incomplete decomposition of the precursor[40]. Carbon contamination in nitride and oxynitride films is a problem as it degrades electrical and optical properties. The carbon contamination detected in TiN films deposited from $Ti(NMe_2)_4$ was over 30 atomic percent and the films also contained high oxygen contamination (13-30%)[24], so although films have been deposited, they can hardly be described as pure titanium nitride.

Dual source precursors react to give the required film, leaving gaseous by-products to exhaust to waste. Examples of the dual source system for titanium nitride films are the reactions of $TiCl_4$ and NH_3 (equation 1.5b) and $TiCl_4$ with N_2/H_2 (equation 1.5c).

$$6TiCl_4 + 8\ NH_3 \rightarrow 6TiN + 24\ HCl + N_2 \qquad \text{(Equ. 1.5b)}$$

$$TiCl_4 + 0.5\ N_2 + 2\ H_2 \rightarrow TiN + 4\ HCl \qquad \text{(Equ. 1.5c)}$$

Advantages of the dual source system are that often the by-products are easier to remove. This is the case in the reaction of $TiCl_4$ and NH_3 where the by-product, HCl, is easily removed by a high process gas flow without damaging or contaminating the freshly formed film (although if it is allowed to linger it reacts with NH_3 to form NH_4Cl that can contaminate the film). The nitrogen sources in reactions to form titanium nitride include nitrogen gas[41], ammonia[42,43] and hydrazine[45]. The disadvantage of the dual source system over the single source system described before is that usually higher temperatures are required to initiate a reaction. Titanium nitride can be prepared from $TiCl_4$ and N_2/H_2 from a temperature as low as 850 °C however, temperatures of between 1000 - 2000 °C are used commercially[42] for durable machine tool coatings[16,42]. These conditions would be too harsh for glass substrates. $TiCl_4$ and NH_3 react together at room temperature to form a complex ($TiCl_n(NH_3)_n$), which can be broken down with heat to TiNCl at 350 °C and TiN above 450 °C[1]. At temperatures between 450 and 600 °C some chlorine and oxygen contamination can remain in the TiN film. A further disadvantage of the dual source system is that blockages often occur at the point of mixing the precursors. The only way to limit this is to mix the precursors very close to the substrate.

Sometimes precursors that can act as single source components are used in a dual source system i.e. Ti $(NR_2)_4$ with NH_3[1](equation 1.5d).

$$Ti(NR_2)_4 + NH_3 \longrightarrow TiN + 3NHR_2 + \bullet NR_2 \quad \text{(Equ. 1.5d)}$$

This has been shown by several research groups to lead to better quality films than using the single source precursor on its own. The reaction proceeds as the $Ti(NR_2)_4$ complex undergoes trans-amination reactions with the ammonia eventually forming multiple Ti-N bonds by successive amine elimination reactions[1]. Again, as with all dual source systems, the problems of prereaction remain, although the problems of impurities appear to be vastly improved[1]. Carbon impurities of just less than 10% have been reported by this method, while the deposition temperatures have been kept low (200 - 450 °C)[30]. These conditions have led to fairly good quality films, although very high purity precursors were used[1].

The downside of the $Ti(NR_2)_4$ and ammonia reaction is the expense of $Ti(NR_2)_4$ compared to the relatively inexpensive and readily available $TiCl_4$ and also the films that are produced still typically have high carbon, hydrocarbon, carbide and oxygen impurities[24,30].

In contrast to titanium nitride films, vanadium nitride films have received much less study. This is surprising as VN films can be formed in a variety of ways, and have properties very similar to those of titanium nitride. Bulk preparation involves the reaction of N_2 or NH_3 with vanadium metal at 1650 °C[49]. The most common method for deposition of VN has involved evaporating vanadium films on to the substrate surface in a controlled atmosphere and then heating the resultant film in a nitrogen atmosphere at between 1000 °C and 1400 °C[35,50-52]. This produces a δ - VN_x phase film. The amount of nitridation changes dependent on the temperature of the annealing. Lower annealing temperatures lead to lower nitrogen content. The nitrogen fills the interstitial sites in the vanadium lattice and when the nitrogen content (x) in VN_x is less than 1, there are vacancies in the cubic structure on the interstitial nitrogen sites. These sites can easily be filled by oxygen or carbon impurities, but despite this, the carbon and oxygen contamination observed in these films formed by PVD has been reported to be in the 0.5 –2.5 % range[3,5]. Lower annealing temperatures of 300 °C can be used in the deposition of VN_x if nitrogen is introduced by ion beam irradiation[53], but this leads to film damage[35], mixed phase products[53], and non-uniform compositions[53].

Vanadium nitride films have been deposited by magnetron sputtering[54]. This involves high purity nitrogen (99.998%) and argon gas (99.9996%), a vanadium target, and steel disc substrates. In this case high purity films are produced with the nitrogen- vanadium ratios from zero to 0.96. The nitrogen partial pressure or the substrate bias voltage[54] can control the stoicheometry.

Lower cost and lower temperature methods of VN_x deposition have not been extensively investigated. CVD methods of preparation of VN involve the use of volatile vanadium chloride (VCl_4) with a nitrogen/hydrogen mixture[1,33]. Molecular precursor routes to vanadium nitrides have been achieved by reaction of ammonia with organometallic dialkylamide complexes such as $V(NMe_2)_4$[1,33]. $V(NMe_2)_4$ has been used to prepare smooth, reflective films with good adhesion at deposition temperatures as low as 200 °C by APCVD [1,33] but the carbon and oxygen contamination in these films was very high (up to 50%), particularly in the 50 Å closest to the film surface.

The reaction for the formation of VN from VCl_4 and ammonia is analogous to the reaction of $TiCl_4$ and NH_3 (equation 1.5e).

$$6VCl_4 + 8NH_3 \rightarrow 6VN + 24HCl + N_2 \qquad \text{(equ. 1.5e)}$$

VCl_4 is preferential to dialkylamide complexes, as a precursor, as theoretically no carbon contamination should occur during CVD deposition. VCl_4 is commercially available and relatively inexpensive compared to $V(NR_2)_4$. $V(NR_2)_4$ is synthesised by reaction of VCl_4 with $LiNR_2$.

Vanadium oxynitride has received very little attention from any of the major coating techniques, probably due to the fact that VN thin film depositions usually have a high percentage oxygen contamination. There are few references to VO_xN_y.

Of those found, none involved thin film preparation only the preparation of VO_xN_y in its bulk form [55-57]. The reason for this lack of study can be put down to the fact that the nitrides are often expected to have better physical, mechanical and chemical properties to oxynitrides. This is not always the case[55].

Mixed metal nitride coatings have only rarely been previously attempted by CVD. Only two examples could be found in the literature. These involved the preparation of FeN_x - TiN films by LPCVD[58] and the preparation of silver, palladium and copper alloys by Aerosol Assisted CVD[27]. Ternary transition metal nitrides have been more commonly prepared by sputtering techniques[59-65], including Ti/V N films[59-60,62-63]. A mixed titanium / vanadium oxide film has been prepared by sputtering[66].

Hoffman has carried out a review of the APCVD of many of the early transition metal nitrides[1,24].

1.6 The theory of heat mirrors

The main intention of coating glass with nitride and oxynitride thin films in this research was to create heat-control mirrors. A heat mirror is a coated substrate that has high transmittance in the visible region (0.3 - 0.77 μm) while providing high reflectance in the infrared region (0.77 μm –100 μm)[40]. The transmittance / reflectance plot for a perfect heat mirror is shown in Fig. 1.6b.

With commercial considerations a heat mirror must have a thin conformal, uniform layered coating, that has enough visible light transmittance to allow typical glass-like appearance.

Some metal coatings such as silver, gold and copper films show the properties associated with heat mirrors, but often conformality, chemical resistance and wear resistance are a problem. Indium doped SnO_2 coatings[67] have improved on this but have proved expensive (Pilkington K – Glass). TiN and other N-doped tin oxides (SnO_2 – F[68] and SnO_2 - Sb) have also shown their suitability as heat mirror coatings.

Fig. 1.6a Diagram of a heat mirror.

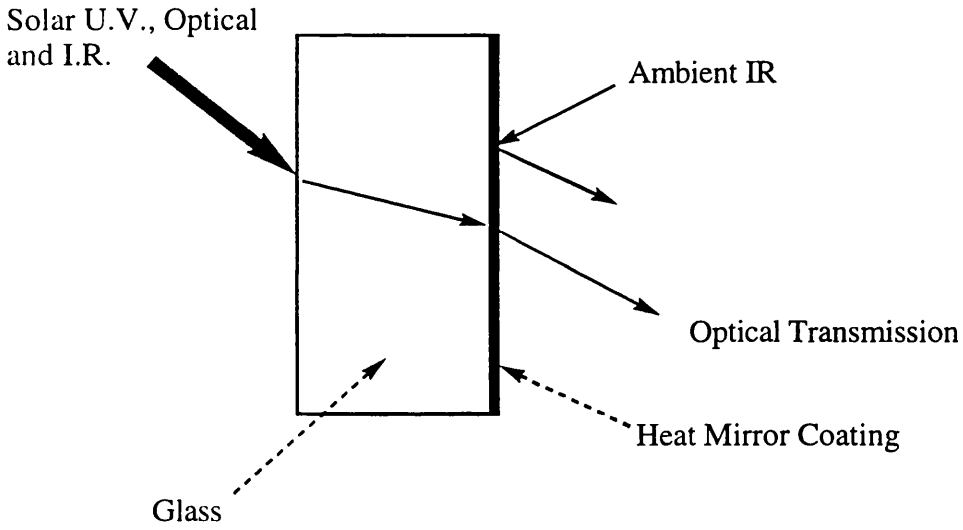

Fig 1.6b Plot of transmittance/ reflectance against wavelength for a perfect heat mirror (1.0 reflectance = 100% reflectance)

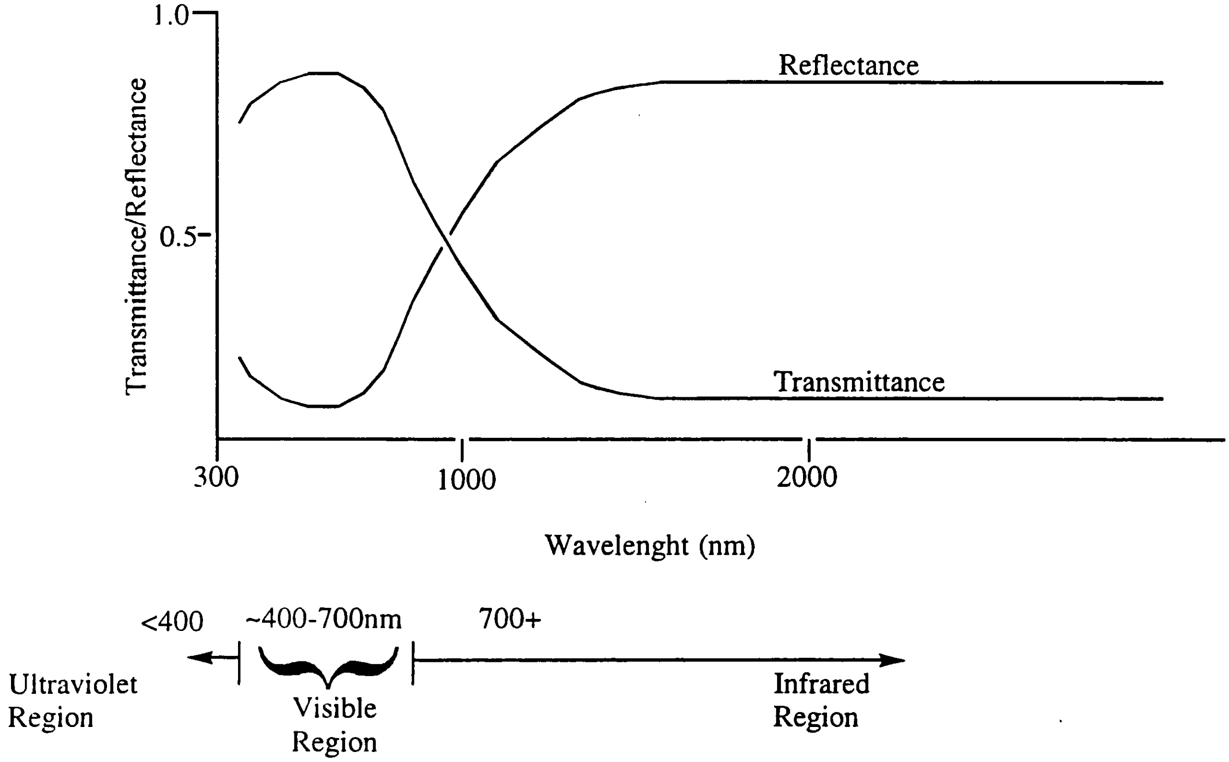

The optical properties of a thin film are able to change the properties of a window. Before deposition of a film the glass substrate, like all glass, has high transmission in the visible region (i.e. it is transparent), and has low reflectance in the infrared (doesn't reflect heat). A spectrum showing the transmission and reflectance properties of glass is shown below in fig. 1.6c.

Fig. 1.6c Plot of transmission / reflectance against wavelength for plain glass.

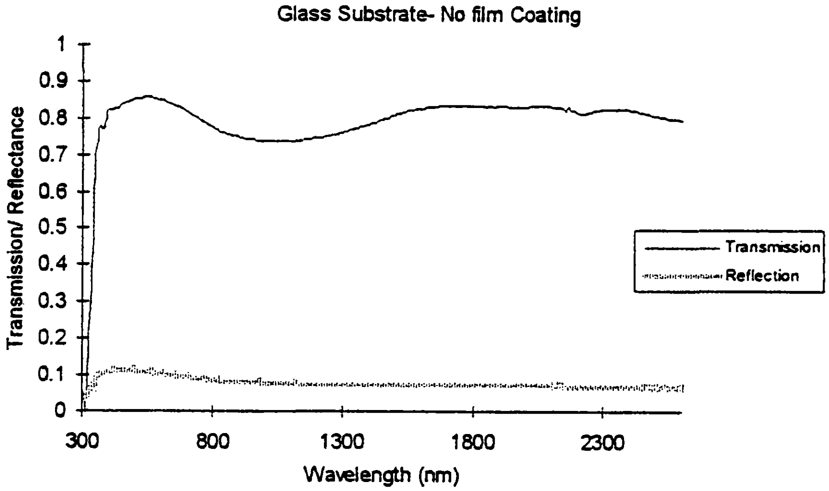

Optical properties of materials originate from the behaviour of free electrons in the conduction bands[8]. The properties of reflectance vs absorbency occurs in metals and metal-like materials due to the large density of closely spaced electron energy states above the Fermi level. Incident photons are accepted over a wide range of wavelengths and are readily absorbed by conduction band electrons. These excited electrons are promoted to higher energy levels where they undergo collisions with lattice ions releasing energy as phonons[8]. When this happens, the lattice is heated, in effect, absorption. Alternatively when the probability of hitting lattice ions is small, the electron can emit a photon and return to the lower energy level. When this happens, the process is essentially a reflection. Heat mirrors exhibit strongly reflective properties in the IR region[8].

Thin films have smaller crystal boundaries and optical properties that are somewhat different to their bulk forms. However the approximations given by the optical properties of the bulk form of metals is close enough to enable a mathematical description of heat–mirror films.

In general the motion of an electron, in an electric field of the form E_0 exp. ($i\omega t$)[69-71], with mass m and charge e, can be described as:

$$md^2x/dt^2 + m\gamma\, dx/dt + \beta x = -e\, E_o \exp(i\omega t) \qquad \text{(Equ. 1.6a)}$$

Where md^2x/dt^2 = inertial force βx = restoring force after its displacement and $m\gamma\, dx/dt$ = damping force (proportional to the velocity of the electron).

The effect of an electric field can be considered similar to the reaction of a wave with the free electrons. The free electrons in the system behave like damped oscillators with natural angular frequencies, ω_o, equal to zero[69].

The damping constant, γ, is a factor that takes into account the collisions of electrons and the crystal lattice[69,70]. It has dimension, 1/time, so it is often treated as an angular frequency. The solution for equation 1.6a gives the following expression:

$$x = \frac{-eE_0}{m\,[(\omega_0^2 - \omega^2)^2 + \gamma\,\omega i\,]} \qquad \text{(Equ. 1.6b)}$$

Polarisation can be expressed by two relationships:

$$P = -Nex \quad \text{and} \quad P = \varepsilon_o\, E_o\, (\varepsilon_r - 1) \qquad \text{(Equ. 1.6c)}$$

(N = electrons per unit volume, ε_0 = permittivity of free space, ε_r = complex dielectric constant)

So

$$\varepsilon_r = 1 + \frac{Ne^2}{\varepsilon_0 m[(\omega_0^2 - \omega^2)^2 + \gamma\,\omega i\,]} \qquad \text{(Equ. 1.6d)}$$

This can also be written as the complex equation,

$$\varepsilon_r = \varepsilon_1 - i\varepsilon_2 \qquad \text{(Equ. 1.6e)}$$

Where the real part:

$$\varepsilon_1 = \frac{Ne^2(\omega_0^2 - \omega^2)}{\varepsilon_0 m[(\omega_0^2 - \omega^2)^2 + \gamma^2\omega^2]} \quad \text{(Equ. 1.6f)}$$

or:

$$\varepsilon_1 = n^2 - k^2 \quad \text{(Equ. 1.6g)}$$

and the imaginary part:

$$\varepsilon_2 = \frac{Ne^2\gamma\omega}{\varepsilon_0 m[(\omega_0^2 - \omega^2)^2 + \gamma^2\omega^2]} \quad \text{(Equ. 1.6h)}$$

$$\varepsilon_2 = 2nk \quad \text{(Equ. 1.6i)}$$

n and k make up the complex refractive index, N.

$N = n - ik$ k = imaginary part of refractive index (Equ. 1.6j)
n = real part

The variation of these two determines the degree of absorbance or reflectance of a material. If a material is highly absorbing, n is usually relatively small compared with k. If a material is dielectric, reflective and useful for optical purposes, k is small compared to n.

Drude expressed ε_1 and ε_2 in terms of frequencies:

$$\varepsilon_1 = n^2 - k^2 = 1 - \omega_p^2 / (\omega^2 + \omega_c^2) \quad \text{(Equ. 1.6k)}$$

$$\varepsilon_2 = 2\,nk = \omega_p^2\gamma / \omega(\omega^2 + \omega_c^2) \quad \text{(Equ. 1.6l)}$$

(ω_p = plasma frequency, ω_c = collision frequency)

At higher frequencies where $\omega \gg \omega_p$ i.e. in the x-ray region ε_2 and k tend to zero and ε_1 tends to n^2 and $1 - \omega_p^2 / (\omega^2 + \omega_c^2)$. So n is positive and the film will appear transparent.

As the frequency is reduced ε_1 will decrease and eventually equal zero when $\omega^2 = \omega_p^2 - \omega_c^2$. This is a transition point. When the frequency gets lower still, ε_1 will become negative, tending towards $1 - (\omega_p^2 / \omega_c^2)$, which is a constant quantity with a negative value. When ε_1 is negative, k^2 is greater than n^2, and a strong absorption and reflection of electromagnetic radiation will be observed.

For most materials, the transition where $\varepsilon_1 = 0$, occurs in the UV region. Materials of use as heat control mirrors will have their transitions in the visible or near IR region of the electromagnetic spectrum[40,69-71].

1.7 Nitrides and oxynitrides as heat control mirrors.

As has been discussed in section 1.31, Chemical Vapour Deposition has provided many examples of metal nitrides thin films. Titanium nitride in particular has been coated by LPCVD[1,43-47,72-74], APCVD[24,30,42], LECVD[16], as well as by sputtering[45,75-79], evaporation[80], and pyrolysis techniques[81]. It has been deposited from single source (e.g. from $Ti(NMe_2)_4$ [1,24] and $Ti(NEt_2)_4$ [1,24]) and dual source precursors (from $TiCl_4$ with N_2 and H_2 [16,41], from $TiCl_4$ and NH_3 [1,46,47], and from $Ti(NMe_2)_4$ and NH_3[72,74]) and also in both cold[1] and hot[41] wall reactors. TiN films have shown very promising features for heat mirror coatings[43]. The transition point from transmission to reflectance occurs in the near IR region of the electromagnetic spectrum[40]. TiN films are also extremely hard and wear resistant[36] ensuring a long lifetime as a coating[82]. Its visible transmission colour (gold), also make it attractive as a coating for windows.

Vanadium nitride shares many of the properties of TiN, but has not been investigated as a solar-control coating. It has been coated as a thin film by several methods including LPCVD[1], sputtering[52,54], APCVD[33], ion beam irradiation[53], from both single and dual source precursors[1,33], and by evaporation techniques[35]. However it is relatively unexplored as a coating on glass, and for its potential as a heat-control mirror. Like TiN, VN has its transition from transmission to reflectance in the near-IR region. Its hardness, similar to TiN, and appearance (black / gold) give it definite potential for use in heat-control mirrors.

Vanadium oxynitride is similar to vanadium nitride in many ways including appearance (gold / black) and hardness. It too has its transition from transmission to reflectance in the near-IR region, a property essential for heat-control mirrors. However, no accounts of vanadium oxynitride as a heat-control mirror appear in the literature.

Chromium oxide films[83] have been deposited on various substrates including glass, using APCVD[84-86] and PVD techniques[87-89]. They have never been investigated for their viability as heat-control mirrors although CrN has been investigated for its optical properties[90]. Chromium oxynitride has not been investigated as a thin film.

By using mixed metal nitrides, the transition from transmission to reflectance could be moved by tailored amounts depending on the exact composition of the film. The appearance could also be changed slightly. A mixed titanium / vanadium oxide film has been prepared for use as a coating on windows[66] although there is no record of mixed metal nitrides being investigated for use as heat-control mirrors in the literature. A mixed chromium / titanium nitride has been prepared[91] but again not for heat-control mirrors, and there are no reports of chromium / titanium oxynitride coatings. These factors have been discussed further in chapter 6.

Of all the nitrides and oxynitrides discussed in this chapter, only titanium nitride has been studied for its potential as a heat-control mirror on glass[40,92].

1.8 APCVD of nitrides and oxynitrides for heat control mirrors

This thesis discusses the design and construction of an Atmospheric Pressure Chemical Vapour Deposition rig. It also describes the APCVD depositions of vanadium nitride, vanadium oxynitride, chromium oxide, chromium oxynitride and mixed metal nitride and oxynitride films. The films have been analysed in detail for use as heat-control mirrors.

Chapter 2

Design and Construction of the APCVD Rig

2.0 Design and construction of an APCVD reactor

A CVD rig was designed and constructed for the study of the atmospheric pressure reaction of $TiCl_4$, VCl_4. VCl_4 / $TiCl_4$, $TiCl_4$ / $CrO_2Cl_2$and CrO_2Cl_2 with ammonia.

APCVD requires inert transport gases (nitrogen or argon), to carry reactive volatile material into mixing chambers (where they will meet ammonia or other precursors), and on into a reactor or coater chamber where deposition will follow. An exhaust system is required to dispose of unreacted material and by-product gases.

Several designs were considered for the pipe framework and mixing chambers. The nature of the chemicals used (NH_3, MCl_n), meant that combination, even at low temperatures, led to the formation of particulate material that blocked the pipework.

The design of the rig can be split into several sections. The coater / furnace, the bubbler (or volataliser), the pipe framework and mixing chamber, and the exhaust. Each of these areas will be dealt with separately.

2.1 The coater / furnace

The coater is the area where final mixing and arranging of the precursor gases and their flow patterns must occur for a trouble-free coating. The coater has an entrance system that not only mixes the gases but changes the flow from an entrance pipe to a uniform flow over the whole substrate. The entrance flange to the coater had to be designed specifically to the dimensions of the coater and substrate. The ¼ inch tube that enters the coater forces the gases into a number of directional changes before the gases can escape in a uniform shape flow (Fig 2.1a, b).

Fig. 2.1a Top view of coater entrance flange.

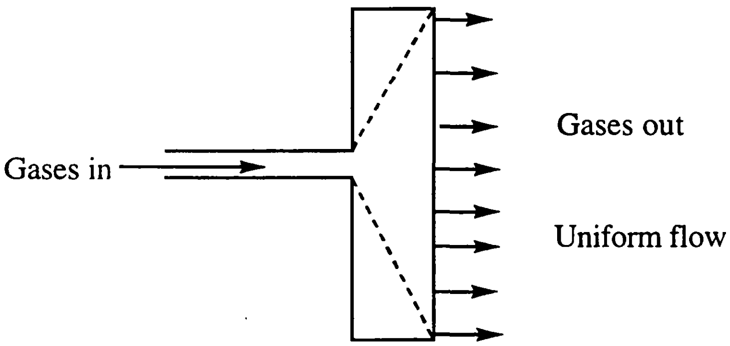

Fig. 2.1b Side view of coater entrance flange.

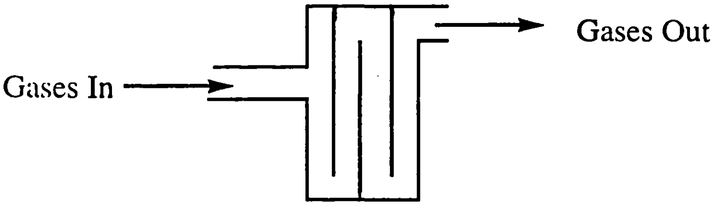

APCVD reactions typically require high temperatures. Other things that must be considered are a uniform heating area that fits the substrate in question and an effective exhaust out of the coater.

The type of coater decided upon for this study is known as a cold wall atmospheric pressure channel flow reactor. A hot wall reactor would have required a heating source around the walls of the reactor[93].

In these studies a graphite block is used in to provide uniform heating to the whole substrate, although this is not entirely effective. The block is heated by three cartridge heaters, which run the length of the graphite block. A temperature difference of around 60 °C across the substrate was noted at 500 °C. These temperature differences could be partially explained by the fact that the investigative measurements were carried out in an open environment to allow access for a thermocouple. This allows cool air from the outside to affect measurements in some areas away from the centre of the graphite block. It also means that overall temperatures across the block would be lower than expected. A table of the coater temperatures measured from various positions across the block is shown below.

Fig 2.1c Readout positions on graphite block.

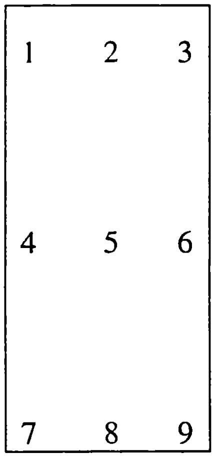

Fig 2.1d Thermocouple readings from positions in Fig 2.1c (with a substrate monitoring thermocouple reading of 500 °C)

Position	Temperature
1	411 °C
2	414 °C
3	410 °C
4	429 °C
5	441 °C
6	434 °C
7	382 °C
8	404 °C
9	404 °C

A graph of the graphite thermocouple temperature against the recorded substrate temperature (measured by placing a thermocouple onto the surface of the graphite block) is shown in figure 2.1e.

Figure 2.1e Plot of graphite thermocouple temperature vs. the recorded substrate temperature

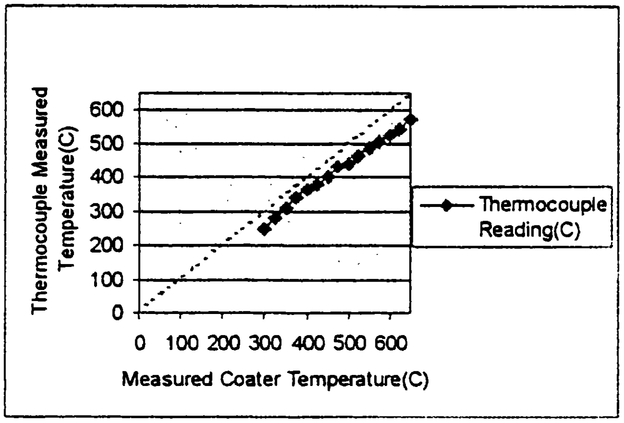

The graphite block measures 100 mm x 230 mm, giving adequate room for the glass substrate measuring 225 x 89 x 4 mm. A diagram of the coater is shown below.

Fig. 2.1f Side view of the coater.

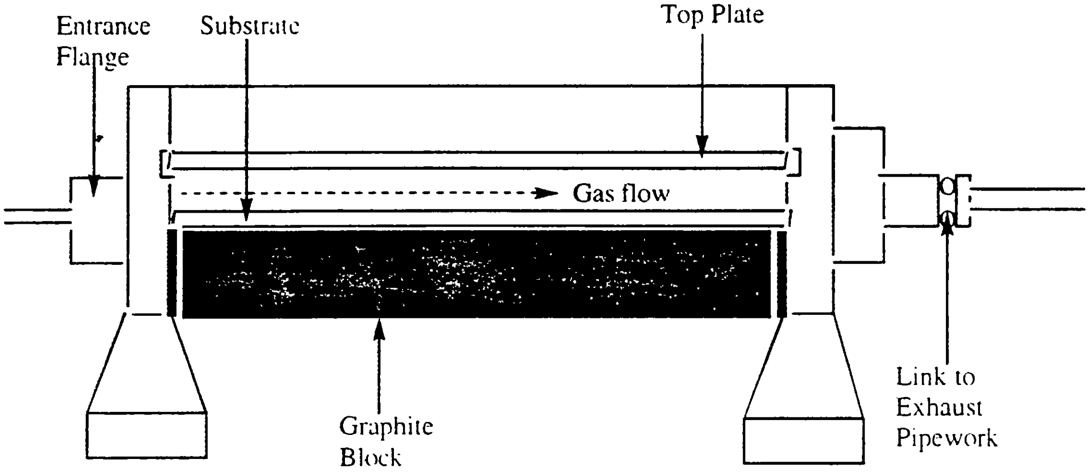

Fig 2.1g View of coater from above.

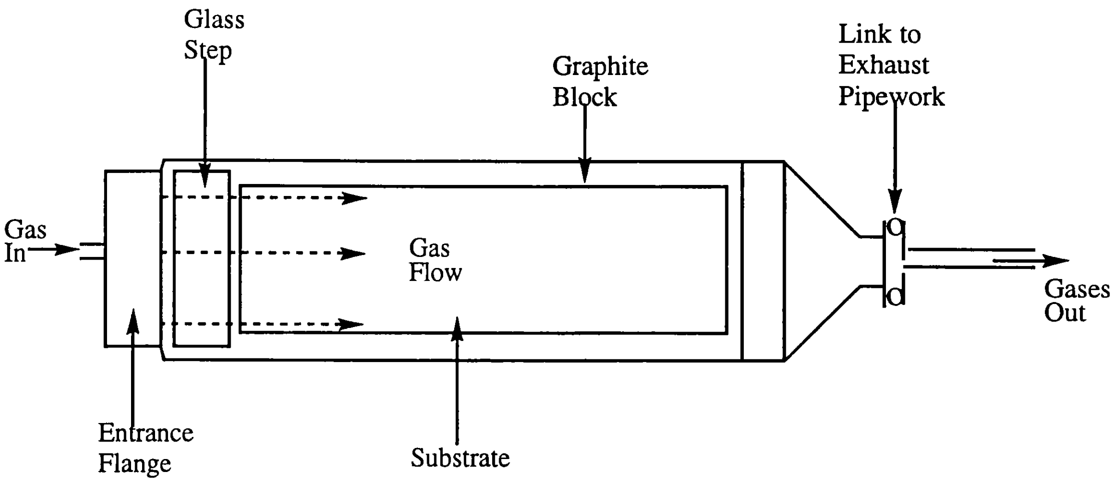

2.11 The substrate

The substrate was specifically designed by Pilkington Glass to aid adhesion of films to the surface while at the same time preventing interdiffusion of ions from the glass into the film. The diffusion barrier layer selected was called Siclon. It is between 50-70 nm thick and contains carbon, silicon and oxygen. This layer helps prevent contaminants such as sodium, potassium and bromine from the bulk glass floating to the surface during deposition and affecting the properties of the film. The glass substrate fitted easily into the coater leaving room at the edges.

2.2 The bubbler / volatiliser

A bubbler is necessary in this system as one of the precursors is always a liquid ($TiCl_4$,VCl_4,$VOCl_3$,CrO_2Cl_2). A bubbler is one of the most effective ways for transport of these materials to the reactor. The precursor is heated in the bubbler to approximately 30 °C below its boiling point in a sealed system. Opening the appropriate valves enables transport gas to flow into the bubbler. The transport gas becomes saturated with the liquid precursor and the resultant gas stream, laden with the precursor vapour, is then transported to the reactor. The bubbler was

Figure 2.2a Bubbler Diagram

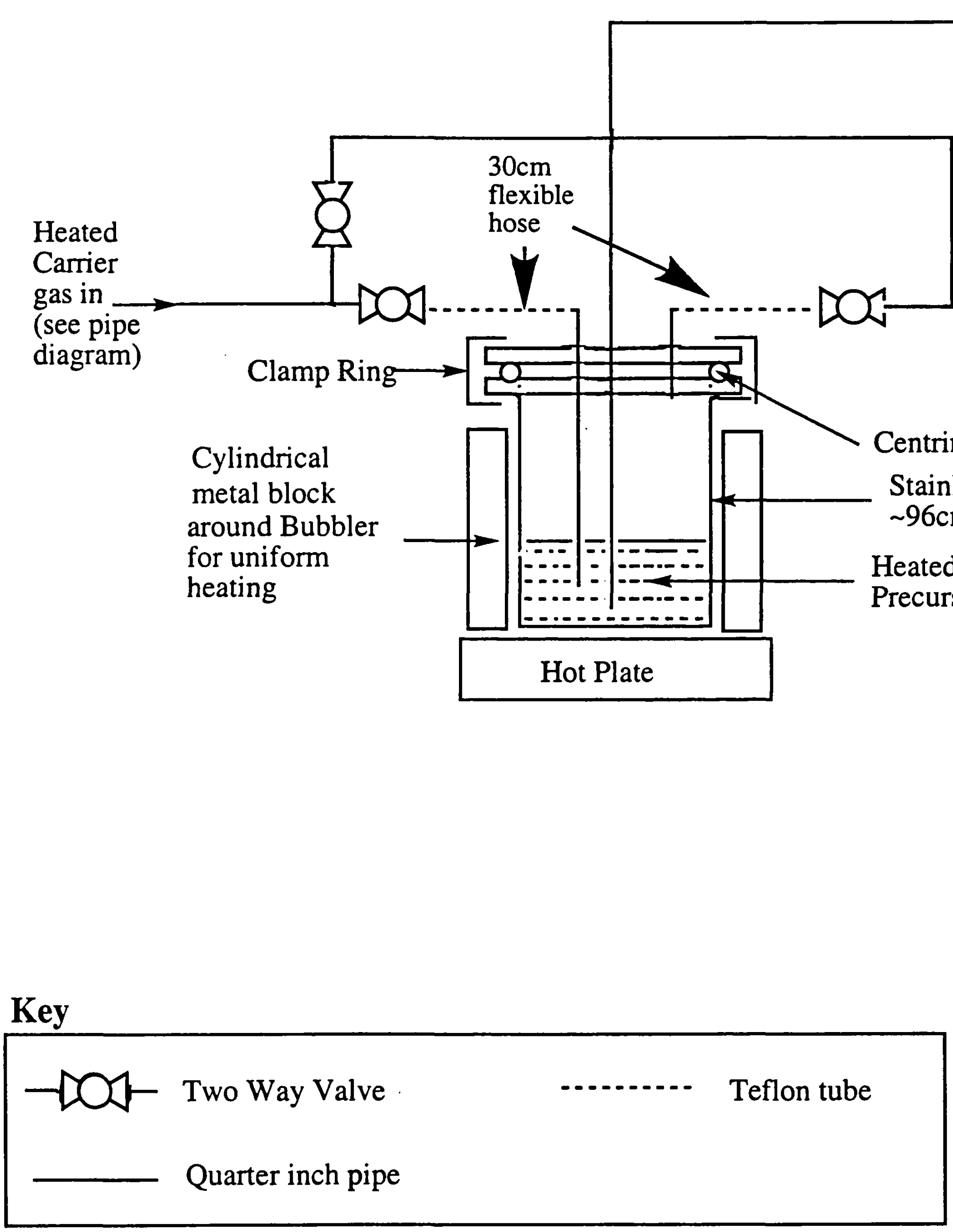

constructed from stainless steel and of dimensions diameter 35 mm, height 100 mm. The bubbler has a volume of approximately 96 cm^3 but was rarely filled over 60 cm^3 (see figure 2.2a).

The valves surrounding the bubbler mean that the transport gases can either by-pass or pass through the bubbler. The by-pass valve is open during warm up and cool down of the rig in order to keep the system purged. When the by-pass valve is closed and the bubbler entrance and exit valves opened a transport gas flows through the bubbler. The gas enters the bubbler via a flexible pipe connected to a stainless steel ¼ inch pipe that extends virtually to the base of the bubbler. The exit to the bubbler is from a hole in the lid, that connects to a flexible pipe and on to the 4-way valve and coater.

A type K thermocouple is used to accurately determine the temperature of the precursor material and to 'police' the heat to the hot plate. A stainless steel cylindrical block has been constructed to surround the relatively thin walled bubbler to ensure uniform heating.

The bubbler and flexible teflon pipework were cleaned following a set of runs with water and acetone. The flexible tubing running in and out of the bubbler was found to be a source of blockages.

Flow rates into the bubbler were calculated to allow only a certain amount of precursor material to enter into the gas flow. As the vapour pressure of each precursor material is slightly different, the temperature of precursor, flow rates through the bubbler and vapour pressure are all important considerations in determining the amount of material that will reach the substrate. The vapour pressure of a precursor was determined at a specific temperature, using one of the charts in figure 2.2b. The amount of material used in grams or $cm^3\ min^{-1}$ can be determined using the following expression.

$$\frac{V_p^T \cdot CF \cdot MW}{(760 - V_p^T)\ 24.4\ D} = \text{Amount of material used in ml / min} \qquad \text{(Equ. 2.2a)}$$

Where V_p^T = Vapour Pressure (Torr) at temperature T (from fig 2.2b).

CF = Carrier Gas Flow rate ($dm^3\ min^{-1}$).

MW = Molecular weight of precursor.

Atmospheric Pressure = 760 Torr

Volume of Gas at STP = 24.4 dm^3

D = Density of precursor

Fig 2.2b Plots of vapour pressure vs. temperature for CrO_2Cl_2, $TiCl_4$, VCl_4 and $VOCl_3$

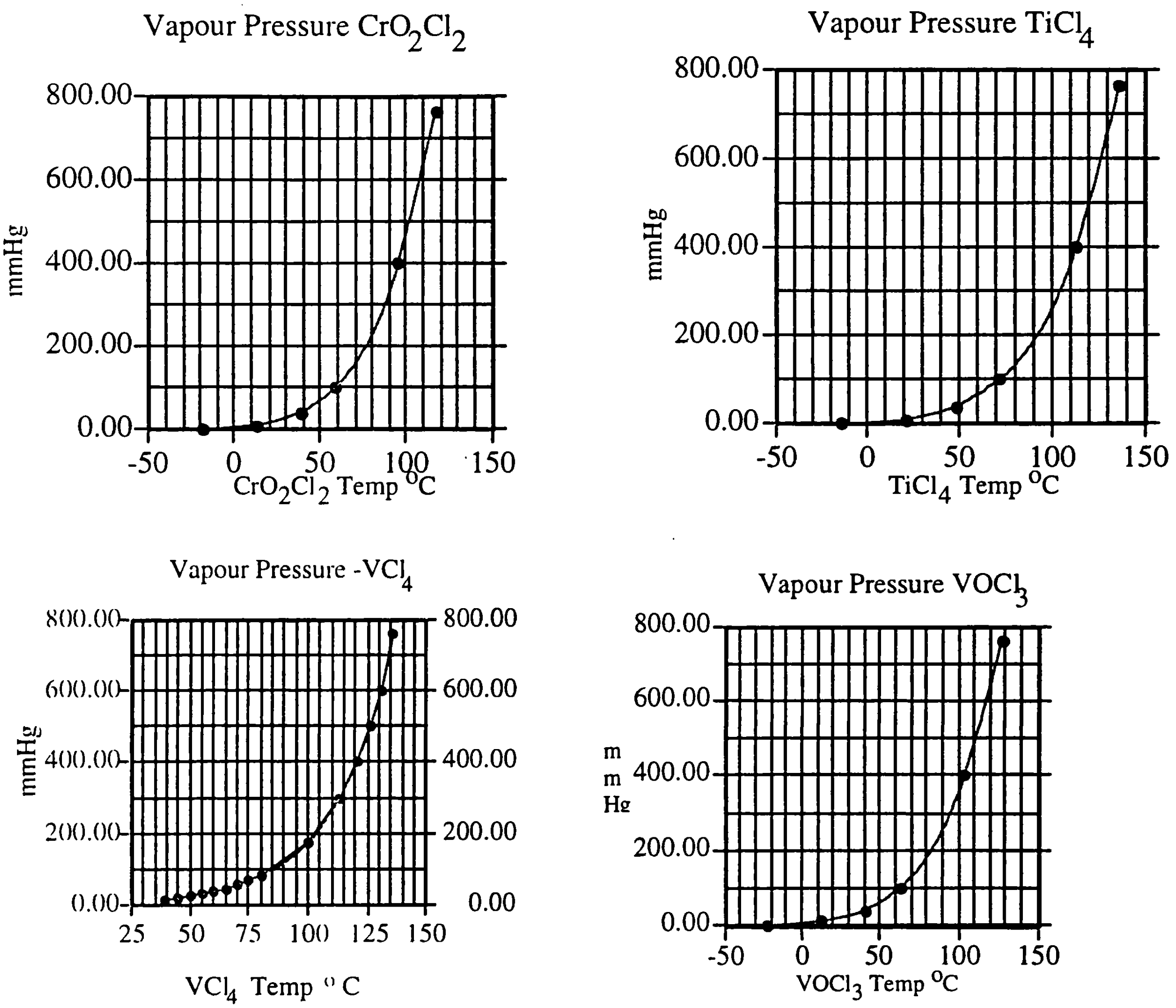

2.3 The pipe framework / mixing chamber

2.31 Initial rig design

Initial design of the pipe framework was intended to fulfil the following criteria: there had to be six separate gas lines, each with a different purpose. These lines were responsible not only for transportation of precursors to the reactor but also to carry enough flow of inert process gas to minimise blockages. The pipework had to be of certain lengths so that the process gas could be heated to an adequate temperature before meeting with the heated precursor vapour. There also had to be shutoff valves and alternative routes so that the reaction start and finish times could be measured accurately. A pipe diagram of the initial pipework plan is shown in figure 2.31a.

Of the six gas lines used in the APCVD rig, five are connected to a pair of nitrogen cylinders and the sixth to an ammonia cylinder. The line connected to the ammonia cylinder is simply known and referred to as the 'NH_3' line. Of the five 'N_2' lines, two are bubbler lines; 'Bubbler 1' and 'Bubbler 2'. This means that they have the option to run through the bubblers after their initial 1.5 metre heat-up period. The two bubbler lines are only able to carry up to 2 dm^3 min^{-1}, of process gas but usually carry ~0.4 dm^3 min^{-1} or less as higher flows can cause the precursor in the bubbler to overflow. The third 'N_2' line is a high flow line, which can accomodate flows of up to 12 dm^3 min^{-1}. Flows of this level are sometimes required in runs where blockages might occur. This line is known as the syringe line as it also has an access point for the addition of a 'dopant' material via a syringe. This means that an initial 1.5 metres of heated pipe is needed before the syringe access, to allow the process gas to heat up. Then a further 1.5 metres of line is needed after the syringe access, all running 'downhill', to insure that the dopant material is able to vaporise before meeting the other precursors in the mixing chamber. In this study the syringe was never used.

The fourth 'N_2' line is known as the 'N_2 / NH_3' line, as it mixes with the 'NH_3' line soon after the ammonia regulator and flow metre. The purpose of this line is to act as a dilutant for the ammonia and to have a 'higher' flow rate to try to prevent blockage further down the pipe (in the mixing chamber). A high flow rate will also prevent back-flow of other gases from the mixing chamber into the ammonia line. Flows of 1 dm^3 min^{-1} or more ammonia were rarely called for, most of the time only 0.5 dm^3 min^{-1} ammonia or less was used. The 'N_2 / NH_3' flow was usually set to around 1.2 dm^3 min^{-1} but was capable of reaching 2 dm^3 min^{-1} maximum

Figure 2.31a Pipe diagram of rig design No. 1

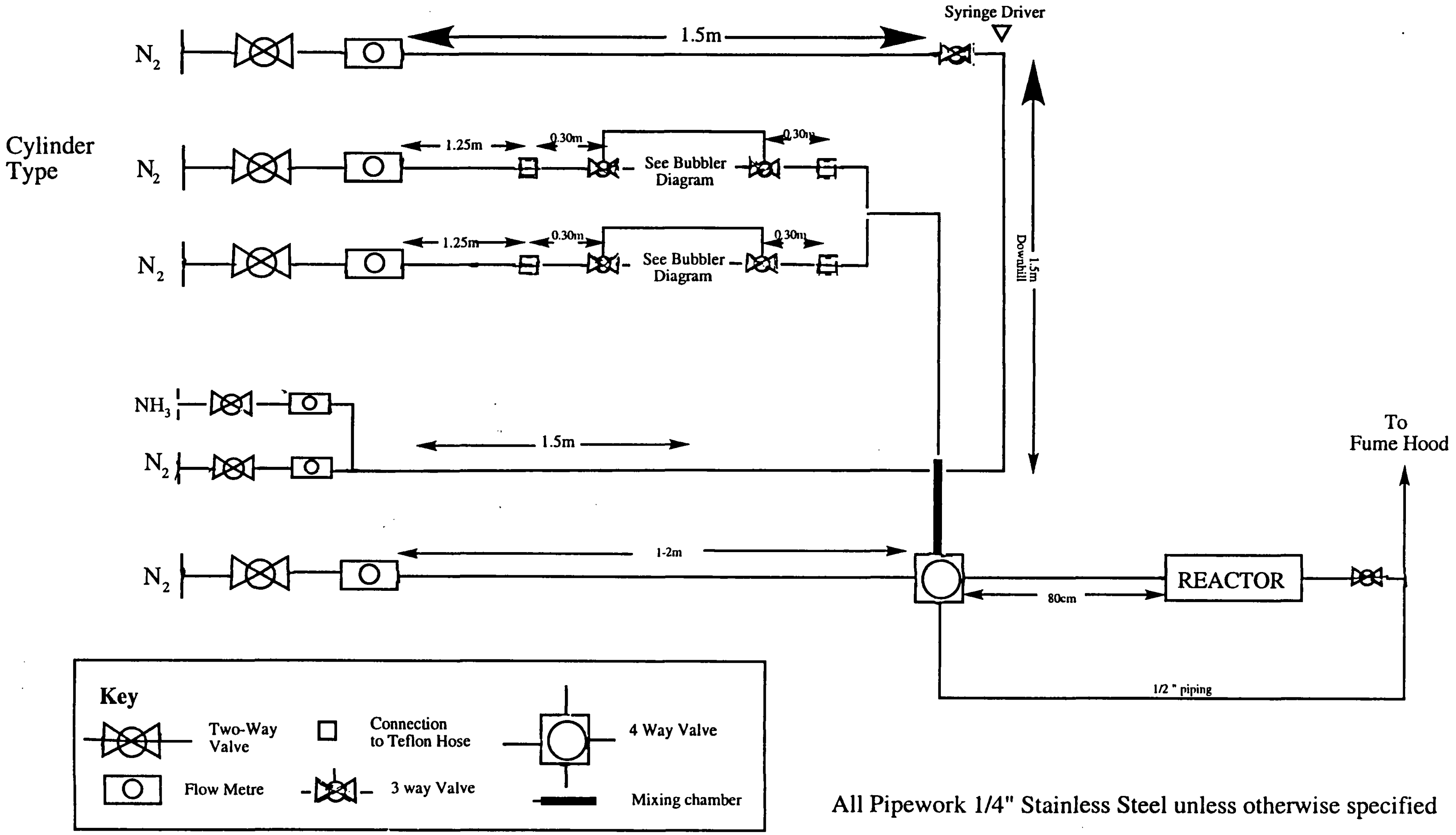

All Pipework 1/4" Stainless Steel unless otherwise specified flow. The final 'N_2' line is known as the 'plain' line, as it carries only nitrogen. It is another high flow line so can handle up to 12 dm^3 min^{-1} of carrier gas flow.

The initial design meant that either the N_2 from the 'plain' line or gases from the other five lines were going through the reactor. This was designed so that nitrogen was always running over the heated substrate. To do this, a four-way valve was added to the pipework about 80 cm from the entrance to the reactor. This allowed N_2 flow from the plain line to be diverted though to the reactor while the substrate was heated to the reaction temperature, as the other five lines all diverted out of the exhaust. When the reaction temperature is obtained the four-way valve is moved anticlockwise through 90 ° and the path of the gases is switched. At the completion of the run the four-way valve can be moved back so nitrogen gas is flowing over the substrate while it is cooling down to room temperature. The action of the four-way valve is represented in figure 2.31b.

Fig. 2.31b Four Way Valve

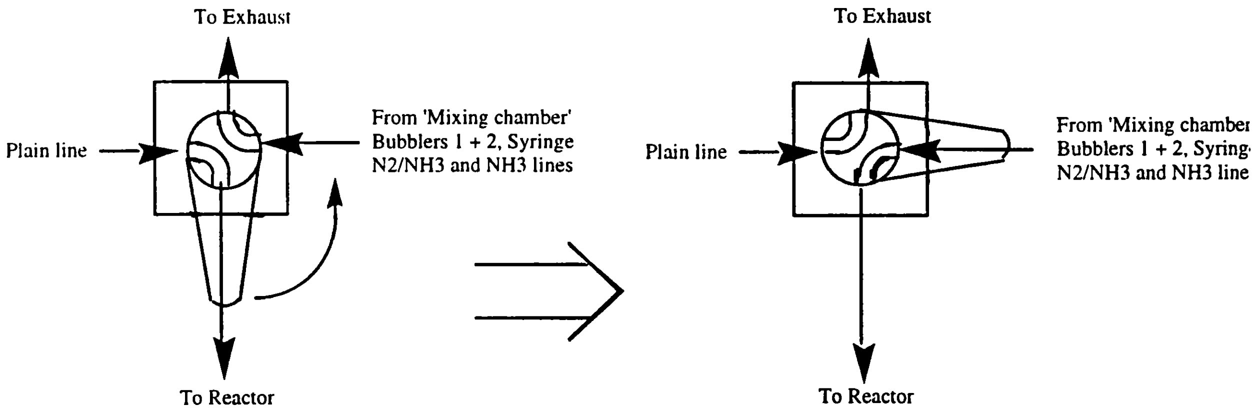

During Substrate Heating

During reaction

This set up allows the precursors to be directed through the coater only when the temperature of the substrate is correct. It also gives control over the time that the precursor gases can flow over the substrate.

2.32 Problems with rig design number 1.

This initial design was soon found to contain some faults that were affecting the quality of the films. The main fault was that blockages occurred in the bubbler pipework and in the mixing chamber. This was put down to the early mixing of the precursors, particularly at the ammonia access point. Additionally, particulate material was building up along the length of pipe leading to the reactor from the four-way valve. It was also found that the plastic material in the four-way valve was chemically and thermally attacked, and in fact, partially melted into the surrounding piping. Some minor changes to the design of the rig were decided upon to rectify these faults.

2.33 Rig design number 2.

The inserts to the four-way valve were removed and in their place some new inserts made from the high melting plastic Vespel were added. To overcome the pre-reaction in the mixing chamber a separate access point for the ammonia (N_2/NH_3 and NH_3 lines), was chosen just before the entrance to the reactor itself. Although pre-reaction is still a problem the part of the pipe-work affected can easily be removed and cleaned with water and acetone following each run. A new pipe diagram for the modified rig is shown in figure 2.33a.

These modifications allowed the original set-up (NH_3 entering previous to the four-way valve) to be used if required by simply opening one valve and closing another. However the new set-up proved successful and the old set-up hasn't been

Figure 2.33a Pipe diagram of rig design No. 2

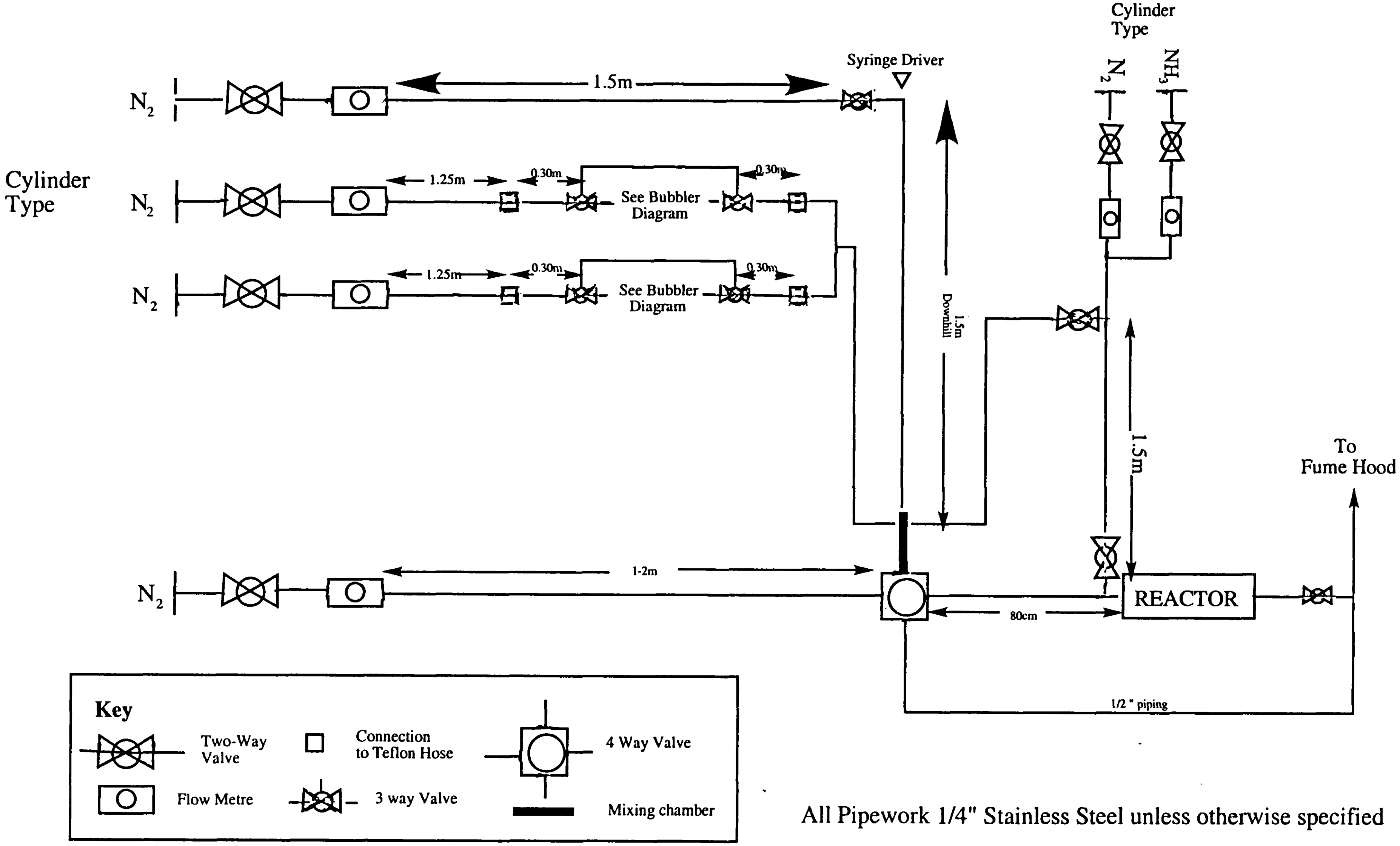

All Pipework 1/4" Stainless Steel unless otherwise specified used since. The Vespel insert, that replaced the previous low melting inserts, have also proved to be a success. They had to be replaced only once during the course of this study.

2.4 The Exhaust

The exhaust line holds a crucial role in the successful running of the rig. It is necessary to aid the transport of by-products and the process gas out of the system in order to avoid particulate build up on the surface of the substrate. The exhaust system has been constructed from ½ inch stainless steel pipework, in an effort to prevent the particulate material formed in the furnace causing blockages in the exhaust. A blockage in this area could cause an explosion of the most vulnerable part of the rig, in the glass tube of the reactor. As can be seen from the exhaust layout a second port was made available so that the system could be connected to a vacuum. The purpose of this was to aid cleaning and to aid the removal of air from the system. Generally this was not used. The exhaust was directed up to the top of the fume cupboard, near to the vent, before the waste was allowed to escape to the atmosphere. The exits to the exhaust had valves added to allow the system to be closed to the atmosphere when it was not in use.

Fig 2.4a Diagram of the exhaust pipework.

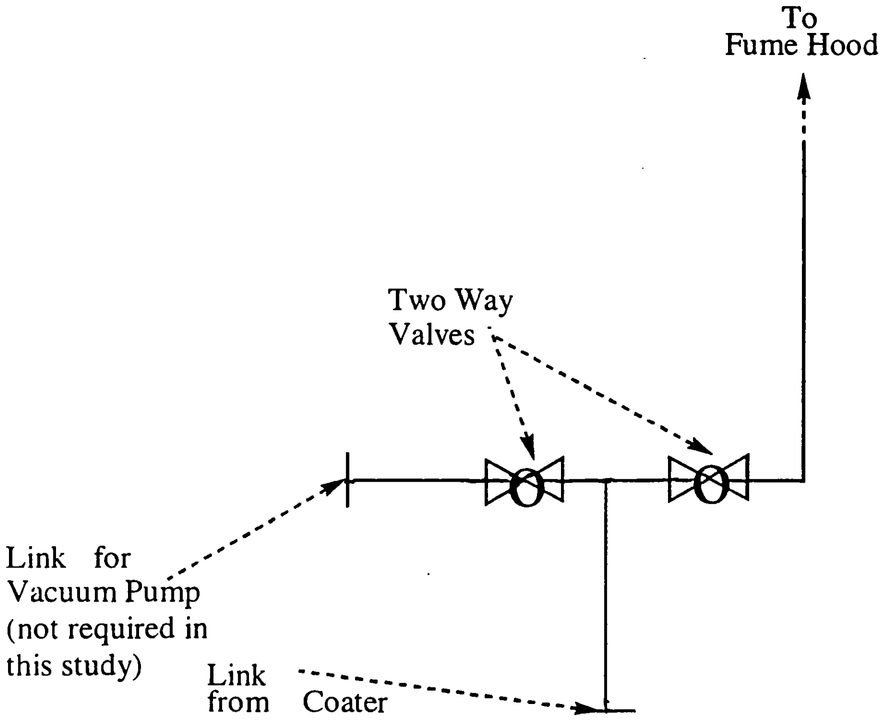

2.5 The control system

It is vital that in a system of this size that there are ways of monitoring the factors that could affect the nature of the films. In the APCVD experiments the temperature of the coater, the temperature of the pipes, the temperature of the precursor and the flow rates of the gases were altered in a systematic way. All of these factors were set, measured and adjusted in the control system part of the rig. A photograph of the control system is shown below.

Fig. 2.5a Photograph of the control system

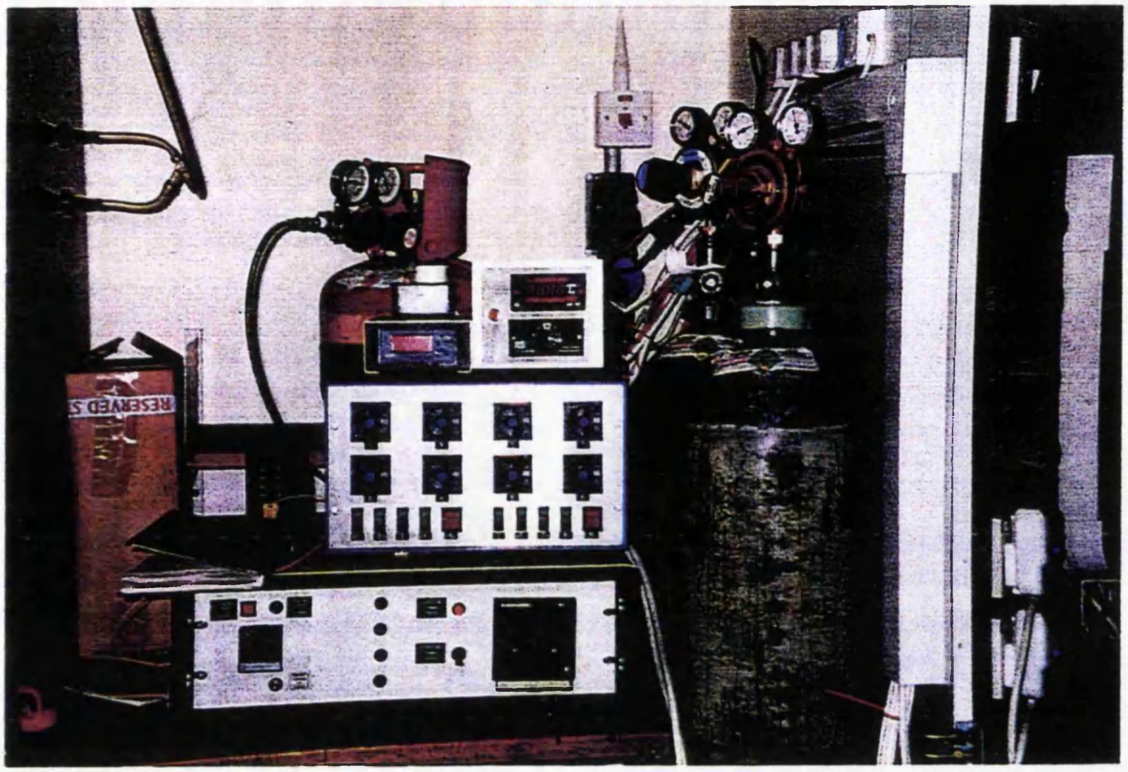

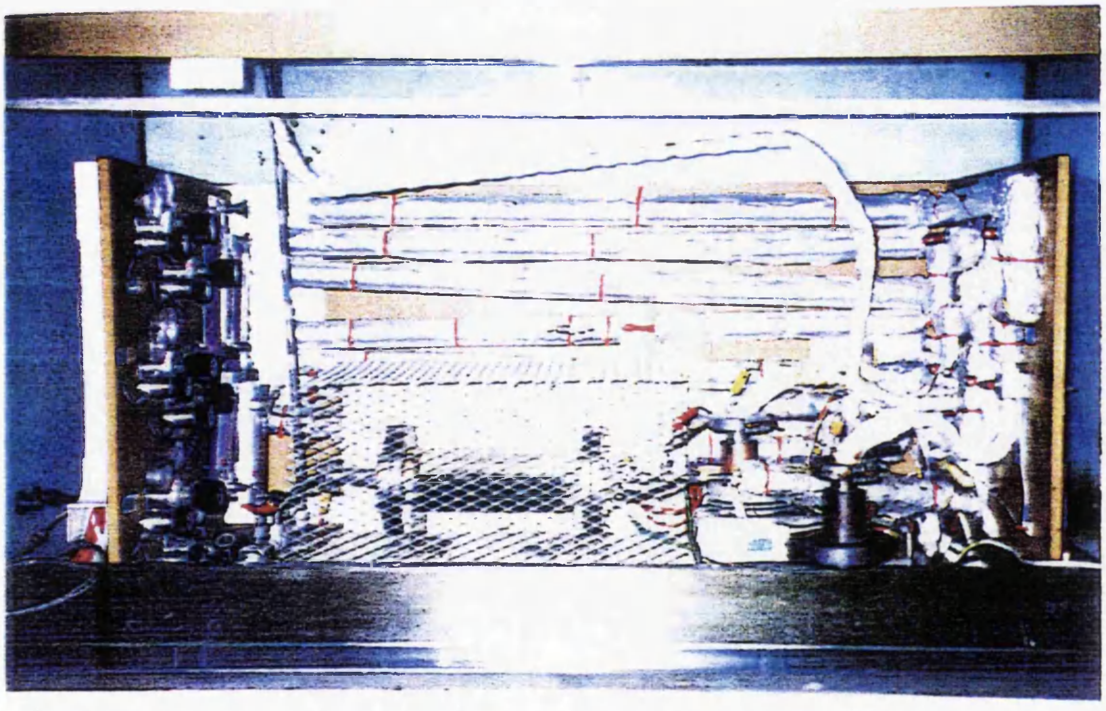

Eight separate heater tapes were used on the rig, each responsible for the heating of a separate length of pipework. These stretches of pipe were numbered one to eight and each had an independent controller. These are displayed in table 2.5b.

Table 2.5b Location of the heater tapes and their jobs.

Heater tape No.	Description	Job
1	Bubbler 1 line	Heat gas before it passes through the bubbler
2	Bubbler 2 line	Same as above
3	Syringe line	Heat process gas before the cross pipe
4	Bubbler1/2 and N_2/NH_3	Heat pipes that contain volatile gases from bubblers
5	Plain Line	Heat process gas in plain line before 4-way
6	Reactor line	Heat pipe from 4-way to entrance of coater
7	4-Way Valve	Keep 4-way valve hot so reactants don't condense
8	Exhaust (from 4 way)	Destroy unreacted reactants before they escape rig

Tape heaters were used to warm the pipes, the temperatures of the pipes were monitored by thermocouples located in certain key areas. Six thermocouples were used. The positions chosen are displayed in table 2.5c.

Table 2.5c Locations of thermocouples for monitoring rig temperatures.

Thermocouple No.	Location
1	Bubbler 1 flexible hose
2	Bubbler 2 valve
3	At cross
4	4-way valve
5	Reactor line
6	Exit point of exhaust gases

In addition to the thermocouples measuring the pipe temperature, there was also a thermocouple for measuring the temperature of the precursor. This thermocouple was located inside the bubbler itself as shown in figure 2.2a. It had the job of not only measuring the precursor temperature but also regulating the power to the hot plate. The temperature was set on the heater and the power was automatically turned off when the thermocouple recorded that the precursor had reached the required temperature. Unfortunately if the temperature of the hotplate was set too high then the temperature of the precursor would often overshoot the set temperature as the hot plate remained hot even though the power to it had been switched off. For this reason the heat up of the precursor had to be done in stages and the temperature allowed to settle, before recommencing the heat up process.

The final piece of equipment in the control system was the reactor control. A special device on this allowed ramping of the temperature at a rate that wouldn't cause damage to the glass. If glass is heated too quickly then cracks can form or the glass can shatter, for this reason the ramp rate of the reactor control was set to 9 °C / min. As already discussed, three cartridge heaters in the graphite block were responsible for the heating of the reactor. There are two thermocouples responsible for regulating the reactor temperature, a cartridge thermocouple and a policeman. The cartridge thermocouple provided the main readout on the controller and it was from this that the ramp rate and power regulation was set. The 'policeman' thermocouple touched the graphite block at the edge and was responsible for making sure that the temperature of the block didn't exceed the temperature set on the control. If the temperature of the block exceeded the temperature set on the policeman then the power to the reactor was cut off. The temperature recorded by this policeman was lower than the temperature recorded by the cartridge thermocouple as the policeman thermocouple had contact with the graphite block rather than the cartridge heater itself. Although the graphite block was an effective heat conductor it was not perfect so some heat was lost. The reactor control also allowed the temperature of the block to be held at a certain temperature for a dwell time before cooling began.

2.6 Comparison with other APCVD rigs

Although atmospheric pressure chemical vapour deposition is relatively common, the rig that has been constructed for this project is quite different to the APCVD rigs that have preceded it. The rig constructed here contains more gas-lines and temperature controllers than typical APCVD apparatus. This sophisticated APCVD rig enables the CVD process to be studied in detail.

Dobkin et al (1990) used an atmospheric pressure continuous belt reactor, for the preparation of tungsten silicide from the reaction of WF_6 and silane or disilane[28]. This sort of preparation has the advantage of offering fast continuous throughput and fast deposition but is pointless for this work where deposition conditions are changed for every run. Dobkin and his co-workers also used two gas precursors, so the need for bubblers and the accompanying complications that this brings were never an issue. Gordon and Hoffman used a similar set up to the reactor used in this work when they carried out APCVD of titanium, zirconium and hafnium nitride thin films[30]. However their rig has only two lines, one which carries the process gas through the bubbler and the other which is responsible for the delivery of the ammonia to the deposition chamber. Extra lines in the rig designed here, limit blockage and also provides a range of extra options, such as the addition of a second precursor through the second bubbler or the potential for dopant addition. Further to this, the use of a plain line and four-way valve in this work means that the length of deposition time can be strictly monitored. The APCVD rig that has been constructed by Mayer for the preparation of tin and fluorine doped indium oxide has 6 separate gas lines and several bubblers but is specific to the preparation of a limited number of materials[94]. Several other APCVD rigs have been described in the literature[29,42,58,95] but none come very close to the specifications for the rig described in this chapter.

The rig constructed for the work in this thesis has many advantages over others described in the literature. The presence of two bubblers gives us the potential to prepare mixed metal coatings, while the number of lines mean that alterations can be made easily to the rig to make it capable of laying virtually any material that can be prepared under atmospheric conditions.

2.7 The future

While this rig has many advantages over the APCVD rigs that have preceded it there is still room for improvement. There are several factors that have been noted over the course of this project that could be upgraded or redesigned to improve the general running and efficiency of the rig. A new rig has been designed and constructed where the problems that have been encountered in this project have been overcome or given a reduced impact by several innovative new design features. None of the work described in this thesis was carried out on the new design, however the author of this thesis designed and oversaw construction of the new rig.

Many problems have been encountered in the apparatus used in this thesis including prereaction which leads to blockages that in turn produce lower quality films with poor conformality and pinhole defects. The reasons attributed as the cause of the blockages are firstly the ¼ inch pipe leading to the entrance to the coater and the T- piece pipe, which means that the ammonia enters the main gas flow at a right angle. To improve on this, the new rig was set up with an ingenious pipe set-up, which saw the ammonia (or second gas precursor), enter the coater flange via a ¼ inch pipe inside a ½ inch. This gave the precursors less chance to mix and react, reducing prereaction considerably.

The second major change to the rig was made at the bubbler. This change was made mainly to make the running of the rig more convenient. In the rig used for this thesis the bubbler is set up with valves followed by the flexible tubes leading to the bubbler. This set up means that the flexible tubes have to be cleaned after each precursor. This is inconvenient and takes a lot of time as the heater tapes have to be undone and the whole bubbler unit taken apart. This set up also means that if a new air sensitive precursor is being added, it has to be added via a syringe in small quantities or poured directly into the bubbler. The new set up has the flexible tubes before the valves as shown in figure 2.7a. With the new set up, the whole unit is small enough to be taken directly into the fume cupboard for addition of a new precursor. This redesign not only saves time but also makes it less likely that the precursor will become contaminated.

Fig 2.7a The new design for the bubbler

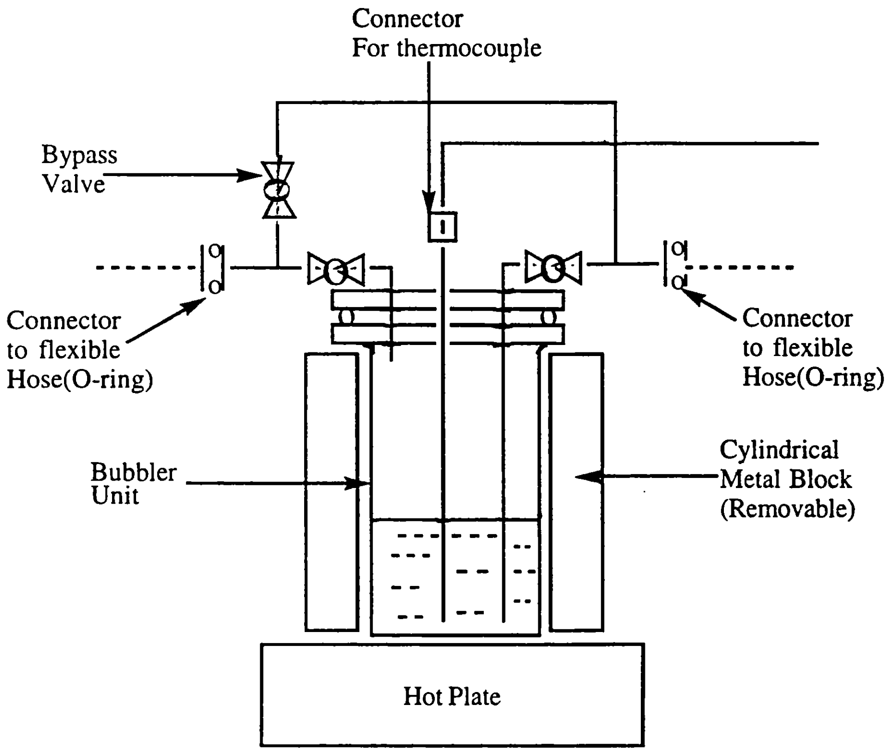

The next change that was made was to the position of the four-way valve. The four-way valve in the current rig is positioned at the back of the rig above the bubbler heaters. This made it hazardous to reach across to operate the four-way to begin a coating. The redesign gave the four-way valve a much more accessible position. The pipe layout of the four-way and surrounding pipework was unchanged.

These changes have been a success with less prereaction and apparently purer films being formed on the new rig.

Chapter 3

Thin Films of Vanadium Nitride

3.1 Experimental details

3.11 Precursor loading

Note: This chapter refers to any film deposited from the reaction of VCl_4 and NH_3 as vanadium nitride (VN). This is despite the films containing notable levels of oxygen.

The liquid precursor, vanadium tetrachloride (Aldrich, 99 %), was used as supplied. It was loaded into the bubbler by transporting it via a syringe from a Sure-seal bottle into the entrance port of the bubbler.

The bubbler was flushed with nitrogen gas (BOC, 99.99 %) for 30 minutes to ensure the absence of air in the vessel. The gas inlet to the bubbler was then closed and the syringe entrance valve opened. The highly reactive VCl_4 was injected as fast as possible into the bubbler via the syringe entrance valve. After addition of VCl_4 this valve was quickly sealed and a small amount of nitrogen gas (0.2 dm^3 min^{-1}) was diverted through the bubbler, (and therefore through the vanadium tetrachloride liquid in the bubbler), for ca. 30 seconds. The gas flow was then redirected through the bubbler bypass. During a typical precursor loading, enough liquid was added to the bubbler to enable approximately 30 deposition experiments (around 30 cm^3 of VCl_4).

3.12 Substrate preparation.

The glass substrates (225 x 89 x 4 mm) were prepared for the APCVD experiments firstly by cleaning with petroleum-ether (60-80 °C), to remove dust and greasy marks and then secondly by rinsing with isopropanol. The glass was then left in an upright position to air-dry prior to use. All contact with the surface of the glass was avoided. The glass substrates were handled by contact with only the edge of the sheets. Once the glass had dried it was visually inspected for marks and if satisfactory was loaded into the coater. This was done so that the precoated side of the glass was facing up and the uncoated side was in contact with the graphite block. The end of the glass was in contact with the step at the entrance to the reactor.

3.13 Final preparation and reaction.

The top sheet of the reactor was reinserted and the reactor reconnected to the exhaust pipework. At this point the heating devices controlling the heater tapes, the graphite block cartridge heaters and the bubbler hotplates were set to their reaction temperatures and heating started. Small flows of nitrogen gas were passed over the substrate and through the pipes during the heating process. Flows of around 1 $dm^3 min^{-1}$ were allowed through each of the high flow nitrogen lines. Flows of 0.5 $dm^3 min^{-1}$ N_2 were put through the bubbler by-pass and N_2/NH_3 line. This helped remove as much air as possible from the pipework and substrate surface and in turn reduce oxygen contamination in the final film.

The coater temperature was ramped up at a rate of approximately 9 °C per minute. This was to avoid cracks in the glass, which may be caused by rapid heating. The bubbler hotplates had no temperature ramp setting, so close monitoring of the precursor temperature was required so that it didn't exceed the required temperature. Failure to do this could lead to the o-ring seal of the bubbler blowing due to excessive pressure. The bubbler temperature set for VCl_4 runs was usually 118 °C (30 °C below the boiling point of VCl_4). This temperature was chosen because it gave sufficient precursor vapour pressure (see fig 2.2b).

Once the temperature of the reactor had stabilised at the deposition temperature, the gas flow rates were raised to the level required for the particular experiment. The ammonia cylinder was opened at this point, if it was required, and the ammonia flow set to the required rate. All the temperatures of the pipes, graphite block and the precursors were noted before the run commenced.

To commence the deposition, the bubbler by-pass valve was closed, the bubbler outlet valve opened and the bubbler inlet valve opened so that nitrogen was allowed to flow through the precursor. The VCl_4 was volatilised into the nitrogen stream at this point. Orange fumes could be seen escaping from the exhaust. To start the run the four-way valve was turned to allow the volatilised VCl_4 to flow through the reaction chamber (rather than being directed through the exhaust). Deposition times were between 20 seconds and 2 minutes.

3.14 Completion of the run and sample preparation for analysis.

The deposition process was halted by initially closing the bubbler inlet and outlet, then reopening the by-pass valve. Finally, the four-way valve was turned back to its original position. The ammonia flow was stopped and the nitrogen gas flow rates reduced to the levels prior to the run. The power to the substrate cartridge heaters, the pipe heaters and the bubbler hot plates was switched off and the rig allowed to cool to room temperature under a flow of nitrogen.

Once the substrate had cooled to room temperature it was removed from the coater, measured with the 4-probe resistance device and assessed visually. The glass was partially cut into approximately 4 cm by 4 cm pieces for glancing angle X-ray diffraction analysis and transmission / reflectance measurements. Some smaller pieces (approximately 1 cm x 1 cm or smaller) were also prepared for SEM and XPS analysis. The procedure for XPS analysis is fairly complex, and is discussed in section 3.2. The remainder of the coated substrate was labelled and stored in air.

Following a run, the rig was cleaned in several key areas, which tended to get the highest build up of powdery by-products. If these areas were not cleared each time then blockages would occur in the following run. The insides of the cold wall reactor and top plate in particular were often covered in a white powdery deposit following a run due to the reaction of co-produced HCl with NH_3 which formed NH_4Cl. The top plate and the inside of the glass tube of the reactor were cleaned by wiping them with a damp cloth followed by a wipe with acetone. The reactor entrance flange and T-piece where ammonia first mixes with the precursor often attracted large deposits of amorphous material during a run. These parts were unscrewed from the rig and washed with water and acetone. They were dried by attaching to an air source and finally left in an oven to dry before being reconnected to the rig. The final area that was found to be a recipient of solid deposit was the coater exhaust pipework. This unit was removed from the rig and connected to an air source to blow the solid out onto a damp cloth. If the next run used the same precursors then this cleaning procedure was usually enough. However, if the next run was to involve a new precursor then a more thorough cleaning procedure was required to ensure that the following runs were not contaminated with precursors from the previous runs.

The unused VCl_4 contained in the bubbler was destroyed at the end of the VN deposition experiments. This was achieved by slowly adding the unused material to isopropanol followed by the dropwise addition of water, (vanadium tetrachloride reacts vigorously with water). The bubbler was then rinsed with copious amounts of water and detergent and cleaned with an abrasive brush. Next, the heater tape and insulating tape were unwound from the flexible Teflon tubing leading to and from the bubbler. The flexible tubes were disconnected from the rig and cleaned thoroughly using water, detergent, pipe cleaners and acetone. The tubes were dried in an oven. If these tubes were not cleaned then cross-contamination of the precursors could occur. Finally, once all the pipes were clean and dry, the bubbler section was rebuilt and flushed with nitrogen to prepare it for the addition of a new precursor.

The purpose of the work in this chapter is to investigate the preparation of vanadium nitride films from the reaction of VCl_4 and ammonia. It concentrates on the effects of varying the reaction conditions on the composition and structures of the films.

XRD, SEM, electron microprobe, XPS and transmission / reflectance analysis were carried out on the films. XRD analysis was carried out on a Philips X-pert diffractometer using unfiltered CuKα (λ_1 = 1.5405 Å, λ_2 =1.5443 Å) radiation in the reflection mode using a glancing incident angle of 1.5 °. Samples were indexed using Unitcell (35-768) and compared with database standards. The crystallite size was estimated using the broadening of the (2 0 0) reflection using the Scherrer equation and ignored any contributions from lattice strain. SEM was obtained on a Hitachi S570 instrument using the KEVEX system. Electron microprobe analysis was carried out on a JEOL EMA instrument and referenced to a polished vanadium standard. XPS experimental information is described in section 3.2.

3.2 XPS analysis

X-ray Photoelectron Spectrometry (XPS) allows the investigation of a small (100 μm) part of the film surface, to reveal information on composition and oxidation state.

3.21 Experimental

XPS spectra were recorded with a VG ESCALAB 220I XL instrument using a focused 300 μm x 300 μm spot.

Sample pieces, approximately 1 cm x 1 cm, were broken from the substrate and brought *via* a sample tube to the XPS apparatus. A sample holder had to be designed and built specifically for the glass samples as typical samples for XPS are pressed powders or crystallites that can be stuck directly onto a conductive pad on the sample holder. A conductive link between the sample and the sample holder / instrument is required to distribute the charge build-up which can occur during XPS analysis. The new sample holder consisted of a stainless steel bridge, which had the dual purposes of holding the sample in place and linking the film to the instrument. Without this link, bombarding the film with X-rays to excite electrons away from the film leads to positive charge build-up on the surface and loss of chemical shift information. Charge could not be neutralised, as the glass upon which the film is deposited is non-conductive. Using an electron flood gun to neutralise the charge does help to an extent, but without the conductive link to Earth, charge build up is a major problem

To get the sample into the analysis chamber (held at $\sim 10^{-10}$ torr), the sample holder and sample were mounted on an extendable arm in a smaller anti-chamber, that could be quickly evacuated down to $\sim 10^{-4}$ Torr. Access could not be gained to the analysis chamber until the vacuum in the anti-chamber was sufficient to restrict contamination. Once the sample was in position, the initial analysis could take place. Monochromatic AlKα radiation was used at a pass energy of 20 eV. Scans were acquired with steps of 50 meV. A flood gun was used to control charging and the binding energies were referenced to an adventitious C 1s peak at 284.8 eV.

Depth profile measurements were obtained using argon sputtering. During the use of the ion gun the chamber pressure was brought up to $\sim 2 \times 10^{-7}$ torr and an additional ion pump used to aid the removal of argon gas and help maintain the vacuum. Once analysis was complete the sample was removed via the smaller port and the vacuum restored to 10^{-10} torr before analysis of a new sample.

3.22 Interpretation of results and theory.

All APCVD films in this study were exposed to air prior to their analysis by XPS. The films collected carbon dioxide and other contaminants on the surface. Because XPS is a purely surface technique (top ten atomic layers interrogated), these contaminants show up and affect the composition analysis of the films. An XPS spectrum of the surface of a representative vanadium nitride film formed in this study is shown in figure 3.22a with a composition analysis in table 3.22b.

Figure 3.22a XPS elemental scan from surface (prior to ion gun use).

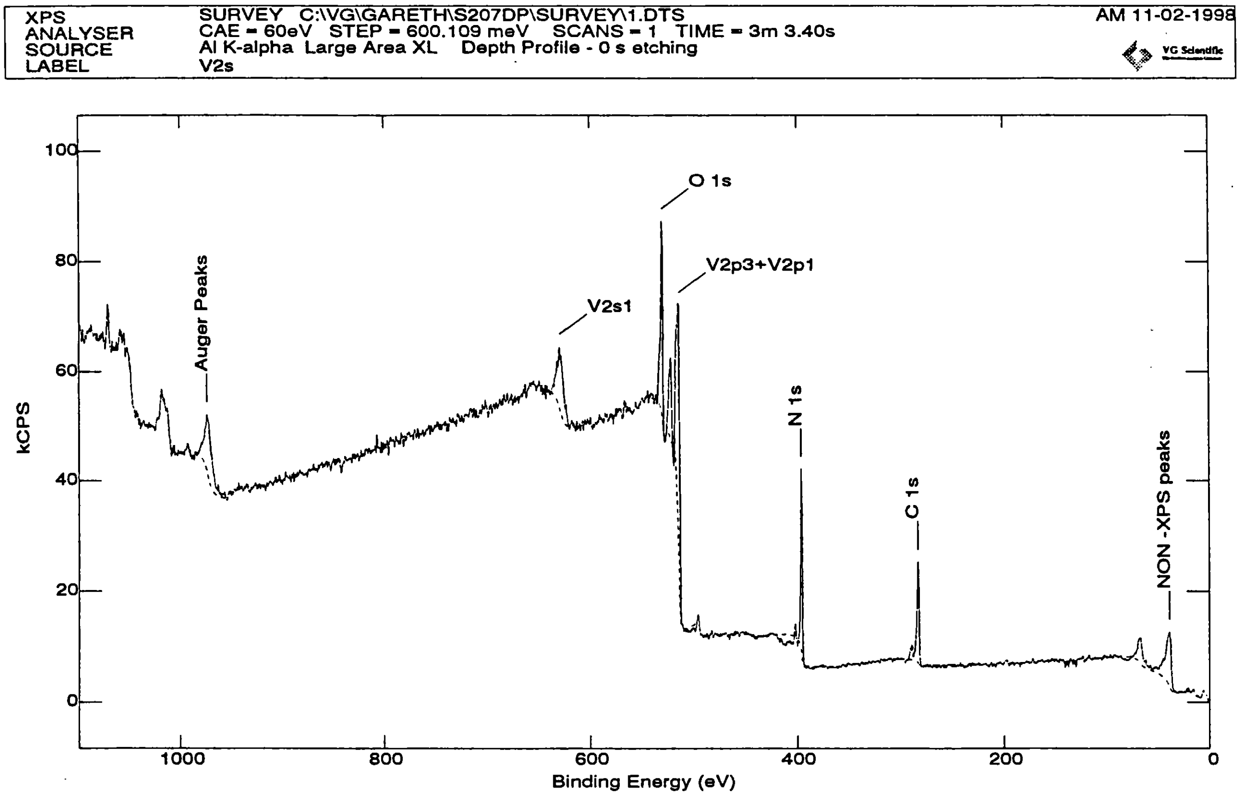

Table 3.22b Composition calculated from figure 3.22a XPS scan.

Element	Chemical Shift (eV)	Elemental % present in bulk
Vanadium	513.71 + 515.8	24.6
Oxygen	529.57 + 531.77	25.5
Nitrogen	396.59 + 398.54	26.4
Carbon	284.25 + 286.27	24.5
Chlorine	-	0

The compositional analysis from XPS enabled a determination of the percentage elemental abundance in the film. This was obtained by integrating the area under each of the XPS peaks and applying a significance factor for each element. The XPS was calibrated against internal machine standards and specific metal nitrides ($TiN_{1.0}$ and $VN_{1.0}$, Alpha Chemicals).

The chemical shift values in table 3.22b are consistent with the values expected from a highly contaminated metal oxynitride surface with absorbed carbon dioxide and elemental carbon (from the high vacuum pumps). For all the elements described two peaks were observed, one due to elements in the bulk material and the other due to oxidised elements on the top most surface layers.

To overcome this problem with XPS compositional information, an argon sputtering gun was used to effectively strip off the films' surface, layer by layer, until the composition measured was self-consistent and the composition of the bulk revealed. The argon sputtering gun that was used wasn't particularly powerful, removing only a few nanometers on each etching. A depth profile, showing how the composition of a representative sample prepared from VCl_4 and NH_3 changed after around 45 minutes of etching is shown in figure 3.22c.

Figure 3.22c Depth profile showing composition change after 45 minutes of etching.

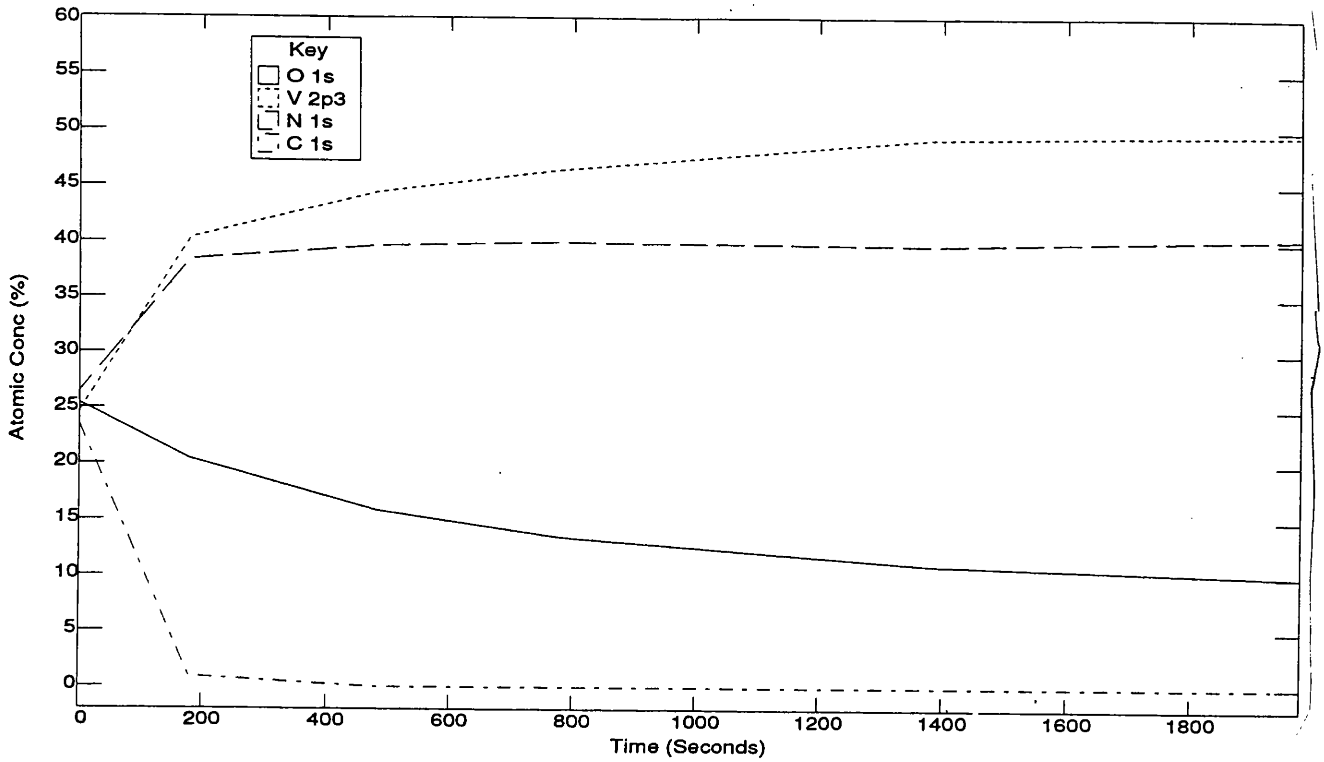

Another feature of XPS is that the binding energies of electrons change depending on which atom they come from, and the local chemical environment of that atom. For example, an electron ejected from surface bound oxygen will have a different environment and hence binding energy to an electron emitted from an oxygen atom in the bulk. The largest shifts in binding energy are due to changes in oxidation state of the element in question. A $2p^3$ electron from a vanadium atom will be slightly harder to remove if the vanadium has a +5 oxidation state (VON) than if it has a +3 (VN) or zero (vanadium metal) oxidation state, due to the electrostatic force. Photoelectrons from atoms in a more electropositive state are emitted with less kinetic energy (and therefore have greater binding energy) and vice-versa for atoms which are more electronegative. Because the kinetic energy ($\frac{1}{2}mv^2$) and frequency (ν) of an excited electron can be measured, binding energies can be calculated by Einstein's equation (equ. 3.2a)

$$h\nu = \text{Binding Energy} + \tfrac{1}{2} mv^2 \qquad \text{(equ. 3.2a)}$$

Oxidation states, and even specific environments (eg whether the carbon is bound to oxygen), may be determined by comparing the binding energy of the peak with known binding energies, obtained from standards. An example of how the binding energy can change is shown in figure 3.22d.

Figure 3.22d XPS chemical shift showing change in vanadium peak position and intensity at various stages of etching

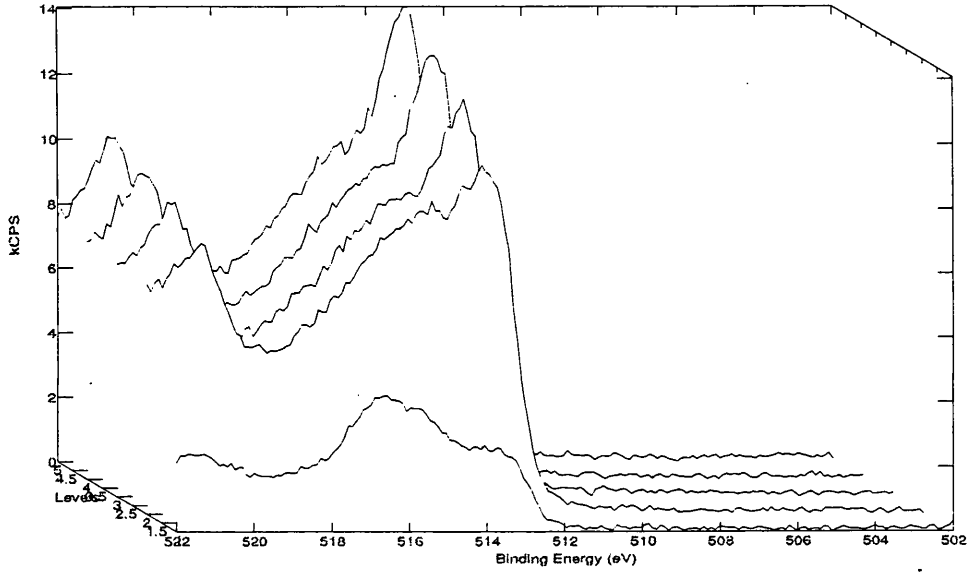

In the example given the peak in the background is due to a surface bound vanadium. As the surface is etched away by the argon ion gun the vanadium peak shifts to the right as its binding energy changes. In the foreground, the peaks are due to vanadium atoms in the bulk which are bound to nitrogen and oxygen.

Once the composition of the film has levelled off in a consistent manner, a final scan of the whole XPS range can take place. The final scan for a film prepared from VCl_4 and NH_3 (fig. 3.2e) and the resultant composition (fig. 3.2f) are shown below. It can be seen from this plot that there are no elements present other than vanadium, nitrogen, small amounts of oxygen and trace amounts of carbon and chlorine.

Figure 3.22e XPS scan of a VN film, following 45 minutes of ion gun use.

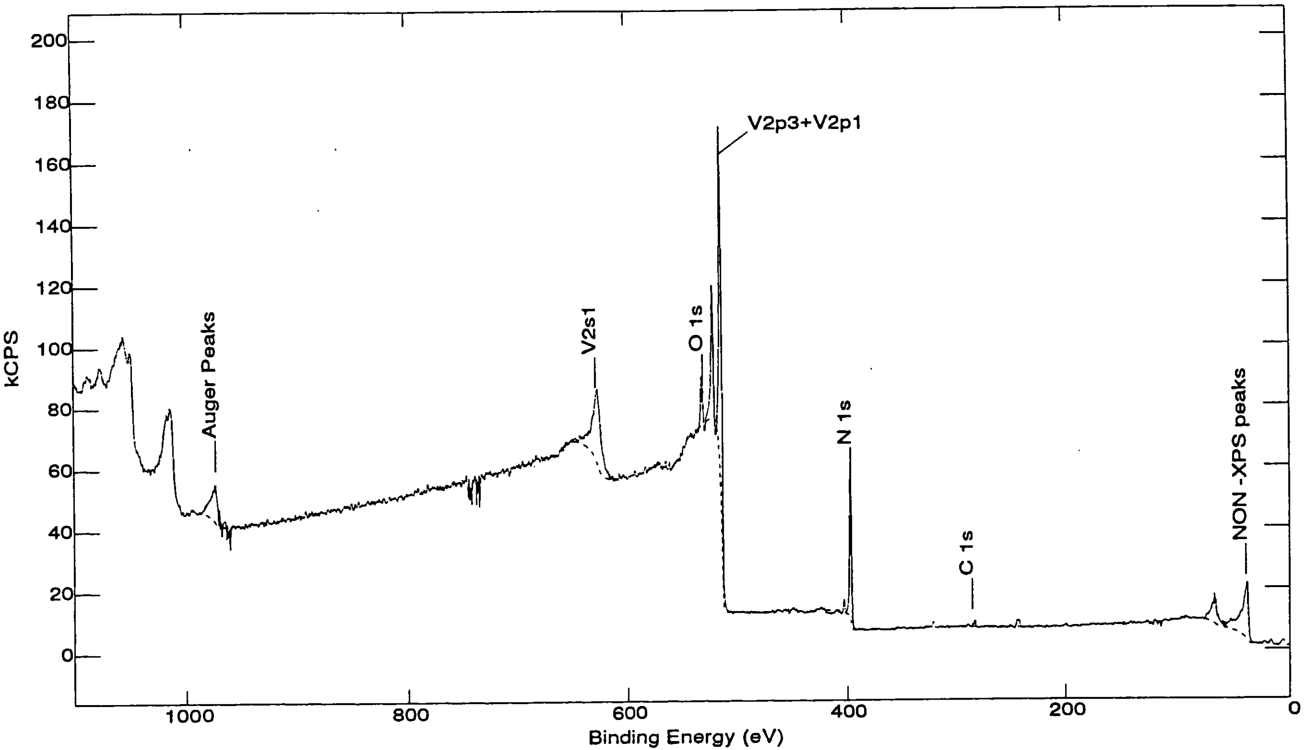

Figure 3.2f Composition calculated from figure 3.22e scan.

Element	Chemical Shift (eV)	Elemental % present in bulk
Vanadium	513.06	49.6
Nitrogen	397.08	40.40
Oxygen	530.78	9.99
Carbon	-	0
Chlorine	-	0

An XPS chemical shift of 513 eV is half way between the expected result for vanadium metal (512.14 eV) and vanadium nitride (514.3 eV). The chemical shift of 515.8 eV observed for vanadium on the surface is typical of vanadium in a high oxidation state such as V_2O_5 (517.65 eV). The XPS values observed for nitrogen and oxygen atoms in the bulk material are both consistent with the XPS chemical shifts expected for a transition metal nitride (396.8 - 398 eV) and oxide (529.5 – 531.3 eV).

3.3 Effect of coater temperature

The first study to be carried out on all the precursor systems was to obtain films at a variety of temperatures to see how the temperature of the coater affected the composition and properties of the film. The deposition temperature has often been found to be the most important variable when forming a film. At too low a coater temperature, reaction of the precursors may not occur and they will be released, unchanged, from the exhaust. In some cases, crystallinity is an important feature required in heat mirror films. Crystallinity may not be observed at lower substrate temperatures, while higher temperatures can encourage impurity incorporation. For a thin film route to be considered useful, the reaction must occur favourably in between these two temperature boundaries. For the commercial float-glass process, the viable substrate temperature range is between 300 °C and 650 °C, with an optimum temperature of 550 °C for the easy addition of any process to the currently-used plant.

For this study, four samples were prepared at temperatures of 350, 450, 550 and 650 °C. The experimental conditions used in this study are detailed in table 3.3a.

Table 3.3a Conditions for preparation of VN_x films in coater temperature variation study.

Variable	Level fixed at
Bubbler Temp.	117 °C
Time of Run	30 secs
Flow through bubbler	0.42 $dm^3\ min^{-1}$
Process flow	5 $dm^3\ min^{-1}$

NH_3 Flow	0.5 dm^3 min^{-1}
N_2/NH_3 flow	1.2 dm^3 min^{-1}

Using the equations in section 2.2, it can be seen that these experimental conditions deliver 0.0074 moles of VCl_4 and 0.0103 moles of ammonia to the reactor during the course of the deposition. From the idealised equation in section 1.5 it can be seen that 6 moles of VCl_4 react with 8 moles of ammonia. So 0.0098 moles of NH_3 would be needed to react with 0.0074 moles of VCl_4. The ammonia was used in excess for this experiment. This was undertaken as stoichiometric VN films were desired, rather than films that had nitrogen vacancies that could be filled by carbon or oxygen contaminants.

Initial assessment of the film quality was carried out by visual inspection. This inspection revealed that the films had uniform coverage over the whole substrate at 350 °C while at 650 °C the progression of the film across the glass was only about 4 cm. This suggests that the reaction occurs much faster at hotter substrate temperatures. All the films are black or grey and most are reflective. The darkness and degree of optical reflection of the films increased with substrate temperature. This can be explained by an increase in film thickness with temperature. It appears that as the substrate temperature increases, the film is progressively formed at the earliest moment the precursors reach the substrate (transport limited regime). This is not really an issue for an industrial process as the substrate would be on a moving conveyor. More particulate build-up is registered in the entrance flange and in the exhaust pipework at higher substrate temperatures.

From the graphs below it can be shown that the deposition temperature shows the highest percentage of vanadium in the film for runs at 450 °C while the oxygen contamination is highest at 350 °C and is at a minimum when the temperature is 450 °C. Nitrogen and carbon incorporation in the films increase with temperature. The carbon contamination is probably due to impurities in the substrate or possibly from the precursors or process gas. Carbon could also be present due to exposure of the film to air following deposition, although usually this type of carbon contamination is surface limited and completely removed by depth profiling.

Figure 3.3b Changes in elemental composition in VN_x films prepared with varying coater temperature (0.42 dm^3 min^{-1} VCl_4 with 0.5 dm^3 min^{-1} NH_3 and 5 dm^3 min^{-1} process gas flow).

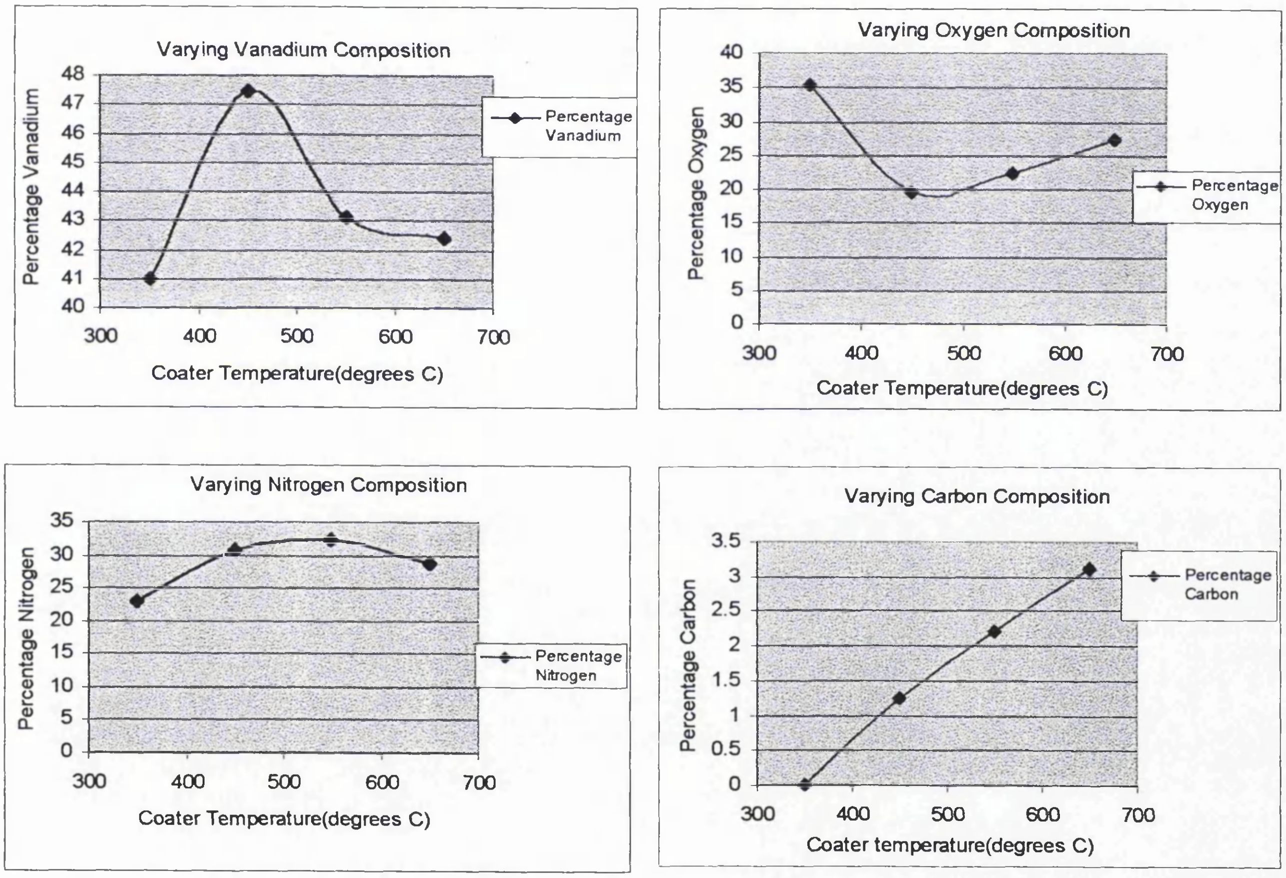

The chemical shifts for vanadium fall at 513.4 eV for the film deposited at 350 °C and are 513.0 eV for the films deposited at higher temperatures. This shows how the higher oxygen contamination in the film deposited at 350 °C has affected the oxidation state of the vanadium. A vanadium chemical shift of around 513 eV is expected for vanadium nitride. Surface vanadium peaks are observed at around 516.8 eV, which can be characterised as highly oxidised states of vanadium such as V_2O_5 (vanadium chemical shift of 517.6 eV). The results in figure 3.3b suggest that at lower substrate temperatures amorphous films are produced which are porous and susceptible to oxygen damage while at higher temperatures, contaminants (eg carbon) are possibly coming up from the substrate. Another source for carbon contamination could be from the nitrogen process gas, as this would cause the contamination to be spread throughout the bulk of the film. Further evidence of this is the higher carbon incorporation with temperature.

Four-probe resistance measurements are a way of assessing the conductivity of the film. The four-probe measurement is related to the resistance and thickness of the film. A four-probe measurement alone provides only an approximation of the sheet resistance. Even so, four-probe measurement is useful as it provides a rough idea of crystallinity (crystalline films tend to be more conductive) and where a thickness is known, the resistance can be determined.

A chart of the four-probe measurements of the films produced from VCl_4 and NH_3 in the temperature range 350 – 650 °C is shown in table 3.3c.

Table 3.3c Four-probe measurements for films grown at different coater temperatures (0.42 $dm^3\ min^{-1}$ VCl_4 with 0.5 $dm^3\ min^{-1}$ NH_3 and 5 $dm^3\ min^{-1}$ process gas flow).

Temperature (°C)	Four-Probe Reading (Ω /□)
350	2450
450	80
550	61
650	178

These results show that although the thickness is not known accurately, the resistance is highest at 350 °C. With increasing substrate temperature, it then drops and stays approximately constant for the films obtained at 450 and 550 °C, then rises for the film deposited at 650 °C. The high resistance measurement for the film obtained at 650 °C could be due to carbon contaminants, which appear in the film at higher temperatures.

Scanning electron micrographs provide information on the film grain sizes. The grain sizes appear to increase with substrate temperature. This could be due to faster film growth rates at higher substrate temperatures.

X-Ray Diffraction measurements give an indication of the crystallinity of the samples. The diffraction patterns are consistent with those expected for vanadium nitride. Further conclusions on the crystallite sizes and composition (from the lattice parameter) can be drawn from peak indexing and evaluating peak size and position. Oxygen contamination will shift the peaks, so altering the lattice parameter. Like four-probe resistance measurements, XRD patterns are affected by the thickness of the sample. By using a glancing incident X-ray angle, the radiation will skim through the film, rather than flooding straight through the amorphous glass. The large hump that appears below 35° on the $2\ \theta$ scale is due to the amorphous glass that does register. A glancing angle of 1.5° will investigate the 300 nm closest to the surface, so if the film is thinner than that, the amorphous glass will have a presence in the spectrum. Films become more crystalline with increasing temperature. This is shown in fig 3.3d.

Fig 3.3d Glancing angle XRD patterns of vanadium nitride films with varying coater temperature (0.42 $dm^3\ min^{-1}$ VCl_4 with 0.5 $dm^3\ min^{-1}$ NH_3 and 5 $dm^3\ min^{-1}$ process gas flow)

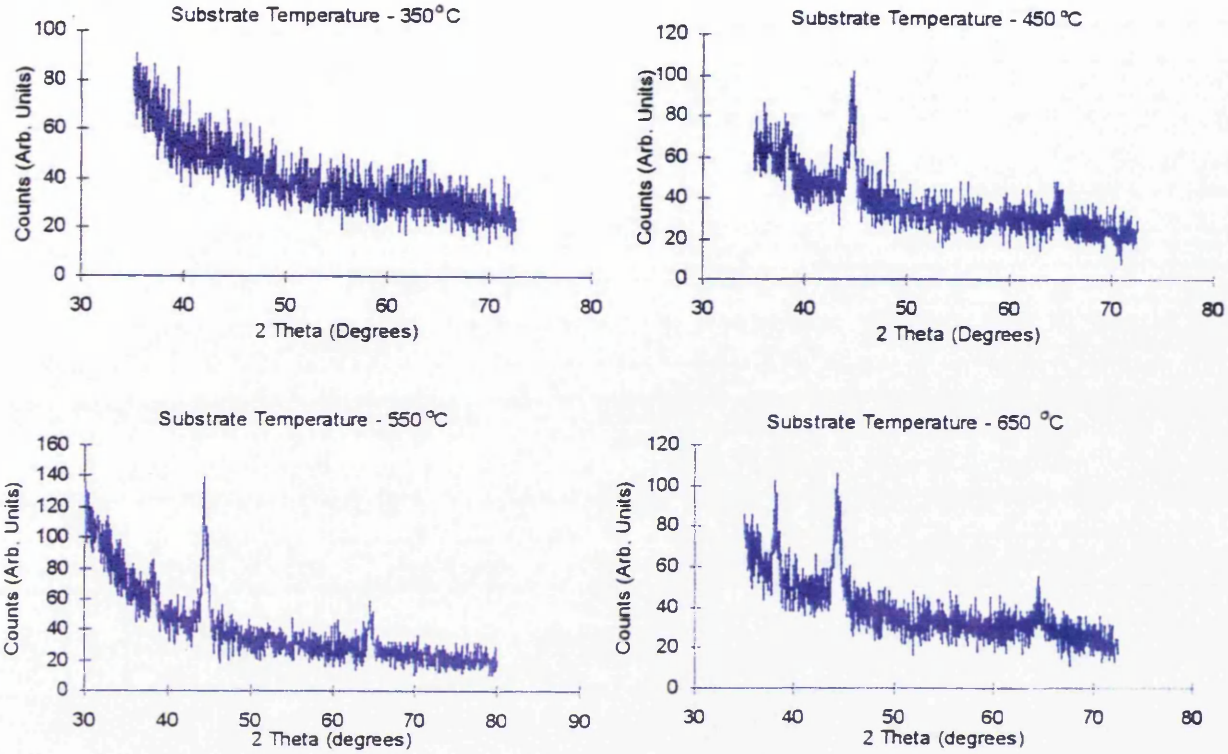

These peaks have been indexed. In all the above cases, other than the almost completely amorphous film deposited at 350 °C, peaks appear due to reflections in the (1 1 1), (2 0 0) and (2 2 0) planes. The X-ray patterns are consistant with a cubic crystal pattern. Further investigation of the indexed peaks can give information on stoichiometry (from Vegards' Law)[96] and crystallite size (from the Scherrer equation)[54].

Table 3.3e Lattice parameter from XRD indexing of spectra in fig. 3.3d with compositional and crystallite size information.

Deposition temperature	Lattice parameter *a* (Å)	Crystallite size Å	N/V ratio from XRD	N/V ratio from XPS
350	-	-	-	0.56 / 1
450	4.072	171	0.70 / 1	0.64 / 1
550	4.078	193	0.77 / 1	0.75 / 1
650	4.088	199	0.80 / 1	0.70 / 1

Discussion by Goldsmidt *et al*[96] has determined that a N/V ratio can be evaluated from the indexing of the peaks and use of Vegards' Law. The figures in table 3.3e show that the ratio of the nitrogen to vanadium estimated from XRD is fairly close to that calculated by XPS, the exception being the film deposited at 650 °C which was calculated to have a higher N/V ratio by XRD than was shown by XPS. This result is despite the belief that oxygen and carbon can also be located in the same interstitial sites. It appears that it is the proportion of nitrogen that shifts the reflections to the greatest extent. The difference between the XPS and XRD measurements could easily be due to the small detection area used by XPS, which limits the sample size to 300 by 300 microns area. For this reason, no definite conclusions on the composition of the film can be made from the XRD lattice parameter. The crystallite sizes are calculated from the width of the (2 0 0) peak at half height. These results show that the grains seen by SEM are in fact made up of many smaller crystallites. The crystallite size does appear to rise consistently with deposition temperature.

The final measurement that will be mentioned in this section is the transmission and reflectance measurements on the film. These measurements show that a rise in substrate temperature has a dramatic affect on the way the film performs as a heat-control mirror. As can be seen in the spectra in fig. 3.3f, at 350 °C there appears to be only minimal heat mirror qualities. All the other temperatures show some heat mirror characteristics as determined by the similarity to the spectra in fig 1.6b in chapter 1. The difference between them is only the degree of IR reflectance and visual transmission, which should, ideally, be as large as possible. The best IR reflectance is in the film produced at 550 °C. The best visual transmission occurs for the film grown at 350 °C, however this film shows no reflectivity properties. For a useful heat-control mirror a combination of good visible region transmission and IR reflectance are required. One or the other on its own is of no use. For this reason, the best overall selection of heat mirror properties is seen in the film deposited at 650 °C as this seems to give a good mix of IR reflectance and visual transmission.

Fig. 3.3f Transmission and reflectance data for VN films deposited with varying coater temperature (0.42 dm^3 min^{-1} VCl$_4$ with 0.5 dm^3 min^{-1} NH$_3$ and 5 dm^3 min^{-1} process gas flow).

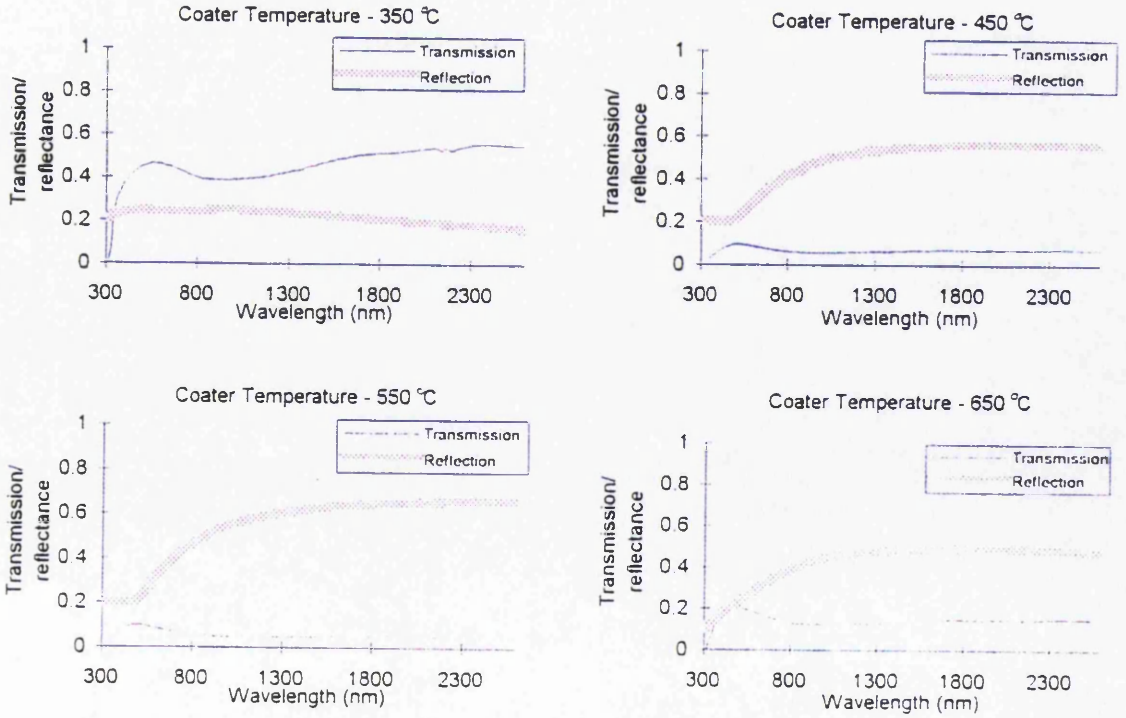

3.4 Effect of ammonia gas flow concentration

Varying the ammonia concentration during deposition affects the composition of the VN film. At high flows of ammonia, it would be expected that the atomic percentage of nitrogen in the film would increase. Again, as with the coater temperature experiments, there appears to be two limits between which the ammonia concentration should be set. Below the lower limit, the required film is not produced. Above the higher level the ammonia is in excess and excessive prereaction means that the build-up of particulate material affects the conformality of the film. Particulate formation from the prereaction is pushed by the gas flow on to the surface of the substrate which can then affect the future film growth (blotchy films are obtained).

No coating was produced without a flow of ammonia.. Runs were carried out under the conditions detailed in table 3.4a. During this study the ammonia flow was varied from 0 dm^3 min^{-1} to 1 dm^3 min^{-1} at intervals of 0.1 dm^3 min^{-1} and one run which was carried out at 2 dm^3 min^{-1}.

Table 3.4a Conditions for ammonia variation study for VN_x films.

Variable	Level fixed at
Coater temp.	500 °C
Bubbler Temp.	117 °C
Time of Run	30secs
Flow through Bubbler	0.42 dm^3 min^{-1}
Process flow	10 dm^3 min^{-1}
N_2/NH_3 flow	1.2 dm^3 min^{-1}

Using the equations in section 1.5 it can be shown that under model conditions 0.0098 moles of ammonia are required to react with 0.00735 moles of VCl_4 to form VN. An ammonia flow of 0.1 dm^3 min^{-1} represents 0.00205 moles. Once the flow of ammonia is 0.5 dm^3 min^{-1} or more, the ammonia is in excess. A flow of 2 dm^3 min^{-1} ammonia represents 0.041 moles. It should be noted that VCl_4 does not react in the deposition chamber in the absence of ammonia so at low ammonia flow rates a thin or patchy film formed. The thickness of the films as determined by SEM are constant for the depositions employing an ammonia flow of above 0.5 dm^3 min^{-1}. All the films produced with variable flows of NH_3 were grey / black and reflective.

The XPS profiles of VN films prepared with different flow rates of ammonia are shown in figure 3.4b. These measurements show that increasing the ammonia flow rate leads to an increase in nitrogen and vanadium concentrations in the films, and also a decrease in the atomic percentage of oxygen. Ammonia helps to inhibit oxygen incorporation in the film. Carbon contamination also appears to drop with ammonia flow rate, although this could not be assessed accurately.

Figure 3.4b Change in elemental composition with changing ammonia flow, from XPS (0.42 dm^3 min^{-1} VCl_4 at 500 °C and 10 dm^3 min^{-1} process gas flow)

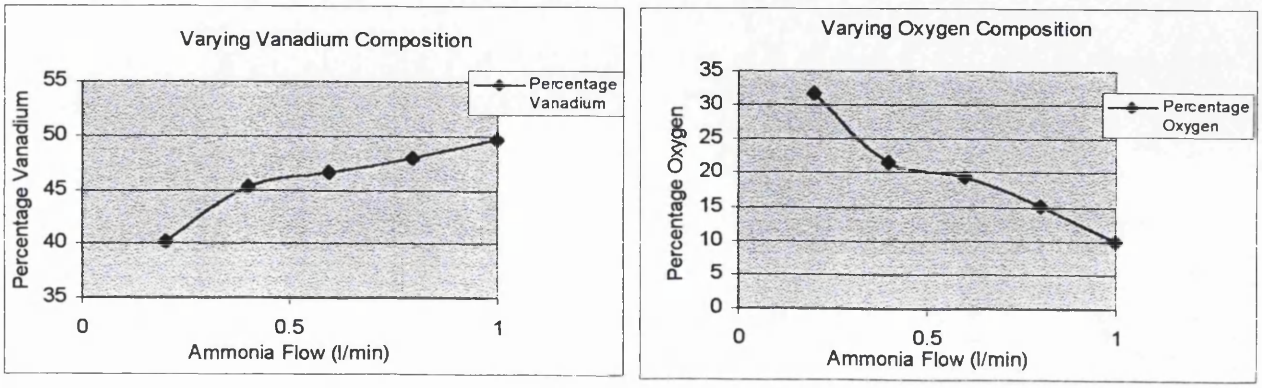

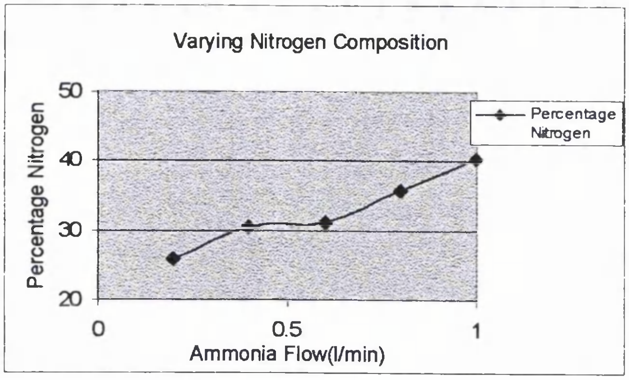

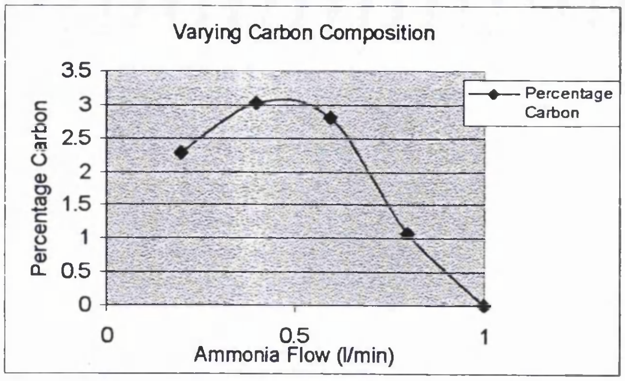

These results suggest that if a method for the addition of the ammonia could be found which cut down on prereaction and consequent particulate formation, then higher ammonia concentration could be routinely used to result in films of better composition. The composition of the film grown at 500 °C with 1 dm^3 min^{-1} flow of ammonia is V_5N_4O. Despite the lower oxygen contamination at higher flow rates of ammonia, the chemical shift for the vanadium peak stays at 513.1 eV for all samples. This is most probably due to vanadium maintaining the same oxidation state.

The four-probe resistance measurements of the films prepared with varying NH_3 flow rates are meaningful as the films are all of a similar thickness (ca 300 nm) (table 3.4c).

Table 3.4c Four-probe measurements for films obtained in the ammonia variation study ($0.42\ dm^3\ min^{-1}$ VCl_4 at 500 °C and $10\ dm^3\ min^{-1}$ process gas flow).

Ammonia Flow (l/min)	Four-probe resistance Reading (σ/▫)
0	Non conductive
0.1	250
0.2	240
0.3	213
0.4	171
0.5	145
0.6	116
0.7	125
0.8	113
0.9	112
1.0	115
2.0	107

Table 3.4c shows that a general trend of a decrease in film resistivity with increasing ammonia flows. It appears from this information that the conductivity of vanadium nitride films is improved if there are less contaminants, such as oxygen and carbon incorporated in the film.

The SEM photos of the VN films produced from different ammonia flows, show that there is not much difference between the particle sizes formed from low and high concentrations of ammonia. When the ammonia flow rate is zero no film is deposited and the SEM photograph shows plain glass. The SEM photos of $0\ dm^3\ min^{-1}$ and $0.6\ dm^3\ min^{-1}$ are shown below in fig. 3.4d.

Figure 3.4d SEM photographs of films deposited with 0 l/min NH_3 (1) and 0.6 l/min NH_3 (2) (0.42 $dm^3\ min^{-1}$ VCl_4 at 500 °C and 10 $dm^3\ min^{-1}$ process gas flow).

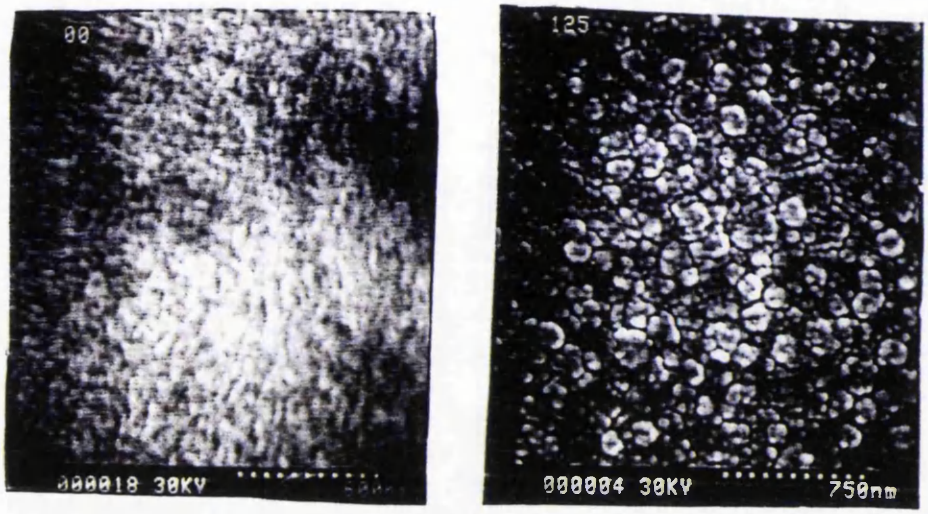

1 2

The photograph in figure 3.4d (2) suggests that the growth mechanism for these films is by an island growth (also known as Volmer-Weber growth) mechanism. This can be identified by the appearance of small islands or grains rather than a smooth single crystal growth.

The XRD spectra for films prepared from VCl_4 and NH_3, obtained with varying ammonia concentration should be similar, as the crystallite sizes and thicknesses are equivalent. The only thing that should change is the exact position of the peaks as the elemental composition of the film changes slightly. The spectra obtained from films deposited with an ammonia flow rate of 0.6, 1.0 and 2.0 $dm^3\ min^{-1}$ are shown in fig. 3.4e.

Figure 3.4e XRD patterns with varying ammonia flow (0.42 dm^3 min^{-1} VCl$_4$ at 500 °C and 10 dm^3 min^{-1} process gas flow).

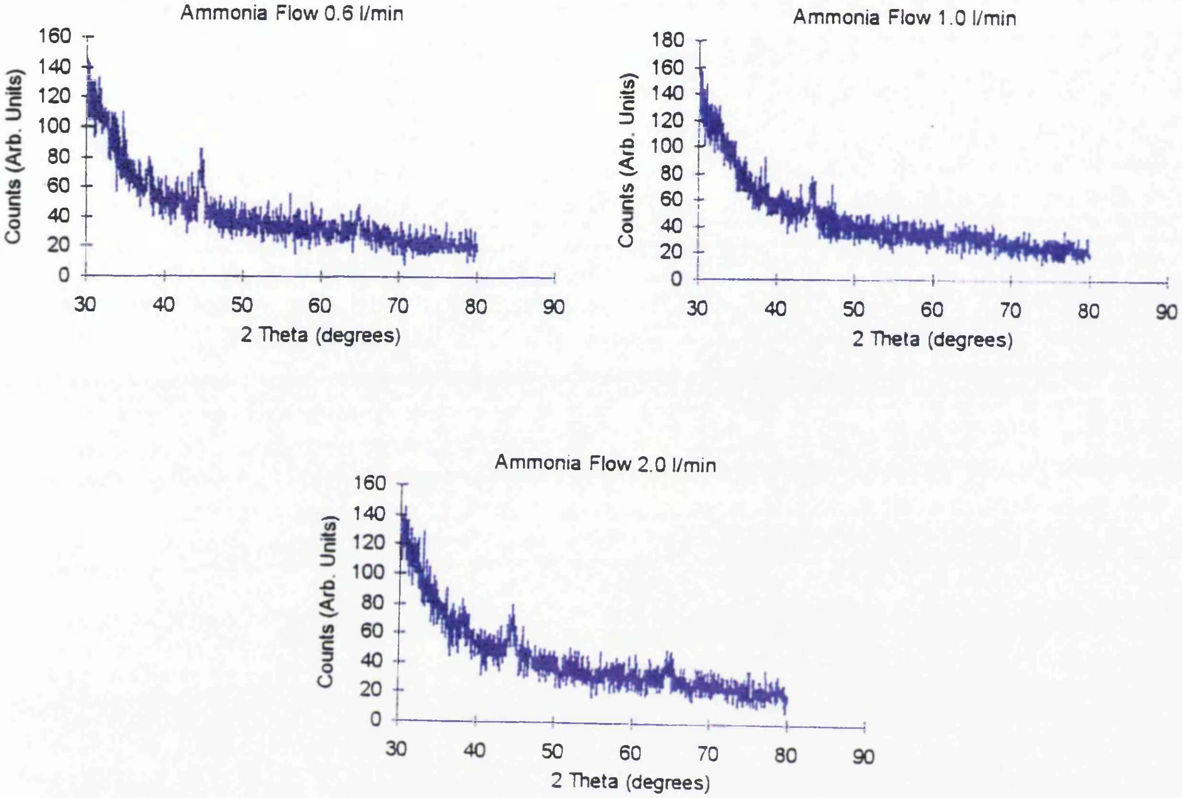

From the spectra shown in fig. 3.4e it can be seen that the crystallinity isn't really good enough to distinguish the peaks very well, but it can clearly be seen that the sharpest peak is at around 45 ° which shows preferred growth in the (2 0 0) direction. Although these peaks are not very clear, they have been indexed and the results are given in table 3.4f.

Table 3.4f Lattice parameters from indexing of XRD peaks in fig. 3.4e and crystallite sizes.

Ammonia flow rate	Lattice parameter a (Å)	Crystallite size Å
0.6	4.070	211
1.0	4.071	226
2.0	4.074	177

It can be seen from table 3.4f that the lattice parameters increase with ammonia flow, relating to a change in chemical composition. The crystallite sizes don't appear to be affected greatly by the ammonia flow rates.

The transmission and reflectance spectra for the films obtained from the variation in ammonia flow-rate experiments are shown in figure 3.4g. As can be seen from the spectra the heat mirror qualities improve as the ammonia flow rate is raised. The transmission properties remain fairly consistent throughout the series but the reflectance properties are much improved when higher flow rates of ammonia are used for the deposition. The best overall heat mirror qualities are seen in the film deposited with an NH_3 flow of 2 dm^3 min^{-1}.

Fig 3.4g Transmission and reflectance spectra for rising ammonia flow rate (0.42 dm^3 min^{-1} VCl_4 at 500 °C and 10 dm^3 min^{-1} process gas flow).

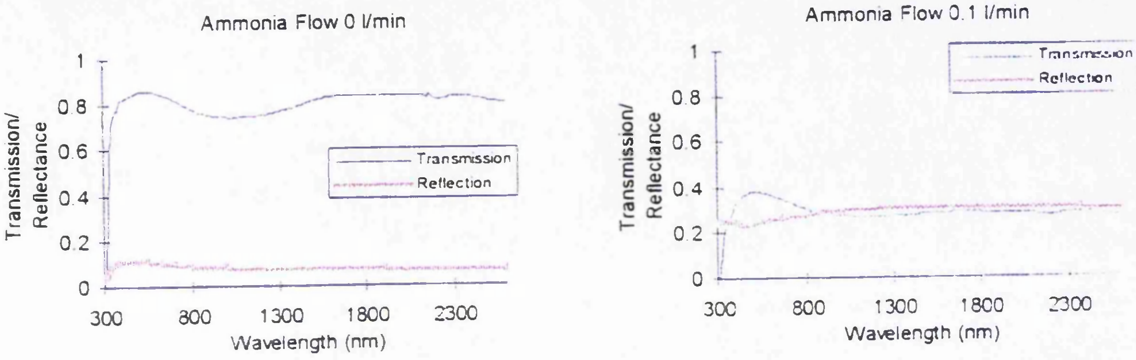

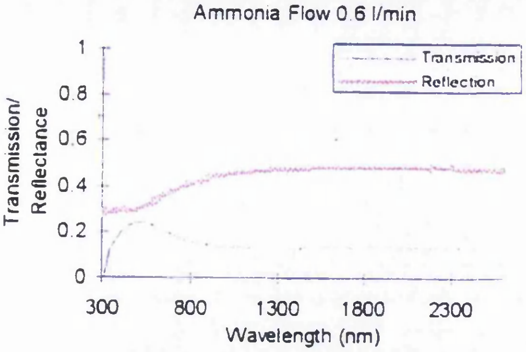
Ammonia Flow 0.6 l/min

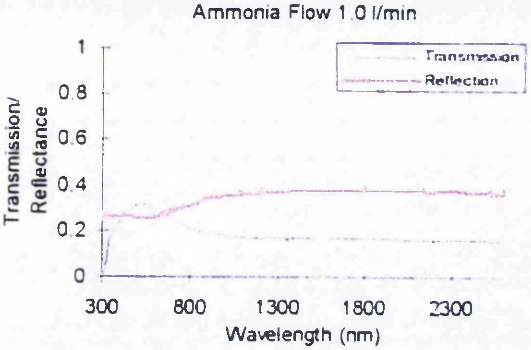
Ammonia Flow 1.0 l/min

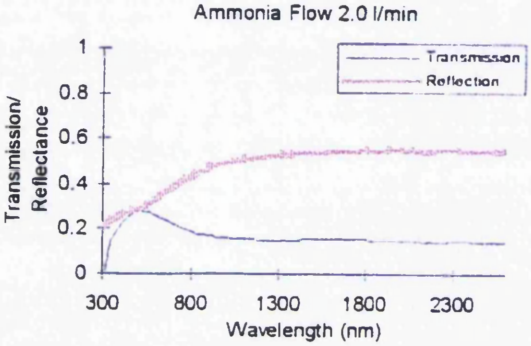
Ammonia Flow 2.0 l/min

Overall, the ammonia variance study has shown that higher flows of ammonia lead to films with lower oxygen and carbon contamination and better conductivity. Crystallinity in the films appears to be independent of the ammonia flow rate. However, heat mirror qualities are improved when higher ammonia flow rates are used. The only negative effect of increasing the flow rate of ammonia is the prereaction. In future studies this could be changed by minor variations to the rig design, especially mixing the gases directly in the reaction chamber.

3.5 Effect of process gas flow

The process gas flow rate is key to the success of a coating. If the flow rate is too low then the blockages caused by prereaction will not be blown out and complete blockages of the reaction lines could occur. If the process gas flow rate is too high then unreacted precursor can be vented out of the exhaust without reacting to form a film. Generally the process gas flow rate is set in order to minimise blockages. For this study, the process gas flow rate was varied from 5 to 10 $dm^3\ min^{-1}$ in steps of 2.5 $dm^3\ min^{-1}$ to see what effect this had on the film. The conditions that remained unchanged throughout the study are listed in table 3.5a.

Table 3.5a Experimental conditions for process gas variation study for VN_x films.

Variable	Level fixed at
Coater temp.	450 °C
Bubbler Temp.	118 °C
Time of Run	30 secs
Flow through Bubbler	0.42 $dm^3\ min^{-1}$ (0.00735 mols VCl_4)
Ammonia flow	0.5 $dm^3\ min^{-1}$ (0.0102 mols)
N_2/NH_3 flow	1.2 $dm^3\ min^{-1}$

For this study ammonia was in slight excess.

The films were initially assessed visually. This revealed, as expected, that films which were grown under lower process gas flow rates appeared darker and thicker and had not formed over as much of the substrate as the films which were grown with higher process gas flow rates. All three of the films appeared grey / black and reflective as with the other VN films reported in the chapter.

As the only factor to change in this study was the process gas flow rate, the XPS data for the films was not expected to show any significant differences in composition. This was shown to be incorrect. Table 3.5b below, shows how the composition of the film varies with increasing process gas flow rate.

Table 3.5b Changes in composition of films formed with process gas flows of 5 dm^3 min^{-1} and 10 dm^3 min^{-1} (0.42 dm^3 min^{-1} VCl_4 at 450 °C and 0.5 dm^3 min^{-1} ammonia gas flow).

Element	At. % (process gas 5 dm^3 min^{-1})	At. % (process gas 10 dm^3 min^{-1})
Vanadium	47.46	41.93
Nitrogen	30.64	31.51
Oxygen	19.57	21.14
Carbon	1.24	3.74
Chlorine	1.09	1.67

This gives the overall composition as $V_5N_3O_2$ when the film is deposited at 5 dm^3 min^{-1} and $V_4N_3O_2$ for the film deposited at 10 dm^3 min^{-1}. This result seems to indicate that higher process gas flow rates lead to slightly higher oxygen impurities. This result lends more evidence to the hypothesis that a source of oxygen contamination in the films comes from impurities in the nitrogen process gas.

Four-probe resistance measurements of the VN films increase for films grown at higher process gas flows. The measurements are shown in table 3.5c.

Table 3.5c Four-probe measurements for varying process gas flow (0.42 dm^3 min^{-1} VCl_4 at 450 °C and 0.5 dm^3 min^{-1} ammonia gas flow).

Process Gas Flow (dm^3 min^{-1})	Four Probe Reading (σ/□)
5	80
7.5	107
10	128

Fig. 3.5d XRD spectra obtained for films grown with varying process gas flow rates (0.42 dm^3 min^{-1} VCl_4 and 0.5 dm^3 min^{-1} ammonia at 450 °C).

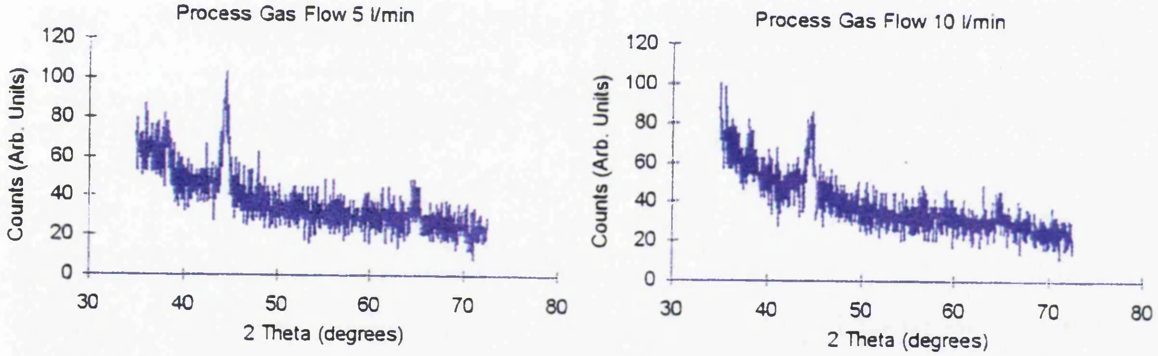

These peaks have been indexed to assess the degree to which changing the process gas flow rate has affected the crystal structure. Sharper peaks were observed for lower process gas flows, figure 3.5d

Table 3.5e Lattice parameters from indexing of XRD peaks in fig. 3.5d and crystallite sizes.

Process gas flow rate (dm^3 min^{-1})	Lattice parameter a (Å)	Crystallite size Å
5	4.072	171
10	4.065	228

The crystallite size increases with higher process gas flow rates. This can be explained by less nucleation sites being allowed to settle and grow into the final film when using higher process gas flow rates.

A decrease in thickness leads to an improvement in the visible transmission properties of the films but also leads to a decrease in the reflectance properties. This can be seen by the reflectance and transmission spectra shown in figure 3.5f.

Figure 3.5f Transmission / reflectance spectra with varying process gas flow rate (0.42 dm^3 min^{-1} VCl_4 and 0.5 dm^3 min^{-1} ammonia at 450 °C).

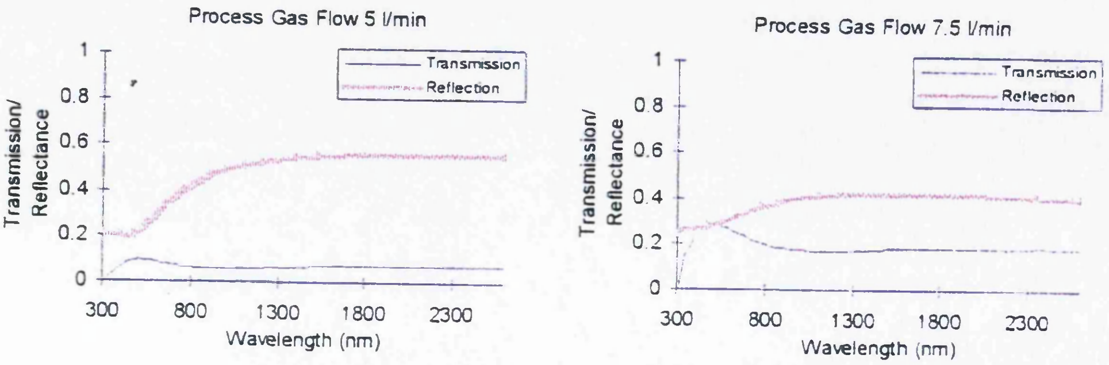

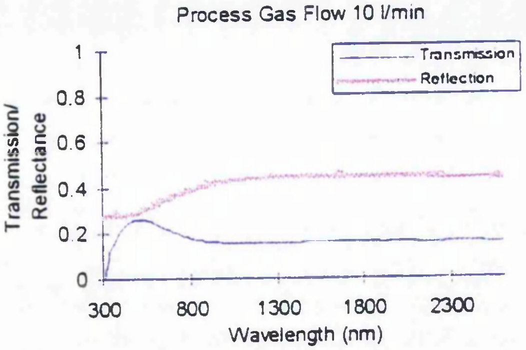

One of the main problems with vanadium nitride heat-control mirrors comes to light with these results. Thicker films have excellent reflectance spectra but are difficult to see through, so have limited use as heat-control mirrors. By making the film thinner, the visual transmission properties have reached a satisfactory level but they are compromised by a decrease in the reflectance properties. The best overall combination of properties is seen in the films deposited at high process gas flow rates.

3.6 Effect of growth times

This study involved changing the length of time for which the film was grown. The deposition time will directly affect the thickness of the film. At longer growth times the amount of particulate build-up can lead to severe blockages in the pipework. In this study all conditions were kept constant except for the deposition time. The shortest time chosen was 20 seconds and the longest time, before severe blockage meant the run had to be stopped, was 2 minutes. Table 3.6a contains a list of the other conditions, which were kept constant throughout the series of runs.

Table 3.6a Experimental conditions for the growth time study for VN_x films.

Variable	Level fixed at
Coater temp.	500 °C
Bubbler Temp.	117 °C
Ammonia Flow	0.8 $dm^3\ min^{-1}$ (0.0164mols)
Flow through Bubbler	0.42 $dm^3\ min^{-1}$ (0.00735mols VCl_4)
Process flow	10 $dm^3\ min^{-1}$
N_2/NH_3 flow	1.2 $dm^3\ min^{-1}$

The figures in table 3.6a correspond to a high excess of ammonia, as this has proved in previous runs to lead to a lowering of the oxygen content of the film (see section 3.4). The films differ in appearance, depending on growth time. The film produced from a 20 second run is pale black in colour and quite transparent. It is reasonably reflective. The film produced from a 2 minute run is very dark and reflective with a metallic lustre.

The XPS depth profiling spectra gave very similar compositions for the films independent of run time. The actual percentages vary by only a few percent. The average composition and the degree to which the four film compositions vary from this average are shown below in table 3.6b.

Table 3.6b Average XPS composition for films produced in growth time study (0.42 $dm^3\ min^{-1}$ VCl_4 and 0.8 $dm^3\ min^{-1}$ ammonia at 500 °C).

Element	Atomic Percentage
Vanadium	47.4 (±0.4 %)
Nitrogen	36.5 (±1.5 %)

Oxygen	15.0 (±2 %)
Carbon	0.5(±0.5 %)
Chlorine	0.00

The reason for the slight variation in the chemical composition is probably due to local impurities in the sample which was used for XPS testing.

Four probe readings from films deposited with different deposition times are given in table 3.6c. It can be seen that the resistance decreases with deposition time. As with the trend shown for the process gas flow rate variation experiment, this can be attributed to film thickness.

Table 3.6c Four probe resistance readings for VN_x films grown for 20, 30, 60 and 120 seconds (0.42 $dm^3\ min^{-1}$ VCl_4 and 0.8 $dm^3\ min^{-1}$ ammonia at 500 °C).

Coating Time(s)	Four Probe Reading (Ω/□)
20	403
30	113
60	70
120	29

The XRD peaks are sharper as the films increase in thickness as shown in the spectra in figure 3.6d.

Figure 3.6d XRD spectra with varying growth times (0.42 dm^3 min^{-1} VCl$_4$ and 0.8 dm^3 min^{-1} ammonia at 500 °C).

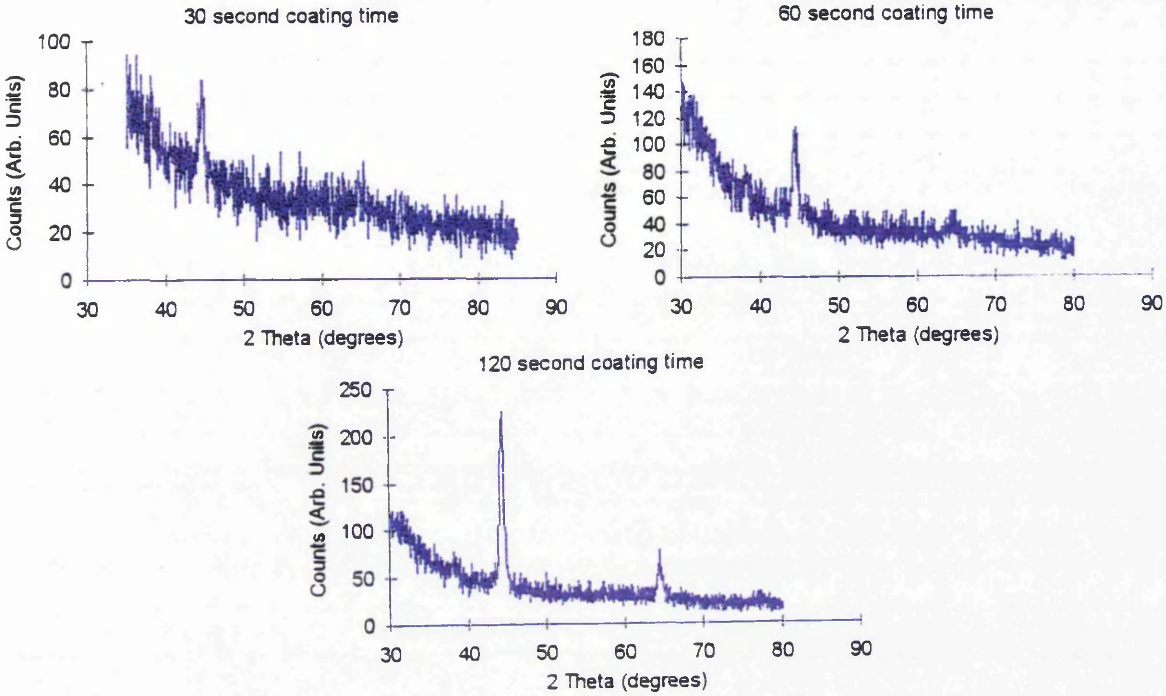
30 second coating time

60 second coating time

120 second coating time

The lattice parameter calculated from the indexing of these peaks is approximately the same for all the compounds with an average of a = 4.082 Å. The preferred orientation, as with all vanadium nitride films grown in this project, is in the (2 0 0) direction. The crystallite size remains fairly consistent and is independent of growth time. A crystallite size of 206 Å has been calculated for the 30 second deposition. The 60 second deposition and 120 second deposition both have similar crystallite sizes (205 Å and 225 Å respectively).

The reflectance and transmission spectra (fig 3.6e) vary as before, with the thicker films having much lower visual transmission.

Fig. 3.6e Transmission and reflectance spectra at varying growth times (0.42 dm^3 min^{-1} VCl_4 and 0.8 dm^3 min^{-1} ammonia at 500 °C).

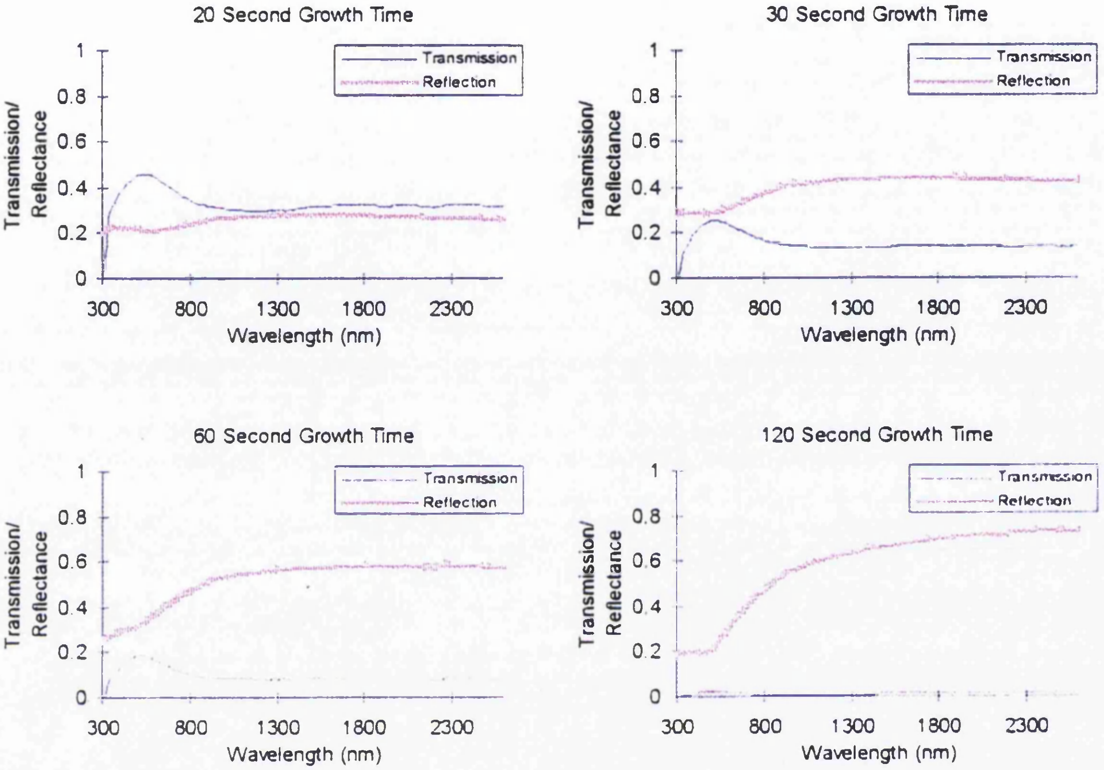

The reflectance shown by the film in the 120 second deposition shows excellent properties for a heat mirror, as the curve dips in the visible region of the spectrum. Unfortunately the visual transmission is so small that the glass is too dark to see through. On the other hand, the visual transmission is excellent in the film deposited over 20 seconds. Over 40 % of light is transmitted in the visible region, which is above the minimum required for commercial windows (30 % transmission in the visible region). However, there is very little difference in the reflectance in the visible and IR regions of the spectrum, meaning this film would find minimal use as a heat-control mirror. The best overall combination of properties appear in the films deposited for between 30 and 60 seconds.

3.7 Effect of annealing

As a final experiment for vanadium nitride films, a film was deposited at 350 °C and then heated to 650 °C. The purpose of this was to see if the properties of the film deposited at 350 °C were still present if the film was annealed at 650 °C. It was uncertain whether the oxygen and carbon were incorporated into the film during deposition, on storage of the films in air or during the cool down period in the coater. Also, films formed at 350 °C have a uniform coating over the whole glass, whereas those formed at higher temperatures formed at just the start of the substrate. That meant that the films formed at higher temperatures were too thick to see through although, they had excellent IR reflective properties. The results from this section are compared with results from section 3.3 and the conditions, apart from the annealing, are identical.

The appearance of the film formed was excellent. The coating was reflective and fairly dark but still transparent. It had fairly good uniformity over the whole substrate. The exact conditions used to prepare it are detailed below in table 3.7a.

Table 3.7a Conditions used for deposition of VN_x film in annealing study.

Variable	Level fixed at
Coater temp.	350 °C
Bubbler Temp.	117 °C
Ammonia Flow	0.5 $dm^3 min^{-1}$ (0.0102mols)
Flow through Bubbler	0.42 $dm^3 min^{-1}$ (0.00735mols VCl_4)
Process flow	10 $dm^3 min^{-1}$
N_2/NH_3 flow	1.2 $dm^3 min^{-1}$
Time of deposition	30 seconds
Annealing temperature	650 °C (for 1hr)

The composition of the film produced by these conditions is shown in table 3.7b.

Table 3.7b XPS composition of film used in annealing study (0.42 dm^3 min^{-1} VCl_4 and 0.5 dm^3 min^{-1} ammonia).

Element	Atomic Percentage
Vanadium	47
Nitrogen	38
Oxygen	12
Carbon	2.9
Chlorine	0.00

These results are a little unexpected as the oxygen percentage is lower than the films produced at 350 °C and 650 °C, (section 3.3), despite the fact that the conditions were exactly the same apart from the annealing stage. The reason for the lower oxygen concentration appears to be due to the fact that the film was annealed under a flow of ammonia. This has allowed nitrogen to replace the oxygen incorporated in the film. This result would suggest that films should be cooled under a flow of ammonia, which hasn't been the case in all the other runs in this chapter. The only anomaly in these results is the fairly high carbon content of 2.87 atomic percent. This is similar to the carbon percentage present in the film produced at 650 °C in section 3.3 and would suggest that the higher temperatures have allowed carbon from the substrate, process gas or even the carbon block on which the substrate rests to become incorporated into the film.

The resistance of the film was calculated at 93 Ω/□ which can be compared with the film of the same thickness deposited in section 3.3, which had a four probe measurement of 2450 Ω /□ . This confirms other conclusions about the crystallinity of the film being a major factor in the resistance.

SEM shows that the grain sizes produced for the annealed VN film are equilavalent to the film produced at 650 °C and perhaps even larger. This is a result of the hour-long annealing process, which has given enough time for the grains to conglomerate together into larger particles. The film prepared at 650 °C in section 3.3 was only held at 650 °C for a few seconds after the deposition had been completed before the substrate was allowed to cool to room temperature.

The XRD for the film produced is shown in figure 3.7c.

Fig 3.7c The XRD pattern produced from a sample deposited at 350 °C and annealed at 650 °C for 1 hour (0.42 dm^3 min^{-1} VCl_4 and 0.5 dm^3 min^{-1} ammonia)

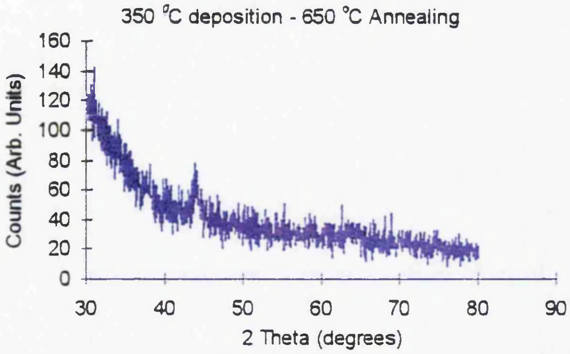

The graph in fig. 3.7c shows that, although the film is crystalline and does show some peaks, the film thickness means that the peaks aren't as sharp as they could be, because the instrument is measuring the amorphous glass. The lattice parameter calculated from the indexed peaks is a = 4.116 Å, a lot closer to the lattice parameter for pure VN (a =

4.139 Å) calculated from the XRD indexing of the (2 0 0) peak. The crystallite size is 175 Å.

The transmission and reflectance spectra for the annealed film are shown in fig 3.7d.

Fig 3.7d Transmission / reflectance spectra for annealed film (0.42 dm^3 min^{-1} VCl_4 and 0.5 dm^3 min^{-1} ammonia).

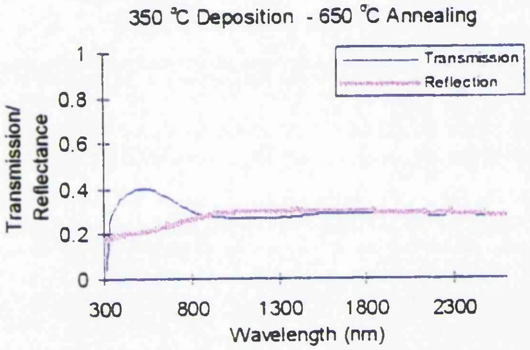

These spectra show a visible transmission better than any other vanadium nitride film but the infrared reflection is still very low. This seems to confirm that thicker films are needed to achieve good reflective properties, even though that leads to lower visible transmission.

3.8 Summary of vanadium nitride films

Following the studies discussed in this chapter the following conclusions have been drawn.

The best quality VN films deposited from the reaction of VCl_4 and NH_3, as determined by composition, are achieved at substrate temperatures between 500 and 600 °C. Above and below this temperature, carbon and oxygen contamination can be a problem.

Higher ammonia flow rates also lead to lower oxygen contamination, but prereaction can be a problem. To overcome prereaction, the new precursor delivery and mixing methods that have been developed and discussed in chapter 2 and 7 should be used. Changing the process gas flow rate and the deposition time do not significantly alter the composition of the film, but do alter film thickness. Prereaction is a problem at all temperatures, but is minimised by higher process gas flow rates. Finally, the annealing experiment has revealed that keeping the deposited film under an ammonia flow during cooling is beneficial as it minimises oxygen contamination.

The chemical shifts of the elements from the XPS spectra, all fall within the boundaries expected for vanadium nitride predicted from the literature[97].

Lattice parameters for VN_x films have varied from 4.06 to 4.11 Å suggesting a large range of compositions are possible and this has been confirmed by the XPS measurements.

Preparing a good quality film, composition-wise and one that fulfils the requirements of a heat mirror are two separate goals, but it does seem that films with lower oxygen contamination do make better heat-control mirrors. Unfortunately, only films with a limited thickness meet the heat mirror goals, as they must have good visual transmission. Nonetheless, many of the films that have been produced in this chapter do fulfil the characteristics of heat-control mirrors and there are some industrial methods available for improving the visual transmission of darker films.

The best reflectance / transmission properties of a vanadium nitride film (good IR reflectance and reasonable visual transmission) are achieved by a film deposited at around 550 °C for 30 seconds, with high ammonia flow and high process gas flow, then annealed at 650 °C and cooled under an ammonia flow.

The results in this chapter compare well with results achieved by other groups, although it is difficult to find other references in the literature, relating to APCVD of VN films or the reaction of VCl_4 and NH_3. Hoffman *et al*[1] have deposited polycrystalline VN_x films by APCVD of $V(NMe_2)_4$ / NH_3. However their results show that over 10% carbon is present, even in films prepared at 400 °C, and carbon contamination is known to increase with deposition temperature for organometallic precursors. Farges *et al*[54] report films of exceptional quality sputtered from vanadium metal and N_2 gas. Their work shows that via sputtering it is possible to control nitrogen composition of δ-VN_x films to within 1 at. %[54]. Although composition control figures are difficult to quote, it can be seen from the ammonia variation study in section 3.4, that nitrogen composition is reproducibly controllable even by APCVD. Sorciano *et al*[51], have reported XRD lattice parameters for pure VN films (a = 4.14 Å) in the region of the lattice parameters in this thesis. Analysis of the bulk vanadium nitride produced by the reaction of V_2O_3 and N_2 at 1000 °C, by Tripathy *et al*[49], showed 8% carbon and over 11% oxygen contamination. This compares well with vanadium nitride prepared in this thesis which has been formed at a much lower temperature and much faster growth rates, resulting in a lot less carbon contamination.

To summarise, vanadium nitride films in this work have been produced faster and in a purer form than many prior methods, particularly when comparing this work with previous APCVD work.

Chapter 4

Thin Films of Vanadium oxynitride

4.1 Experimental details

The experimental procedure for preparing vanadium oxynitride thin films is as described in chapter 3 (section 3.1) except for the following changes.

Vanadium oxychloride ($VOCl_3$) was purchased from Aldrich (99%) and used instead of VCl_4. It is an orange liquid at room temperature, with a boiling point of 126.5 °C.

Bubbler temperatures were set to around 96 °C as this provided a good vapour pressure of vanadium oxychloride (see graph 2.2b).

The intended coating from this series of experiments is vanadium oxynitride (VO_xN_y). Prior to this work, this material had only been prepared and characterised as a bulk material (see section 1.5). In the context of this work it was not known whether the oxygen in the film introduced from the precursor would affect the quality of the heat-control mirror. For compositional purposes it was important to learn how altering the amounts of precursors could vary the oxygen and nitrogen levels in the final film and how these levels would affect the physical properties of the film.

$$VOCl_3 + NH_3 \rightarrow VON + 3\,HCl \qquad \text{(Equ. 4.1a)}$$

From equ. 4.1a and the vapour pressure charts in fig. 2.2b it can be seen that for a 30 s deposition a flow of N_2 of 0.42 l/min through the bubbler will yield 0.00678 moles of $VOCl_3$ at 98° C. Using a flow of 0.3 l/min of ammonia will yield a similar molar equivalent 0.00615moles, therefore any flow of NH_3 above 0.3 l/min, will have the ammonia in excess, and below 0.3 l/min NH_3, the $VOCl_3$ will be in excess. Unlike the reaction of vanadium tetrachloride and ammonia, where the vanadium is reduced from V^{4+} (in the precursor) to V^{3+}(in the film), the $VOCl_3$ precursor has V in the +5 oxidation state and in the product, V can have varied oxidation states depending on the values of x and y in VO_xN_y. This may lead to different film properties to those observed for VN.

4.2 Effect of coater temperature

This study is similar in many ways to the VCl_4/NH_3 study. Like the VCl_4/NH_3 prepared films the composition of the film is affected by the coater temperature. In this study films were grown at 350, 450, 550 and 650 °C, all other factors being kept constant (table 4.2a).

Table 4.2a Factors kept constant for coater temperature study.

Variable	Level fixed at
Bubbler Temp.	98 °C
Time of Run	30 secs
Flow through Bubbler	0.42 $dm^3\ min^{-1}$ (0.0068 mols)
Process flow	5 $dm^3\ min^{-1}$
NH_3 Flow	0.5 $dm^3\ min^{-1}$ (0.0102 mols)
N_2/NH_3 flow	1.2 $dm^3\ min^{-1}$

According to equation 4.1a, $VOCl_3$ and NH_3 react in a 1:1 ratio to form VON, therefore, from table 4.2a, it can be seen that the ammonia is in excess for these experiments.

At a low process gas flow rate (5 $dm^3\ min^{-1}$), all the runs experienced prereaction, formation of particulates and some blocking of the pipes, except the run carried out at 350 °C. These blockages were caused by the precursors reacting prior to the reaction chamber. The blockages affected the visual quality of the films, with the films produced at 450, 550 and 650 °C looking splattered and non-uniform in places. The run at 650 °C had blockages in the pipework after only 5 seconds and the film only formed along the first 3 cm of the substrate. The film was splattered and patchy. Because of this, films were also produced at higher process gas flow rates. All the conditions described in table 4.1a were kept constant except the flow rate of the process gas was raised to 10 dm^3 min^{-1}. An increased process gas flow rate did not affect the amounts of precursor reaching the substrate, only their concentrations in the inert process gas. Visually, the films produced with a higher process gas flow rate were better; prereaction affected the films to a lesser extent. The film produced at 650 °C only progressed 6 cm along the substrate and was very dark but contained no particulates. The results obtained from both the high and low process gas flow rates will be described.

XPS has been used to obtain depth profiles and compositions for the films produced from $VOCl_3$ and NH_3. An XPS spectrum of a typical film prepared at 550 °C with 10 dm^3 min^{-1} process gas flow and with the experimental conditions as detailed in table 4.2a is shown in figure 4.2b.

Fig. 4.2b XPS data from VO_xN_y film prepared at 550 °C from reaction of $VOCl_3 + NH_3$ with 10 dm^3 min^{-1} process gas flow.

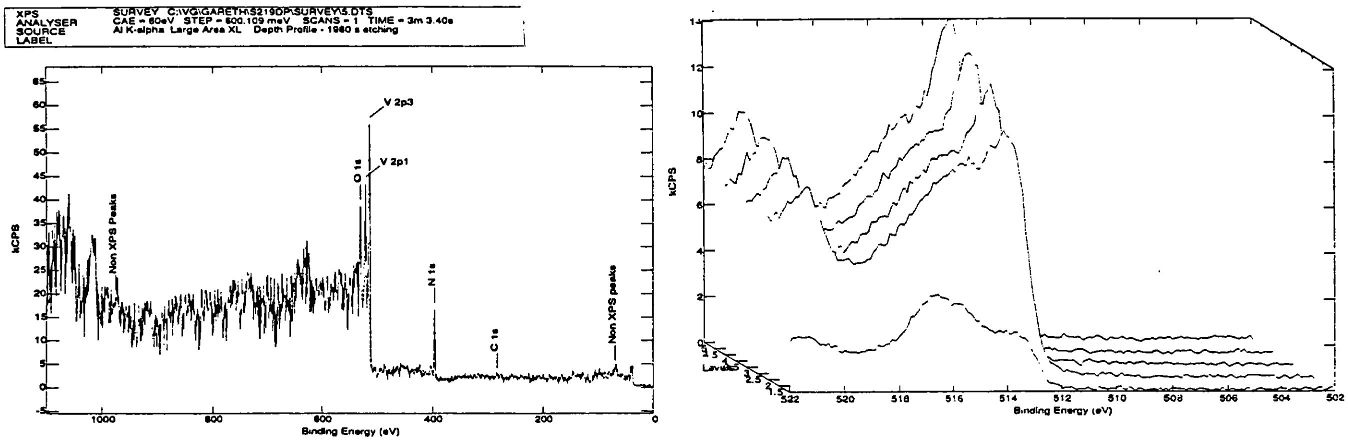

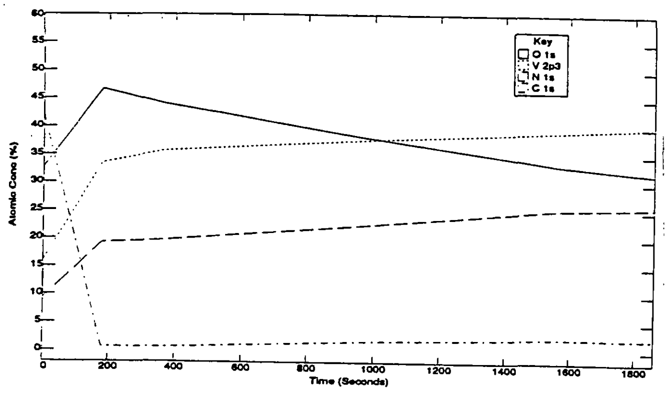

Element	Chemical Shift	Elemental % present in bulk
Vanadium	513.02eV	44.7
Oxygen	530.67eV	32.1
Nitrogen	397.08eV	21.9
Carbon	282eV	1.3
Chlorine	-	0

The composition of the film prepared from the reaction of $VOCl_3$ (0.42 dm^3 min^{-1}) and NH_3 (0.25 dm^3 min^{-1}) with 10 dm^3 min^{-1} process gas flow at 550 °C is $VO_{0.75}N_{0.5}$. This data can be compared with XPS spectra obtained from a VN film in section 3.2. The chemical shifts observed for V, O and N peaks in vanadium oxynitride are very similar to those observed for the VCl_4/NH_3 films in chapter three. This isn't surprising as the VCl_4/NH_3 prepared films contain oxygen contamination. A chemical shift of 517.1 eV was observed for the surface bound vanadium and is consistent with vanadium in a higher oxidation state such as V_2O_5 (517.65 eV). An observed XPS chemical shift of 513 eV is observed for the bulk vanadium oxynitride film after sputtering. This value is halfway between the expected result for vanadium metal (512.14 eV) and vanadium nitride (514.3 eV). The XPS values observed for nitrogen and oxygen in the bulk material are both consistent with the XPS chemical shifts expected for a transition metal nitride (396.8 - 398 eV) and oxide (529.5 – 531.3 eV).

XPS data has been used to obtain compositions for films in the coater temperature study. First to be described are the films produced at the low process gas flow rate of 5 dm^3 min^{-1}. Graphs of how the elemental percentage varies with film deposition temperature are shown in figure 4.2c.

Fig. 4.2c Variation in XPS composition with varying temperature (0.42 dm^3 min^{-1} VOCl$_3$ and 0.5 dm^3 min^{-1} ammonia at 5 dm^3 min^{-1}).

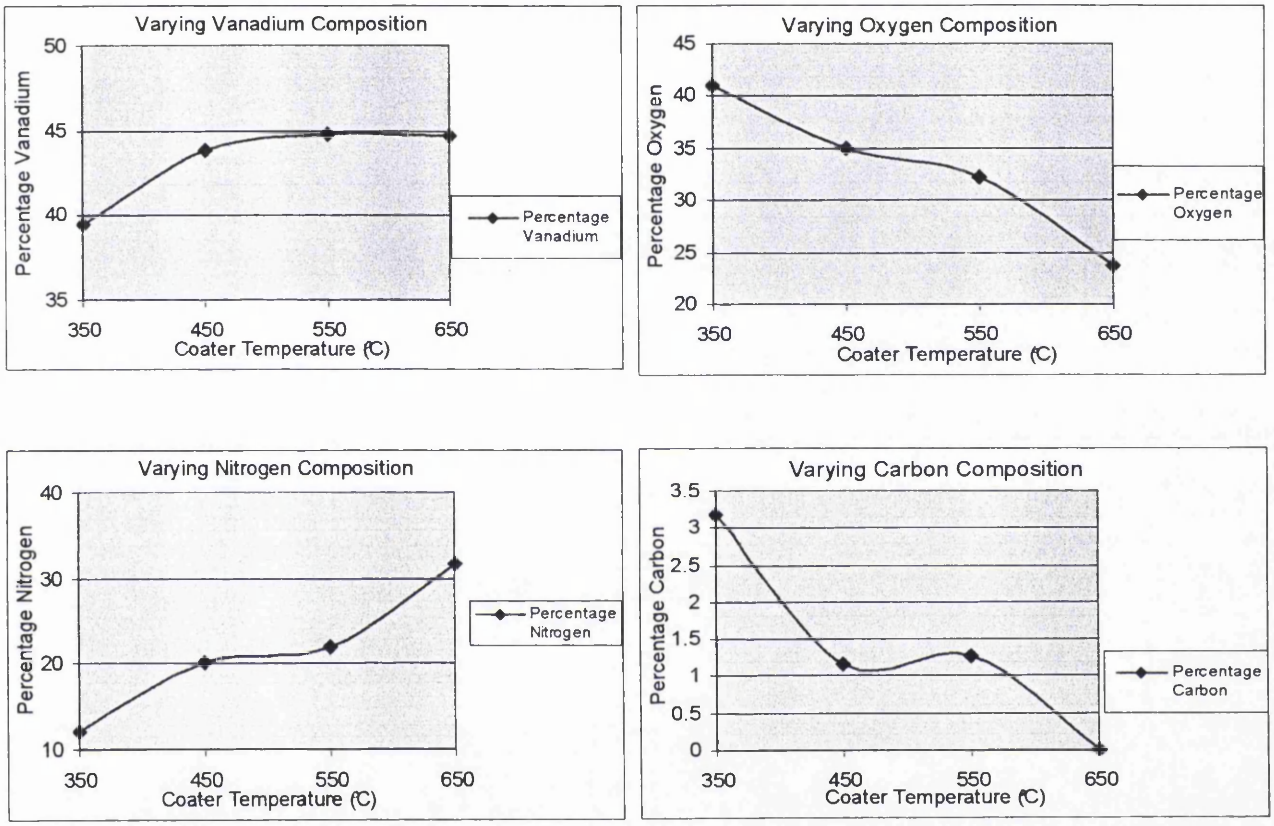

Chlorine was only seen in the film deposited at 350 °C, and assessed at 4.2 at. %. In all films deposited at temperatures above 350 °C no chlorine was detected. Fig. 4.2d shows the graphs of elemental variation in composition of the VO$_x$N$_y$ films against substrate temperature at the higher process gas flow rate of 10 dm^3 min^{-1}.

Fig. 4.2d Variation in XPS composition with varying temperature (0.42 dm^3 min^{-1} VOCl$_3$ and 0.5 dm^3 min^{-1}ammonia at 10 dm^3 min^{-1}).

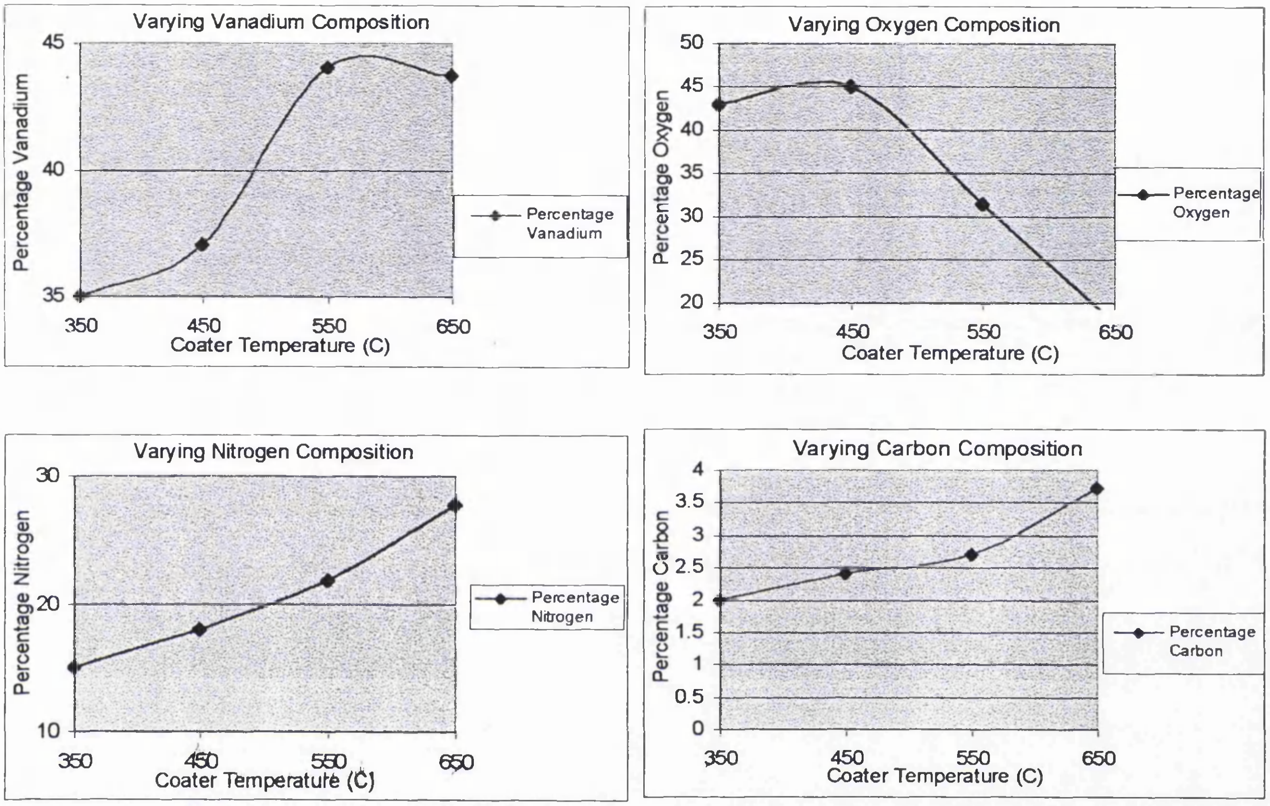

At higher process gas flows chlorine was again observed only in films deposited at 350 °C (7 at. %). It appears that lower substrate temperatures are not enough to break down the VOCl$_3$ completely. This may be due to a similar reaction occuring to that which has already been reported in the literature for reaction of TiCl$_4$ and ammonia (described in section 1.5), where TiNCl is formed below 550 °C. Substrate temperatures above 550 °C are able to break TiNCl down to TiN[1].

From figures 4.2c and 4.2d it can be seen that with increased deposition temperature the amount of oxygen in the film drops. In fact, at higher temperatures the composition is similar to that of the films prepared from VCl$_4$ and NH$_3$ in chapter 3 where oxygen was a contaminant. It is difficult to explain this result especially in light of the result seen in section 3.3, where the oxygen contamination actually started to rise again at higher coater temperatures. In this set of data the oxygen atomic percent drops significantly between 550 and 650 °C. This could be explained by the fact that there is a difference between oxygen from the precursor and oxygen contamination from the process gas.

Chlorine contamination is only seen at 350 °C in the films prepared from $VOCl_3$ and NH_3, which is different from the VCl_4 / NH_3 films, where chlorine contamination wasn't seen at all. This suggests that a VN_xCl_y intermediate is not formed in these cases or if it did form it breaks down to VN_x at lower temperatures than a $VO_xN_yCl_z$ intermediate breaks down to VO_xN_y. Carbon contamination rises slightly at higher substrate temperatures. The carbon is probably due to contamination from the N_2 process gas and the higher substrate temperatures would leave the film more susceptible to attack.

The other important thing to note, by comparing figures 4.2c and 4.2d, is that as the flow rate of the process gas increases, despite keeping all other factors the same, the composition of the film is altered. This has been summarised in table 4.2e.

Table. 4.2e Variation in XPS composition with varying temperature (0.42 $dm^3\ min^{-1}$ $VOCl_3$ and 0.5 $dm^3\ min^{-1}$ ammonia at 450 °C).

Element	At. % (5 $dm^3\ min^{-1}$)	At. % (10 $dm^3\ min^{-1}$)
Vanadium	44	37
Oxygen	35	45
Nitrogen	20	18
Carbon	1.15	2.4

The atomic percentage of oxygen present in the vanadium oxynitride films, in particular, is significantly higher at higher process gas flow rate. The probable reason for this is that the reaction of ammonia with vanadium oxychloride is slow and the longer the ammonia is given to react with the vanadium oxychloride at the substrate surface, the more nitrogen is absorbed into the growing film. At higher deposition temperatures, the difference between the elemental compositions of the VO_xN_y films obtained at the two different flow rates isn't as significant. The carrier gas being a source of oxygen contamination can also explain this result, so at higher flows of carrier gas more oxygen is incorporated in the film.

Four probe sheet-resistance measurements give an idea of the conductivity of these films, although, again, these results are distorted by the differences in film thickness. Films formed at lower temperatures are thinner than those formed at higher temperatures for reasons discussed in section 3.3. Films formed at higher process gas flow rates are also thinner than those deposited at low process gas flow rates. These readings are still useful to look at, as they still give an idea on the improvement in conductivity. The measured four probe resistance readings are given in table 4.2f and 4.2g.

Table 4.2f Four-probe readings at low flow rate (0.42 $dm^3 min^{-1}$ $VOCl_3$ and 0.5 $dm^3 min^{-1}$ ammonia at 5 $dm^3 min^{-1}$).

Temperature (°C)	Four-Probe Reading (Ω/□)
350	333
450	86
550	29
650	30

Table 4.2g Four-probe readings at high flow rate (0.42 dm^3 min^{-1} $VOCl_3$ and 0.5 dm^3 min^{-1} ammonia at 10 dm^3 min^{-1} process gas flow)

Temperature (°C)	Four-Probe Reading (Ω/□)
350	15800
450	72
550	31
650	80

These results show that the sheet resistance decreases with an increase in substrate temperature up to 550 °C and then increases slightly for the films grown at 650 °C even though the oxygen atomic percent in the film is lower. This result could be due to an increase in carbon contamination for the film grown at 650 °C. There isn't much change in the resistance between the films deposited at low flow rates compared with those deposited at high process gas flow rates.

The XRD patterns of the films grown from $VOCl_3$/ NH_3 show that the crystallinity is affected by decomposition temperature. The XRD patterns observed for the films grown from $VOCl_3$/ NH_3 are similar to those observed from VN films, indicating a similar crystal structure for VO_xN_y, as shown in fig 4.2h.

Fig. 4.2h XRD spectra with varying substrate temperature, at low process gas flow (0.42 $dm^3 min^{-1}$ $VOCl_3$ and 0.5 $dm^3 min^{-1}$ ammonia at 5 $dm^3 min^{-1}$ process gas flow).

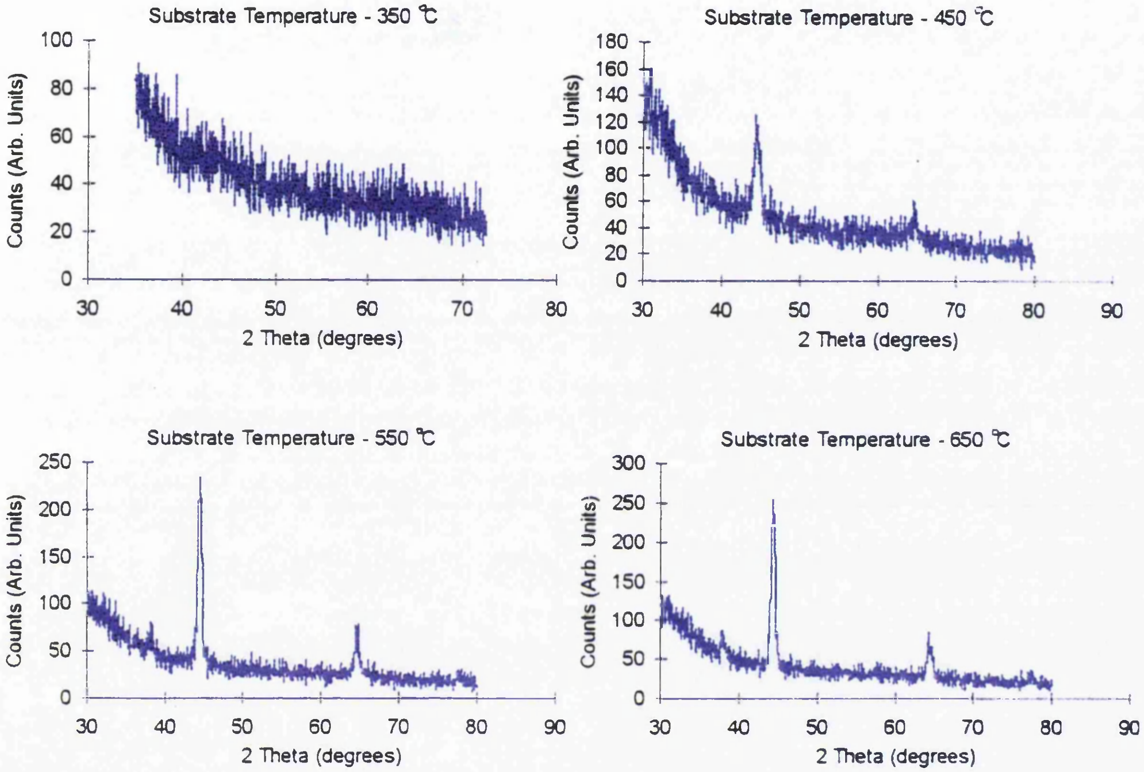

These results show that the coating is more crystalline at higher deposition temperatures. Similar XRD patterns are seen from VN films obtained from VCl_4/NH_3 at 450 °C as are seen from VO_xN_y films at 420 °C, so the onset of crystallinity for these two types of films is different despite the similarity of the final composition.

The spectra shown in figure 4.2h have been indexed and show strong preferential growth in the (2 0 0) direction. The lattice parameter for $VO_{0.9}$ is a = 4.12 Å and for VN is a = 4.139 Å, so the expected value for VO_xN_y should be similar. Crystallite sizes have also been calculated using the Scherrer equation using the width at half height of the (2 0 0) reflection. Values for these calculations are given in table 4.2i.

Table 4.2i Lattice parameters and crystallite sizes for VO_xN_y films in coater temperature study (0.42 $dm^3\ min^{-1}$ $VOCl_3$ and 0.5 $dm^3\ min^{-1}$ ammonia at 5 $dm^3\ min^{-1}$) (from fig. 4.2h).

Deposition temperature (°C)	Lattice parameter a (Å)	Crystallite size Å
350	-	-
450	4.074	121
550	4.072	240
650	4.093	252

The crystallite size increases with deposition temperature. Larger crystallites are expected at higher substrate temperatures as faster growth rates should occur.

The flow rate of the process gas doesn't seem to affect the grain size observed by SEM, although XRD has already shown the crystallite size to increase with deposition temperature.

The reflectance and transmission spectra for VO_xN_y films are expected to be inferior to those obtained from VCl_4 / NH_3 deposited films due to the extra oxygen (which seemed to damage the reflectance properties for VCl_4 / NH_3 deposited films). However, there are a number of things that bring some promise to the vanadium oxynitride films, such as the lower temperature onset of crystallinity. The reflectance and transmission spectra shown in fig. 4.2j are from the films of VO_xN_y deposited at the low process gas flow rate.

Fig. 4.2j Transmission and reflectance spectra for films in coater temperature study ($0.42\ dm^3\ min^{-1}$ $VOCl_3$ and $0.5\ dm^3\ min^{-1}$ ammonia).

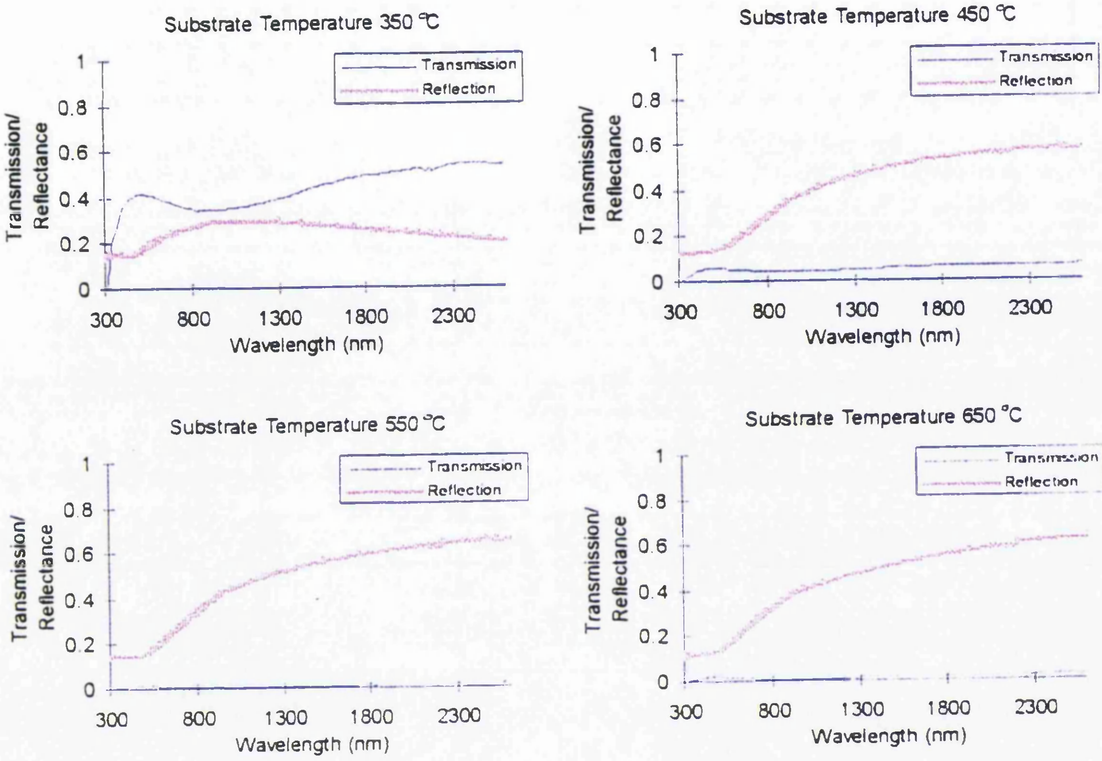

As can be seen from these spectra at the low process gas flow rates the reflectance is excellent in the infrared region but the visual transmission is very poor and gets worse for films prepared at higher deposition temperatures.

4.3 Effect of ammonia gas flow concentration

The variation of the ammonia flow rate is another way of affecting the values of x and y in VO_xN_y. In this study films were grown with ammonia flow rates of between 0 and 1 $dm^3\ min^{-1}$ in steps of 0.1 $dm^3\ min^{-1}$ to discover how much x and y could be varied. All other factors were kept constant and these are displayed in table 4.3a.

Table 4.3a Conditions for variation in ammonia flow on VO_xN_y films.

Variable	Level fixed at
Bubbler Temp.	98 °C
Time of Run	30 secs
Flow through Bubbler	0.42 dm^3 min^{-1} (0.0068mols)
Process flow	10 dm^3 min^{-1}
Coater Temperature	500 °C
N_2/NH_3 flow	1.2 dm^3 min^{-1}

A flow of 0.42 dm^3 min^{-1} through the bubbler corresponds to 0.00678 moles of $VOCl_3$ over a 30 second time period at 98 °C. According to equation 4.1a, 1 mole of $VOCl_3$ reacts with 1 mole NH_3 to form 1 mole VO_xN_y. 0.1 dm^3 min^{-1} NH_3 corresponds to 0.00205 moles so at this flow rate the $VOCl_3$ is in excess. 0.3 dm^3 min^{-1} of NH_3 provides 0.00615 moles; with this flow the concentration of the precursors are balanced. At 1.0 dm^3 min^{-1} NH_3, 0.0205 moles of ammonia are reaching the coater so the ammonia is in excess.

Due to the thickness and poor visual transmission of the films produced with a process gas flow rate of 5 dm^3 min^{-1} a process gas flow rate of 10 dm^3 min^{-1} was chosen for this study.

Visually, the films varied very little with an increase in ammonia flow rate. The exception to this, as in section 3.4, was when an ammonia flow rate of 0 dm^3 min^{-1} was used. As with the vanadium nitride depositions, no film was formed when no ammonia was used. When the $VOCl_3$ was in excess (ammonia flow rate 0.1 dm^3 min^{-1}), the film appeared streaky. This was due to the non-uniform flow of the ammonia through the coater and local preferences for deposition. At flows of 0.2 dm^3

min^{-1} and above the films appear uniform with a bronze / black metallic lustre. The films appeared reflective and had an appreciable amount of visual transmission.

XPS analysis was carried out to discover the effect of varying the ammonia gas flow rate on the composition of the film.

Fig. 4.3b Plots of XPS composition vs. ammonia flow rate for VO_xN_y films (0.42 dm^3 min^{-1} $VOCl_3$ at 500 °C and 10 dm^3 min^{-1} process gas flow).

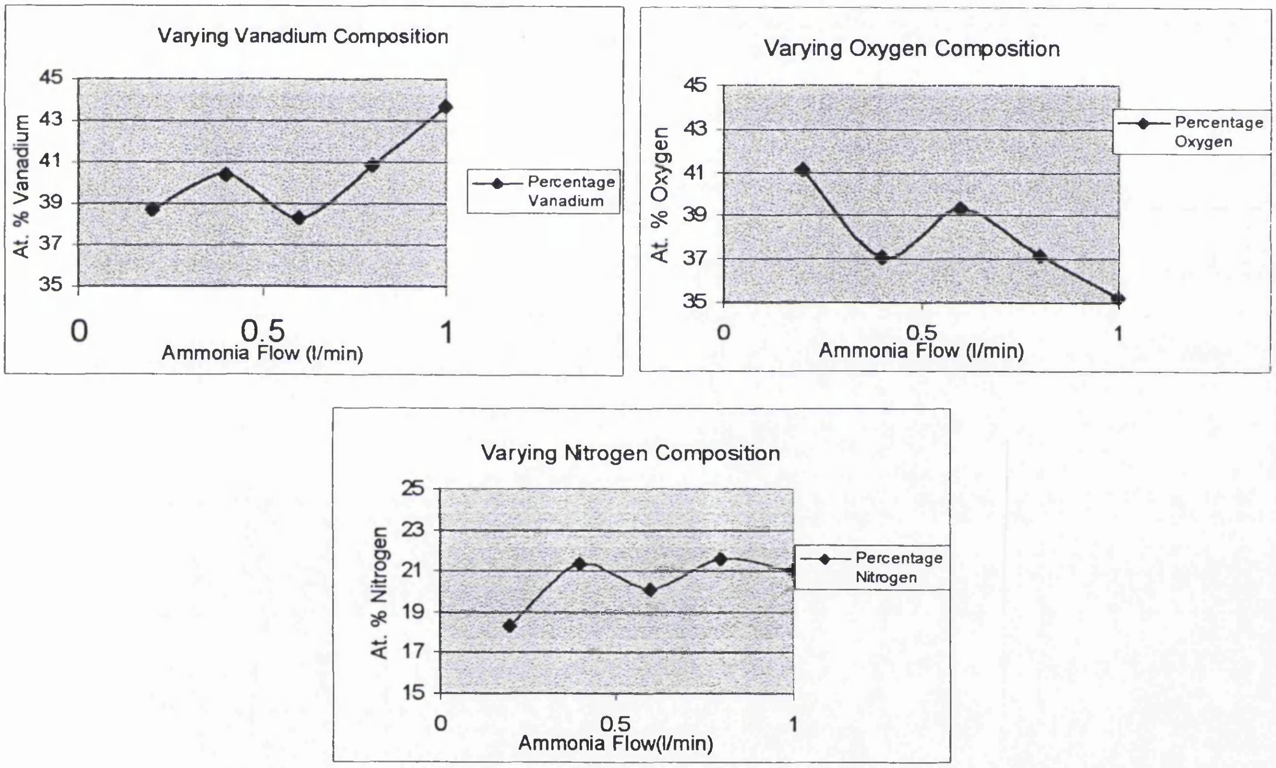

These spectra show that the elemental composition of the films change very little with increasing ammonia flows and certainly not to the same extent as that seen in the vanadium nitride films reported in chapter 3. There was a slight change in the composition of the films with increasing ammonia flow rates with a small increase in the observed vanadium and nitrogen content and a corresponding decrease in the observed oxygen and carbon contents. Despite this, the oxygen atomic percentage in the films are still over 35 % even with an ammonia flow rate of 1.0 dm^3 min^{-1}. However, the ratio of vanadium to oxygen is lower in the film (1:0.8, V:O) at higher flows of ammonia, than it is in the precursor (1:1, V:O). All carbon compositional values were below 2 atomic percent.

As the ammonia flow rate increases a lowering of oxygen content in the film has lead to an increase in the conductance observed by four probe resistance measurements. This is shown in table 4.3c.

Table 4.3c Four-probe readings at low flow rate (0.42 dm^3 min^{-1} $VOCl_3$ at 500 °C and 10 dm^3 min^{-1} process gas flow).

NH_3 Flow Rate (dm^3 min^{-1})	Four-Probe Reading (Ω/□)
0	No Coating
0.1	104
0.2	74
0.3	70
0.4	63
0.5	58
0.6	51
0.7	48
0.8	39
0.9	46
1.0	42

Lower four-probe resistance measurements of the vanadium oxynitride films were observed with increasing ammonia flows, with the exception of the film prepared with a flow of 0.8 dm^3 min^{-1}, where an anomalous result appears. It seems from this data that there is a limit to the decrease in the sheet resistance and that level is probably at around 1.2 – 1.5 dm^3 min^{-1} NH_3. Surprisingly, the films have a lower sheet resistance than the vanadium nitride films deposited under the same conditions despite the larger oxygen content. This is probably due to the higher degree of crystallinity in the vanadium oxynitride films.

XRD proves that the vanadium oxynitride films are more crystalline than vanadium nitride films prepared in chapter 3 under similar conditions. The XRD patterns shown below can be compared with the similar spectra for VN films in figure 3.4e.

Fig 4.3d XRD patterns with varying ammonia flow (0.42 dm^3 min^{-1} $VOCl_3$ at 500 °C and 10 dm^3 min^{-1} process gas flow).

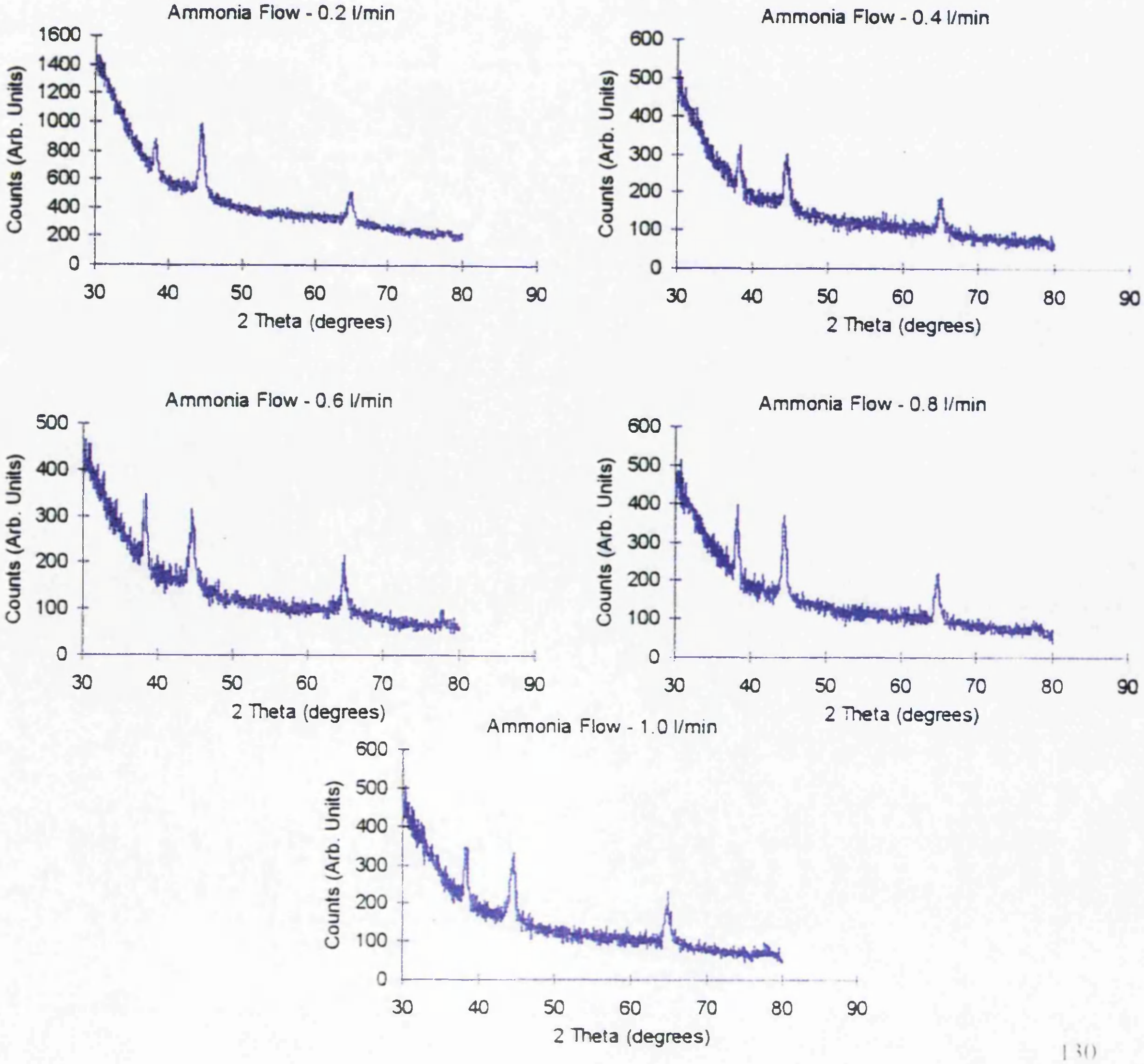

As can be seen from the spectra in 4.3d the reflections change very little as the ammonia flow rate is raised. One thing that is different for the XRD patterns of the VO_xN_y films is the preferred orientation. This seems to shift from (2 0 0) at low ammonia flows to (1 1 1) at higher flows.

The reflections have been indexed. Crystallite sizes have been evaluated using the Scherrer equation (table 4.3e).

Table 4.3e Lattice parameters and crystallite sizes for VO_xN_y films in ammonia study from peaks in fig. 4.3d.

Ammonia flow rate	Lattice parameter *a*	Crystallite size Å
0.2	4.063	152
0.4	4.061	144
0.6	4.062	133
0.8	4.069	201
1.0	4.066	130

The results displayed in table 4.3e show that the crystallite size and the lattice parameter vary very little from sample to sample. This seems to suggest that a high excess of ammonia does not lead to larger crystallites or a change in the lattice parameter.

Changing the ammonia flow rate affects the sheet resistance but not the composition or crystallinity of the films. In figure 4.3f below, the transmission and reflectance spectra are given for films obtained with differing ammonia flow rates.

Fig 4.3f Reflectance / transmission spectra for varying ammonia flow rate (0.42 dm^3 min^{-1} $VOCl_3$ at 500 °C and 10 dm^3 min^{-1} process gas flow).

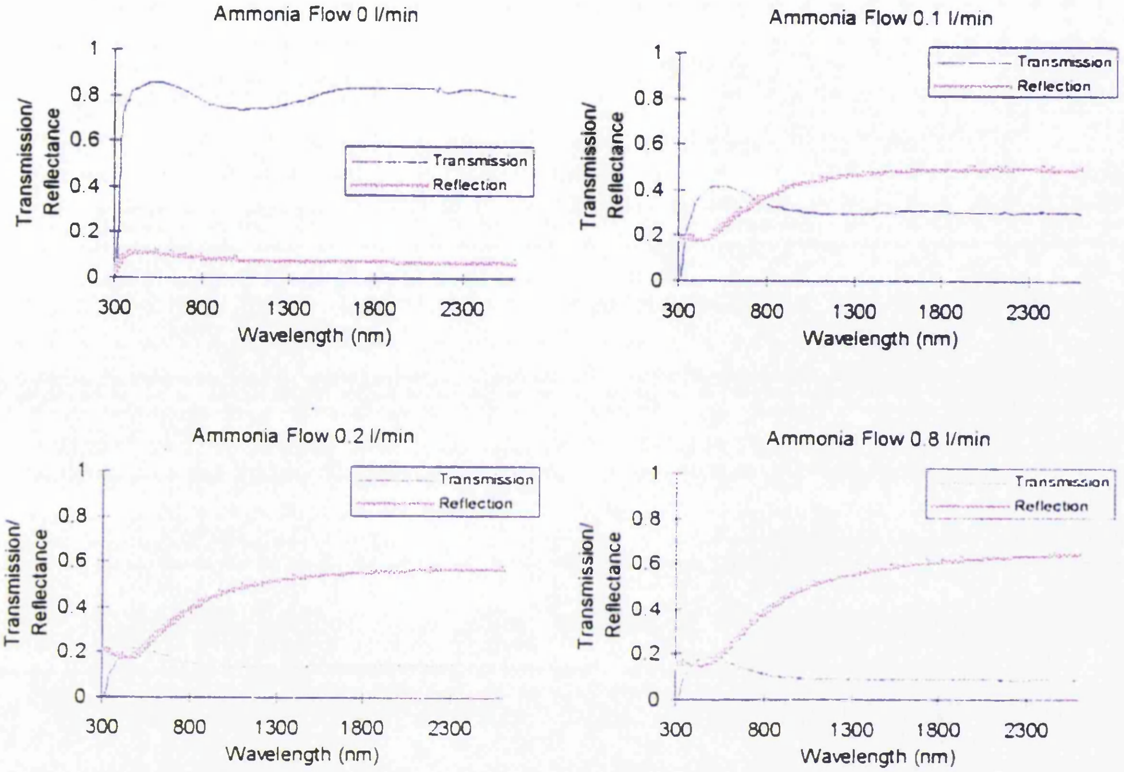

As can be seen from these spectra, films produced at ammonia flow levels above 0.2 dm^3 min^{-1} show very little difference in the transmission or reflectance properties. In comparison with the spectra obtained for the equivalent study with vanadium nitride films (section 3.4), the spectra obtained here show that vanadium oxynitride has a much greater potential for use as a heat-control mirror. This is a completely unexpected result considering the amount of nitrogen present in the films. Even with an ammonia flow rate of 0.1 dm^3 min^{-1} the visual transmission is 40 % and the infrared reflectance shows the required properties for a heat-control mirror. The only problem with the film deposited with a 0.1 dm^3 min^{-1} flow of NH_3 is its streaky appearance which is due to the uneven flow of ammonia over the substrate. This could be remedied relatively simply by using an entrance flange of appropriate design.

4.4 Effect of growth times

Films of VN (section 3.5) lose many of their heat-control properties as coating times are reduced but the vanadium oxynitride films examined in this chapter show that good reflectance properties can be produced with shorter deposition times. These films also have good visual transmission. The effect of changing the deposition time from 15 seconds up to 210 seconds was examined while keeping other factors constant. The conditions employed for this study are displayed in table 4.4a.

Table 4.4a Deposition conditions used for growth time study on VO_xN_y films.

Variable	Level fixed at
Bubbler Temp.	98 °C
Flow through Bubbler	0.42 dm^3 min^{-1} (0.0068 mols)
Process flow	10 dm^3 min^{-1}
Coater Temperature	500 °C
N_2/NH_3 flow	1.2 dm^3 min^{-1}
Ammonia flow rate	0.8 dm^3 min^{-1} (0.0164mols)

A high excess of ammonia was used for this series of experiments. XPS analysis was carried out on several films and the compositional analysis was shown to be invariant with deposition time. The average film composition is displayed below in table 4.4b.

Table 4.4b Average composition of vanadium oxynitride films deposited for 15, 20, 30, 60 and 210 seconds (0.42 $dm^3\ min^{-1}$ $VOCl_3$ at 500 °C and 10 $dm^3\ min^{-1}$ process gas flow).

Element	Atomic Percentage
Vanadium	40.81 (±0.1)
Nitrogen	21.03 (±0.5)
Oxygen	37.85 (±0.65)
Carbon	0.36 (±0.06)
Chlorine	0

These elemental percentages suggest a composition close to $VON_{0.5}$, which would indicate a mix of V^{3+} and V^{4+}. The XPS chemical shift for vanadium consistently appears at 513.2 eV, a value expected for vanadium in a low oxidation state.

Visually, the films changed considerably as the deposition time was altered. A fifteen second deposition leads to a dark, metallic, transparent film that is uniform over the whole substrate. A 210 s deposition time produced a black, metallic, reflective coating which was non-transparent. Some small pinholes where dust and prereacted material had landed on the substrate during deposition were also observed for the 210 s run.

The film produced over a 210 s period was thick enough to run an electron probe colour mapping experiment on it. The result of this is shown in the photograph in fig 4.4c.

Fig. 4.4c Electron probe colour mapping to show VO_xN_y film thickness (0.42 $dm^3\ min^{-1}$ $VOCl_3$ at 500 °C and 10 $dm^3\ min^{-1}$ process gas flow).

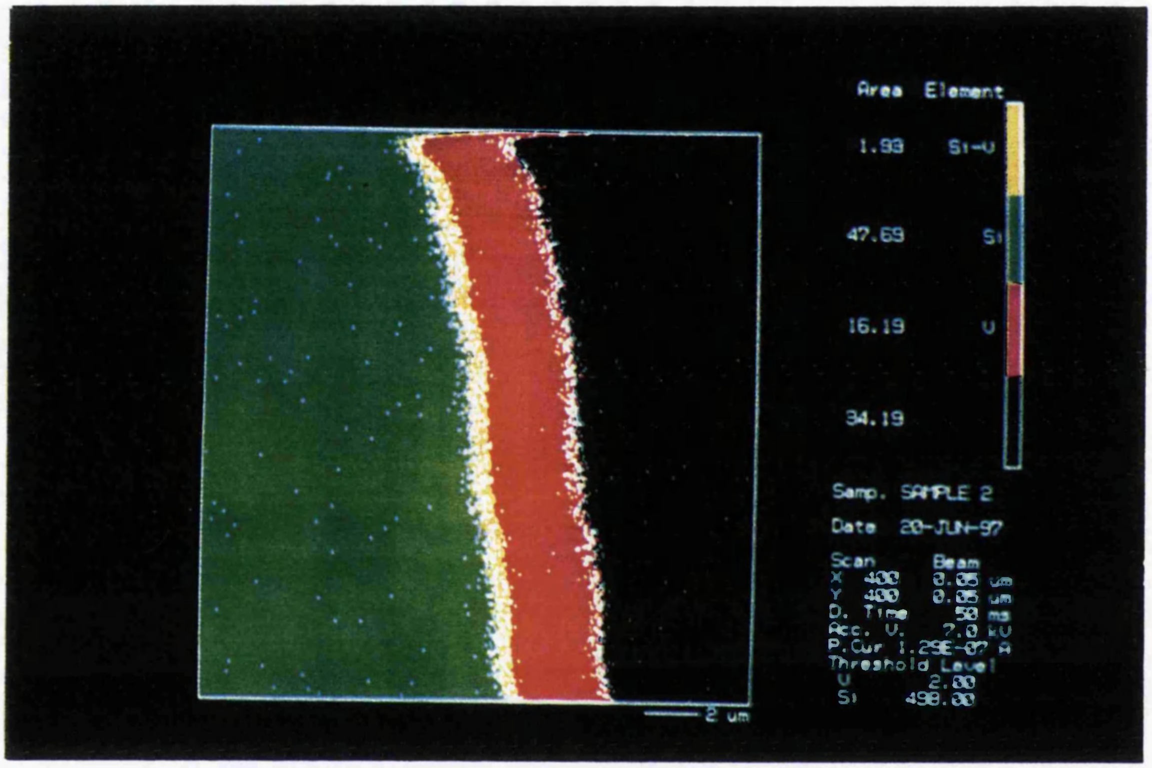

KEY (Green : silicon present. Red : vanadium present)

The clear boundary between the vanadium and silicon (in fig. 4.4c), shows that no vanadium is absorbed into the substrate or silicon absorbed into the coating. The thickness of this film is 1.68 μm. This enables us to correlate the thickness of some of the other vanadium oxynitride films produced in this work with the SEM film thickness measurements. The approximate thicknesses of the films produced in this time study are listed in table 4.4d below. These values are only approximate, but are the best estimate based on the information available. Some correlating SEM and step measurement data was obtained, although diamond polishing (needed for preparation of the sample) lead to the films peeling away and some inconsistent results.

Table 4.4d Estimates of VO_xN_y film thickness from electron probe and SEM measurements.

Deposition Time (s)	Approximate Thickness
15	120 nm
20	160 nm
25	200 nm
30	240 nm
60	480 nm
210	1680 nm

The four-probe resistance readings are affected by the thickness of the film (table 4.4e).

Table 4.4e Four-probe readings for varying growth time (0.42 $dm^3 min^{-1}$ $VOCl_3$ at 500 °C and 10 $dm^3 min^{-1}$ process gas flow).

Deposition Time (s)	Four-Probe Reading (Ω/□)
15	57
20	57
25	44
30	39
60	15
210	5

From these results it can be seen that the conductivity of the films increases with growth time. These results can be compared with those from vanadium nitride films in section 3.5 where a four-probe reading of 70 Ω/□ was achieved with a film deposited over 60 seconds. The result from the vanadium oxynitride equivalent is almost 5 times lower at 15 Ω/□. Visually the films look very similar.

The XRD spectra for the thicker films are expected to show better quality patterns as the glancing angle x-ray beam is only passing through the deposited film and not through the amorphous glass material. This will be achieved if the film is thicker than approximately 300 nm. The spectra that have been collected for the growth time study are displayed in fig. 4.4f.

Fig. 4.4f XRD spectra from films grown for 30 and 210 seconds (0.42 dm^3 min^{-1} $VOCl_3$ at 500 °C and 10 dm^3 min^{-1} process gas flow).

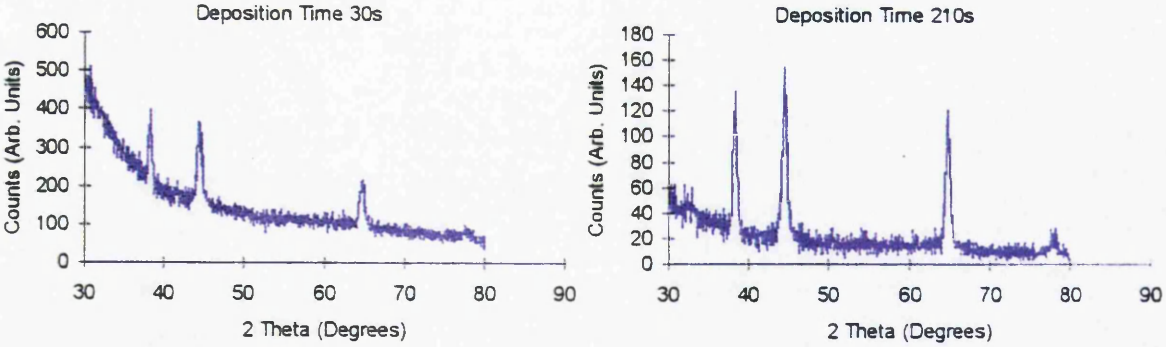

As can be seen from the data in fig 4.4f, the broad reflection at ~30 ° due to the amorphous character of the glass is much less apparent for the film deposited over 210 seconds than for the one prepared over 30 seconds. According to the estimated thicknesses in table 4.4e, the film deposited over 30 seconds is only 240 nm thick, which ties in with the theory mentioned earlier that films under 300 nm thick are thin enough for the x-ray beam to be analysing the amorphous glass substrate as well as the film on the surface. The slight rise to the left of the XRD spectrum for the film deposited over 210 seconds is probably due to some amorphous character in the actual film.

The films prepared in this study have been indexed. The XRD spectra show a preferred growth in the (1 1 1) direction. The lattice parameters and crystallite sizes for vanadium oxynitride films grown for 30, 60 and 210 seconds have been calculated (table 4.4g).

Table 4.4g Lattice parameters and crystallite sizes for VO_xN_y films in ammonia study (0.42 $dm^3 min^{-1}$ $VOCl_3$ at 500 °C and 10 $dm^3 min^{-1}$ process gas flow).

Growth time (s)	Lattice parameter *a*	Crystallite size Å
30	4.069	201
60	4.060	214
210	4.065	173

The values in table 4.4g show that the crystallite sizes and lattice parameters are not particularly affected by varying the growth time.

Reflectance and transmission spectra were collected from the films of different thickness to discover whether the thinner films in particular had any potential as heat-control mirrors. The results are displayed in fig. 4.4h.

Fig. 4.4h Reflectance and transmission data for films with varying thickness (0.42 dm^3 min^{-1} $VOCl_3$ at 500 °C and 10 dm^3 min^{-1} process gas flow).

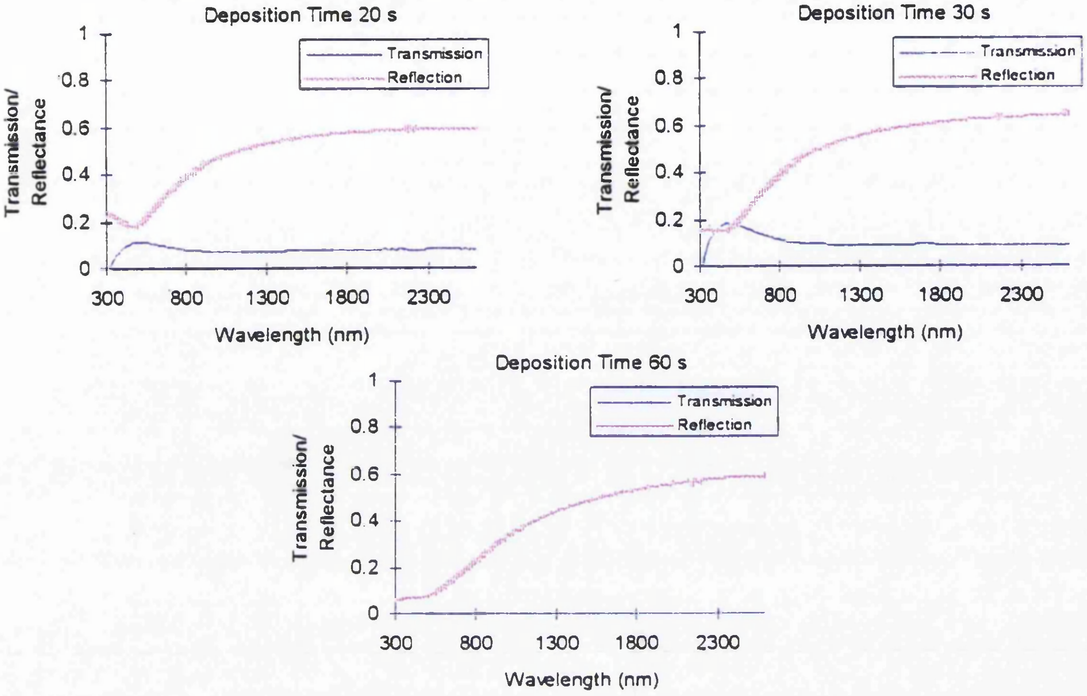

These spectra show that the IR reflectance properties stay remarkably similar whatever deposition time is used, while the visual transmission is obviously a lot poorer for thicker films. The film deposited over 210 seconds shows virtually no transmission at any wavelength. Contrary to the results for vanadium nitride films in section 3.5, IR reflectance doesn't deteriorate to the same extent for thinner films.

4.5 Effect of annealing

As with vanadium nitride films, it was interesting to discover whether the effect of annealing vanadium oxynitride films under a flow of ammonia would have an effect on the appearance and composition of the film. In this study two films were prepared. Both films were deposited at 350 °C for only 20 seconds. This time length was selected based on results from section 4.4; it was felt that longer depositions led to films that were too thick for heat-mirror application. The films were annealed at 650 and 500 °C respectively under a nitrogen / ammonia flow for one hour. The other conditions utilised in the experiment are displayed in table 4.5a.

Table 4.5a Deposition conditions for annealing study on VO_xN_y films.

Variable	Level fixed at
Deposition Temp.	350 °C
Bubbler Temp.	98 °C
Ammonia Flow	0.8 $dm^3\ min^{-1}$ (0.0164 mols)
Flow through Bubbler	0.42 $dm^3\ min^{-1}$ (0.0068 mols)
Process flow	10 $dm^3\ min^{-1}$
N_2/NH_3 flow	1.2 $dm^3\ min^{-1}$
Time of deposition	20 seconds

The visual appearance of these two films was very different. The film annealed at 650 °C was very reflective and was fairly dark and metallic in appearance. The film annealed at 500 °C had poor reflectivity and a non-metallic appearance.

The composition of the film annealed at 650 °C as determined by XPS analysis is displayed below in table 4.5b.

Table 4.5b XPS analysis of annealed film (0.42 $dm^3\ min^{-1}$ $VOCl_3$ and 0.8 $dm^3\ min^{-1}$ ammonia).

Element	Annealed at 650 °C At. %
Vanadium	49.44
Nitrogen	33.76
Oxygen	14.16
Carbon	2.64
Chlorine	0.00

The vanadium XPS chemical shift for the 650 °C sample was observed at 512.80 eV suggesting much more vanadium metal character (V metal: 512.14 eV) than vanadium nitride character (514.3 eV). This chemical shift is lower than vanadium chemical shifts observed for other films deposited from $VOCl_3$ and NH_3 that invariably have a vanadium chemical shift above 513 eV.

The results from this data (table 4.5b) more or less confirm what was speculated in section 3.6. Annealing under ammonia at high temperatures leads to nitrogen-oxygen exchange within the crystal lattice. This nitrogen-oxygen exchange is evident, as an oxygen percentage of 15 % or lower would be low for a film prepared from VCl_4 and NH_3, whereas films prepared from $VOCl_3$ / NH_3 typically have a much higher oxygen content of the order of 35-40 %. It appears that this transfer can only take place at high temperatures as the film annealed at 500 °C has retained the appearance and composition of a film deposited at 350 °C and cooled without annealing.

The four-probe resistance measurements further confirm this, as the reading for the film annealed at 650 °C is 55 Ω/□, whereas the reading for the film annealed at 500 °C is 750 Ω/□. As the films are both of the same thickness, these measurements correspond to quite a difference in the conductivity of the films. The thickness of these films is around 160 nm.

Figure 4.5c XRD spectra for annealing study (0.42 dm^3 min^{-1} $VOCl_3$ and 0.8 dm^3 min^{-1} ammonia).

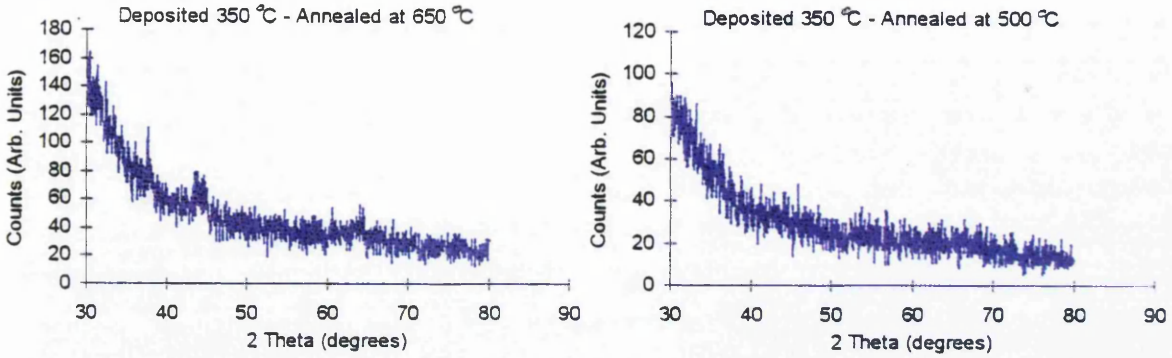

Neither of the annealed films prepared from $VOCl_3$ / NH_3 are very crystalline, although they are both thin. It is possible that a higher degree of crystallinity could have been achieved with a longer annealing time. The film annealed at 650 °C does show very weak peaks, which have been indexed. The lattice parameter, *a*, has been calculated as 4.124 Å and the crystallite size is 71 Å. Both of these figures should be treated with caution.

The transmission and reflectance spectra obtained for the annealed films are displayed in fig 4.5d.

Fig. 4.5d Transmission and reflectance spectra for VO_xN_y annealed films (0.42 dm^3 min^{-1} $VOCl_3$ and 0.8 dm^3 min^{-1} ammonia)

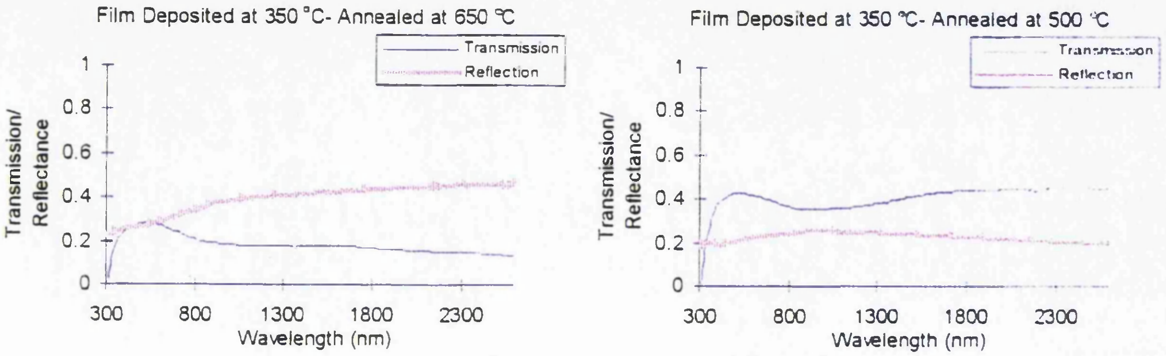

These spectra again confirm what has been shown before in this study about the film annealed at 500 °C. It appears that 500 °C isn't a high enough temperature to have much affect on a film which has been deposited at 350 °C. However, 650 °C is a sufficiently high annealing temperature to allow the crystal structure to reform on the surface of the glass and even accept nitrogen-oxygen transfer into its lattice. The heat-mirror qualities are present in the film annealed at 650 °C but are not particularly good. This is perhaps due to the lower atomic percentage of oxygen present. Earlier films in this chapter have shown much more promise as heat-control mirrors, with higher amounts of oxygen present in the crystal structure.

4.6 Summary of vanadium oxynitride films

The composition of films obtained from the reaction of $VOCl_3$ and NH_3 can change dependent on reaction conditions. The oxygen concentration in the VO_xN_y films is lower when the substrate temperature is high or when the ammonia flow rate is high. The nitrogen concentration is lower when the substrate temperature is low or the ammonia flow rate is low. The oxygen concentration (x) varied between 0.29 and 1.22. The nitrogen concentration (y) varied between 0.43 and 0.68. The lowest carbon and chlorine contamination was found for films deposited at 450 °C or above.

Crystallinity increased with substrate deposition temperature and deposition time.

The best sheet resistance measurements were recorded for films deposited above 500 °C with high ammonia flow rates, and low process gas flow rates.

The largest crystallite sizes were observed when the substrate temperatures were 500 °C and above.

The films with the best heat-control mirror properties were those deposited at substrate temperatures of 450 to 550 °C. Infrared reflectance was better for films prepared with higher deposition temperatures and lower process gas flow rates. High ammonia flow rates also lead to improved IR reflectance. IR reflectance was not particularly affected by growth time. The best all-round heat mirror qualities were found for a film prepared at 500 °C with a high process gas flow rate and low ammonia flow rate.

Annealing lead to films of composition close to that of vanadium nitride. This occurred through nitrogen-oxygen substitution. This only took place at high annealing temperatures. Annealing did not improve heat-control mirror properties.

It is difficult to compare this work to previously published work as no study of VO_xN_y films has been previously undertaken. In one of the few papers regarding the synthesis of vanadium oxynitride, Raskolenko *et al*[55] have reported vanadium oxynitride prepared by self-proprogating high temperature synthesis. The lattice parameters for the material produced was in the range a = 4.076 Å to a = 4.128 Å, equivalent to the range of lattice parameters that have been observed in this thesis, however their work has concentrated on VO_xN_y as a bulk material rather than a thin film, as presented here. Zaninulin *et al*[56] reported a wide range of stoicheometries from $VN_{0.11}O_{1.20}$ (a = 4.076 Å), to $VN_{0.93}O_{0.12}$ (a = 4.128 Å) for bulk vanadium oxynitride. These stoicheometries compare to those reported in this thesis from $VN_{0.43}O_{1.22}$ (amorphous), to $VN_{0.68}O_{0.29}$ (a = 4.124 Å).

In summary the vanadium oxynitride films prepared in this thesis compare very well with results cited elsewhere in the literature, although this appears to be the first time that VN_xO_y has been specifically deposited as a thin film.

Chapter 5

Thin Films of Chromium Oxide and Oxynitride

5.1 Experimental details

The APCVD experimental conditions for chromium oxynitride and oxide film deposition is identical to the procedure described in chapter 3 (section 3.1) except for the following changes:

Chromyl chloride (CrO_2Cl_2) was purchased from Aldrich (99 %). It is a red liquid with boiling point 117 °C.

Bubbler temperatures were set to around 77 °C as this provided a good vapour pressure of chromyl chloride (see figure 2.2b).

The intended coating from this series of experiments is chromium oxynitride (CrO_xN_y). Prior to this work, CrO_xN_y has not been reported.

Chromyl chloride is a highly oxidising and air sensitive liquid. It was provided by Aldrich Chemical Co. in glass ampoules. To add CrO_2Cl_2 to the bubbler meant first preparing the bubbler by purging with nitrogen for several minutes. The seal around the lid of the bubbler was loosened. The top of the ampoule was scored with a glass knife. The lid to the bubbler was removed and the nitrogen flow stopped and the contents of the ampoule quickly poured into the bubbler vessel. The lid to the bubbler was replaced and the seals tightened. Finally, a small flow of nitrogen (ca. 0.2 dm^3 min^{-1}) was allowed to pass through the bubbler and its contents. This entire process was completed within 5-10 seconds in order to minimise air reacting with the precursor.

The proposed equation for the APCVD reaction of chromyl chloride and ammonia is shown in equation 5.11.

$$6\ CrO_2Cl_2 + 8\ NH_3 \rightarrow 6\ CrO_xN_y + 12\ HCl + 6\ H_2 + (4\text{-}3y)\ N_2 + (6\text{-}3x)\ O_2 \quad \text{(eq. 5.11)}$$

5.2 Effect of coater temperature

This study was carried out to look into the effects of changing the substrate temperature on the final composition of the film. In the previous work described in this thesis, films prepared at lower temperatures were amorphous, had high levels of contamination and didn't have heat mirror qualities comparable to the same materials prepared at higher temperatures. The purpose of this study was to find out at what deposition temperature chromium oxynitride films became crystalline and how the composition and optical properties of the film changed with deposition temperature. As before, films were deposited from the chromyl chloride precursor at coater temperatures of 350, 450, 550 and 650 °C. The deposition conditions used in the experiments are displayed in table 5.2a.

Table 5.2a Deposition conditions for the reaction of chromyl chloride with ammonia for coater temperature variance study.

Variable	Level fixed at
Bubbler Temp.	77 °C
Time of Run	240 seconds
Flow through Bubbler	0.25 dm^3 min^{-1} (0.0146 mols)
Process flow	6 dm^3 min^{-1}
NH_3 Flow	0.2 dm^3 min^{-1} (0.0328 mols)
N_2/NH_3 flow	1.2 dm^3 min^{-1}

Ammonia was used in excess for these experiments, based on the results from previous chapters. The films were metallic-bronze in appearance, changing to a green/brown colour where the film was thicker. The uniformity for all films was poor with only the initial 5-10 cm of the substrate covered at all substrate temperatures. Similar to all the results quoted for VN and VO_xN_y coatings, adhesion to the surface of the substrate was excellent. Prereaction was a problem, as there was quite a high build up of green powder in the entrance flange to the coater. Despite this, there were no blockages during a 4-minute run.

XPS analysis was carried out on the films to monitor the effect of coater temperature on film composition. This analysis yielded an unexpected result. It was found that despite the use of ammonia, the final composition of the film contained no nitrogen, and in fact, produced a film made up of only chromium and oxygen. There are at least three distinct reported stoichiometries for chromium oxide. These are CrO_3, Cr_2O_3 and CrO_2. The XPS analysis result for the film deposited at 650 °C is shown in figure 5.2b.

Fig 5.2b XPS compositional analysis for film deposited from chromyl chloride (0.25 dm^3 min^{-1}) and ammonia (0.2 dm^3 min^{-1}) with a substrate temperature of 650 °C.

Element	At. % present
Chromium	39.85
Oxygen	59.8
Nitrogen	0
Carbon	0.3
Chlorine	0

This compositional analysis of the film prepared at 650 °C suggests a Cr_2O_3 film (expected: chromium 40 %, oxygen 60 %; found: chromium 39.85 %, oxygen 59.8 %) formed. A four-probe resistance device was used to determine the resistance of the chromium oxide films. This showed that all films were insulating.

Glancing angle XRD analysis was used to assess the crystallinity of the films. As can be seen from a representative spectrum (fig. 5.2c) the films were amorphous. The XRD results are puzzling, as chromium oxide films prepared by other methods at similar temperatures have shown crystallinity[84,85,87]. All glancing angle XRD analysis on chromium oxide films were run for 12 hours.

Fig. 5.2c XRD spectrum of film deposited from the reaction of chromyl chloride with ammonia at a substrate temperature of 650 °C (0.25 dm^3 min^{-1} CrO_2Cl_2 and 0.2 dm^3 min^{-1} NH_3).

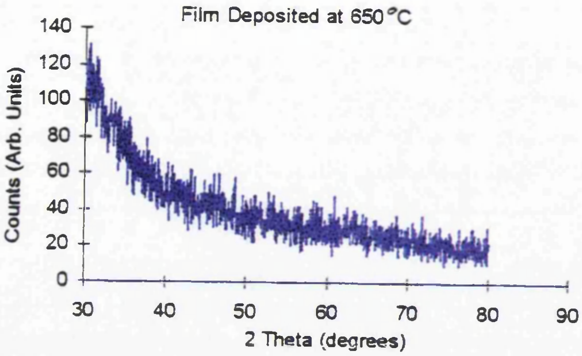

SEM photographs showed that the particle size wasn't really affected by a rise in substrate temperature. An SEM photograph of the film deposited at 650 °C is shown below in fig. 5.2d.

Fig. 5.2d SEM photograph of a Cr_2O_3 film deposited at 650 °C (0.25 dm^3 min^{-1} CrO_2Cl_2 and 0.2 dm^3 min^{-1} NH_3).

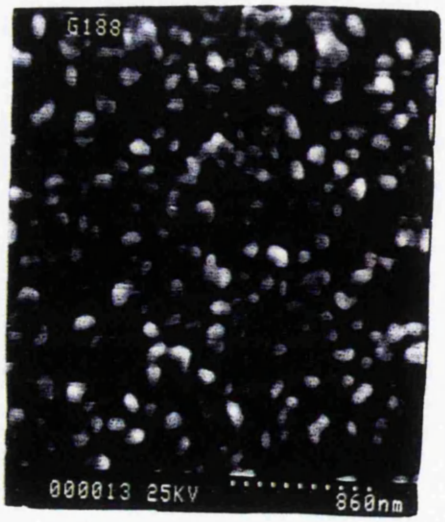

To complete this study the films were analysed for their heat mirror qualities. The transmission and reflectance spectra obtained from these films are displayed below in fig. 5.2e.

Fig 5.2e Transmission / reflectance spectra for coater temperature study ($0.25\ dm^3\ min^{-1}$ CrO_2Cl_2 and $0.2\ dm^3\ min^{-1}$ NH_3).

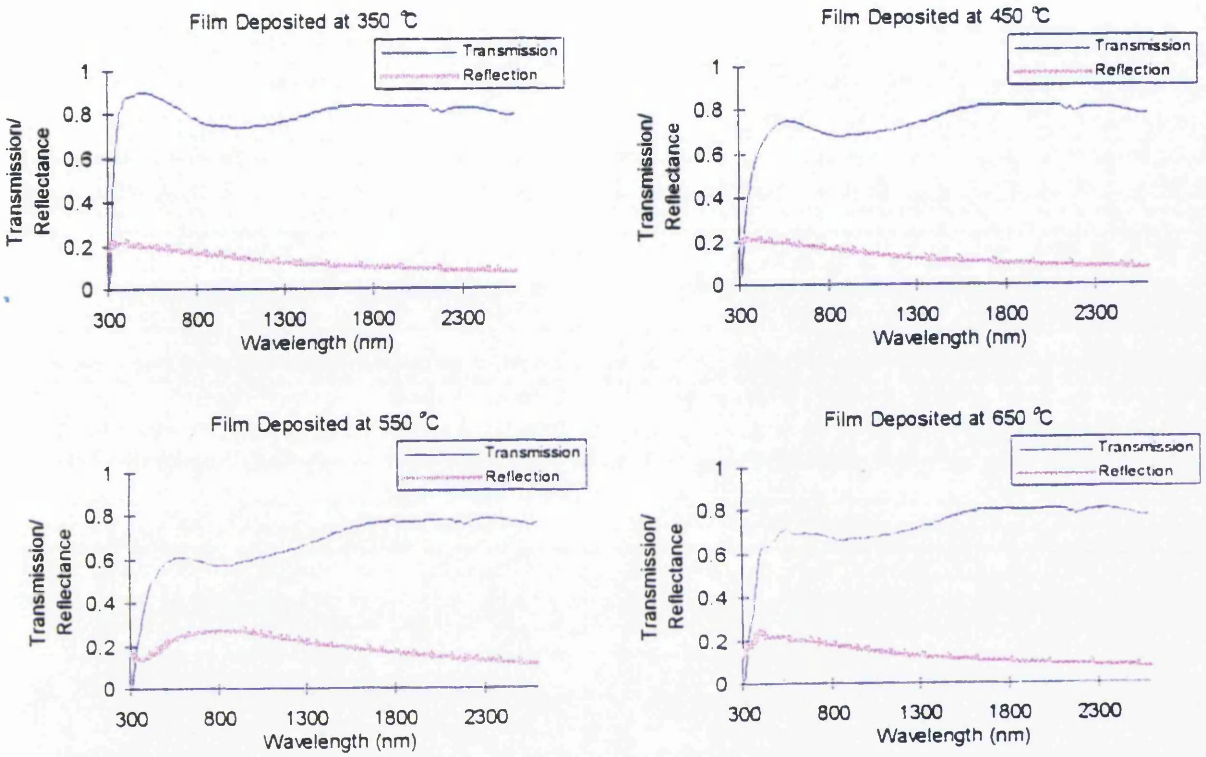

The spectra in fig. 5.2e show that the chromium oxide films deposited by APCVD at 350 – 650 °C cannot be used as heat-control mirrors. Their characteristics are not unlike the reflectance and transmission properties displayed by plain glass (see fig. 1.6c).

5.3 Effect of ammonia gas flow concentration

The results from section 5.2 show that there was no nitrogen incorporated into the films prepared from the reaction of CrO_2Cl_2 with NH_3 despite the use of excess ammonia in the deposition process. In this section the effects of changing the ammonia flow rate and coating without ammonia will be presented.

In this study films were deposited with an ammonia flow rate of 0, 0.2, 0.6 and 1 dm^3 min^{-1}. All other factors were kept constant. The conditions which weren't changed during the study are displayed below in table 5.3a.

Table 5.3a Conditions for ammonia flow rate study on films deposited from chromyl chloride and ammonia.

Variable	Level fixed at
Bubbler Temp.	77 °C
Time of Run	240 seconds
Flow through Bubbler	0.25 dm^3 min^{-1} (0.0146 mols)
Process flow	6 dm^3 min^{-1}
Substrate temp.	500 °C
N_2/NH_3 flow	1.2 dm^3 min^{-1}

A flow of rate of 1.0 dm^3 min^{-1} of ammonia for four minutes is equivalent to 0.164 moles. According to equation 5.11, chromyl chloride reacts with ammonia in a 1:1.33 ratio. Only 0.0146 moles of chromyl chloride should pass through the reaction chamber during the course of the reaction so the NH_3 is in excess with a flow of 0.2 dm^3 min^{-1}.

It was found that a film formed even when only CrO_2Cl_2 was used without ammonia. This was not really a surprise as the films prepared prior to this contained no nitrogen. The film deposited without ammonia had a completely different visual appearance to the films deposited in the presence of ammonia. The film deposited with no ammonia was dark green, appeared thick, and covered most of the substrate. The films deposited with ammonia were all thin, slightly metallic looking and covered the first few centimetres of the substrate.

The compositions of the films from XPS obtained from the reaction of CrO_2Cl_2 and ammonia with a flow rate of 0, 0.6 and 1.0 $dm^3 min^{-1}$ are shown in table 5.3b.

Table 5.3b Compositions of films deposited with varying ammonia flow (0.25 $dm^3 min^{-1}$ CrO_2Cl_2 at 650 °C).

Conditions/ Composition	Ammonia flow 0 $dm^3 min^{-1}$	Ammonia flow 0.6 $dm^3 min^{-1}$	Ammonia flow 1.0 $dm^3 min^{-1}$
Chromium	13.76	36.2	29.07
Oxygen	37.06	61.9	58.07
Carbon	49.18	0	0
Nitrogen	0	0	6.74
Chlorine	0	1.8	5.32

As can be seen from the data in table 5.3b, film composition is considerably different for those prepared in the presence of ammonia. The amount of nitrogen present in the films never exceeds 7 atomic %. The high percentage of carbon in the film deposited in the absence of ammonia is surprising. Indeed the XPS depth profile (fig. 5.3c) shows that the composition on the surface to be the same as it is in the bulk. It appears that the film is porous and highly reactive in air.

Fig 5.3c Depth profile of the film produced from APCVD reaction of CrO_2Cl_2 in the absence of ammonia (0.25 dm^3 min^{-1} CrO_2Cl_2 at 650 °C)

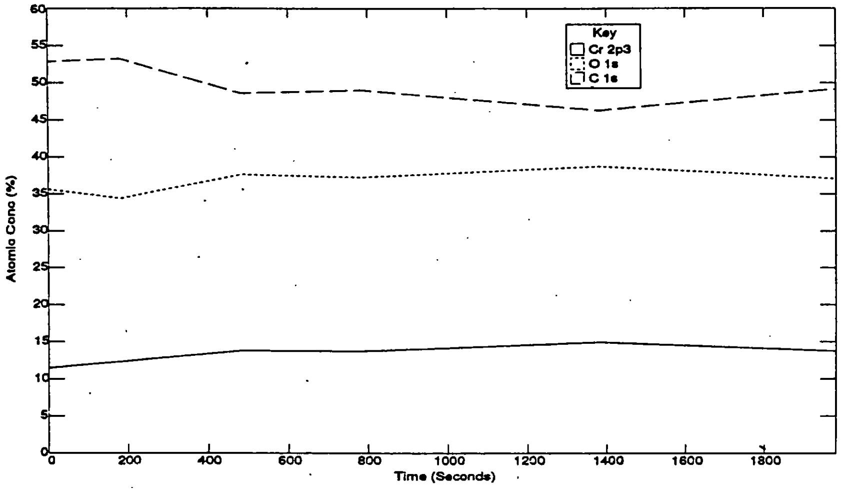

It appears from this study that the presence of ammonia somehow regulates the composition of the films. This could occur by ammonia facilitating the removal of contaminants and by-products during film deposition. A new equation for the reaction of chromyl chloride and ammonia consistent with these results is shown below (equation 5.31).

$$4CrO_2Cl_2 + 8NH_3 \rightarrow 2Cr_2O_3 + 6NH_4Cl + O_2 + N_2 + Cl_2 \quad \text{(eq. 5.31)}$$

Exceptionally high levels of ammonia result in some nitrogen incorporation in the film as shown by the film deposited with 1.0 dm^3 min^{-1} NH_3 (table 5.3b). Four-probe resistance measurements on all films prepared with a variable NH_3 flow show that they are insulating. Glancing angle XRD carried out on these films has shown some reflections for the film deposited without ammonia. The XRD spectra obtained from these films are shown below in fig. 5.3d.

Fig 5.3d XRD information for films deposited in varying flows of ammonia (0.25 dm^3 min^{-1} CrO_2Cl_2 at 650 °C).

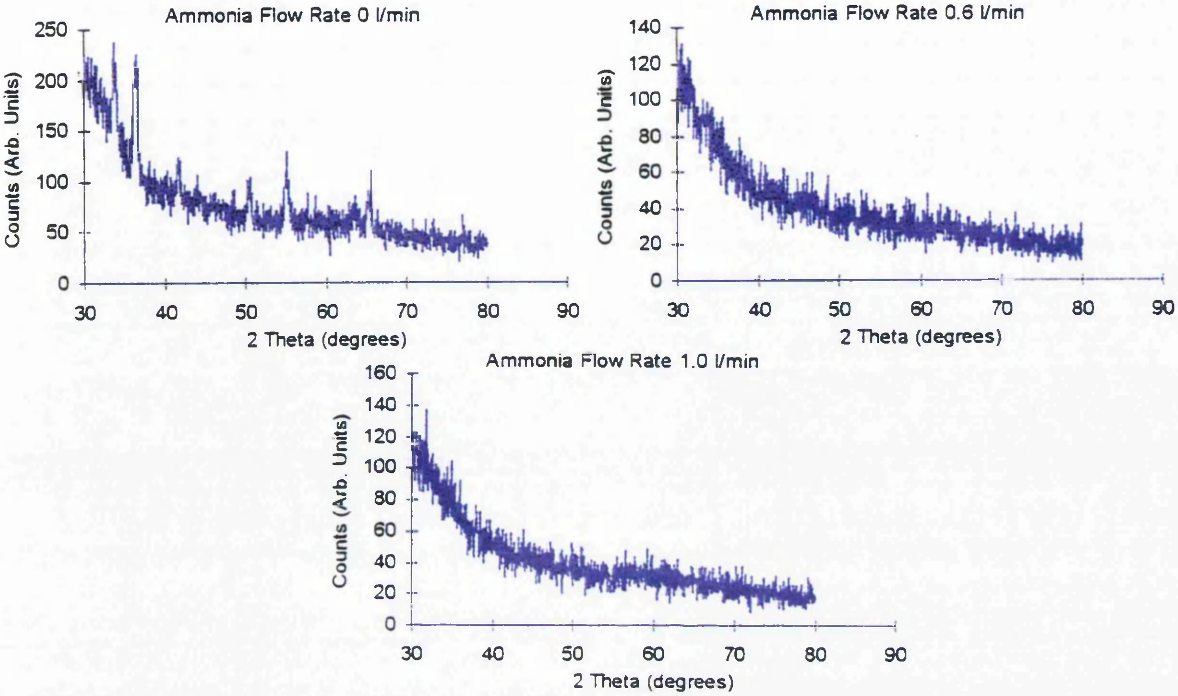

As can be seen from the spectra in fig.5.3d, only the film deposited in the absence of ammonia is crystalline. This XRD pattern relates closely to the pattern expected for Cr_2O_3. If some crystalline Cr_2O_3 is present, the extra carbon and oxygen in the film could have originated from the porous film reacting in air. Films deposited at higher flow rates of ammonia are amorphous. The reason for this is not known.

There is a definite difference in the appearance of the films produced with and without ammonia. Below, in fig 5.3e, SEM photographs from the film deposited with no ammonia and from the film deposited with 0.6 dm^3 min^{-1} ammonia are presented.

Fig 5.3e SEM of film prepared with no ammonia (1) and film deposited with 0.6 dm^3 min^{-1} ammonia (2) (0.25 dm^3 min^{-1} CrO_2Cl_2 at 650 °C).

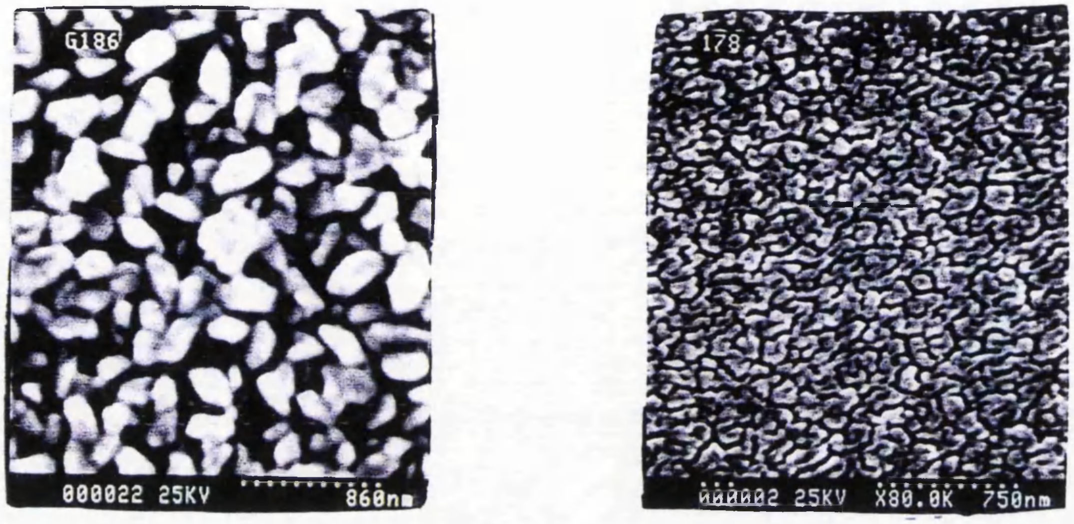

1 2

The transmission and reflectance spectra are displayed in fig. 5.3f.

Fig. 5.3f Transmission and reflectance spectra of films deposited from chromyl chloride and ammonia from the ammonia flow rate study (0.25 dm^3 min^{-1} CrO_2Cl_2 at 650 °C).

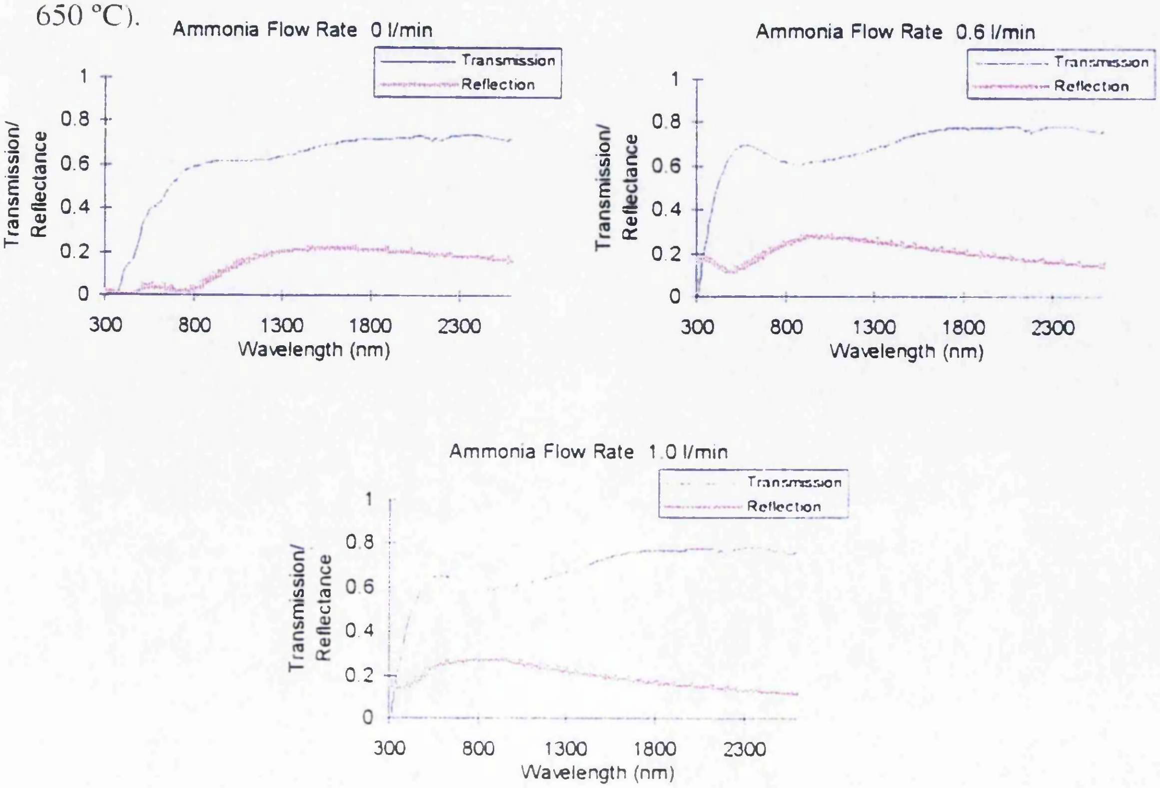

As can be seen from the spectra in fig 5.3f, the reflectance does rise slightly in the infrared region when no ammonia was used during deposition. It also rises where higher flow rates of ammonia have been used, but overall none of these films have optical properties that would make them suitable for use as heat-control mirrors.

5.4 Effect of process gas flow

Films in the previous sections have been prepared with a process gas flow of 6 dm^3 min^{-1}. This has led to attractive coatings, but also to a high build up of particulates at the entrance flange to the coater. The purpose of this study was to investigate what effect raising the process gas flow rate to 10 dm^3 min^{-1} had not only on the degree of prereaction but also to see how it affected the appearance and composition of the film. All factors were kept constant for this study other than the process gas flow rate. The conditions used for this study are displayed below in table 5.4a.

Table 5.4a Conditions for process gas variation study on films deposited from chromyl chloride and ammonia.

Variable	Level fixed at
Bubbler Temp.	77 °C
Time of Run	240 seconds
Flow through Bubbler	0.25 dm^3 min^{-1}
Ammonia flow	0.8 dm^3 min^{-1}
Substrate temp.	550 °C
N_2/NH_3 flow	1.2 dm^3 min^{-1}

The first thing of note from this study was the change in the visual appearance of the films. The film deposited with a process gas flow rate of 6 dm^3 min^{-1}, was bronze with mustard yellow areas at the sides where the film was thicker. It had good adhesion to the substrate surface and progressed only around 4-5 cm along the substrate. The film deposited under a process gas flow rate of 10 $dm^3 min^{-1}$ was also bronze, although it was lighter in colour than the film deposited with a process gas flow rate of 6 $dm^3 min^{-1}$, this film progressed 7 cm along the substrate. Adhesion and metallic lustre were maintained in both films.

In table 5.4b are details of the composition analysed by XPS.

Table 5.4b Composition of a film prepared with a 6 $dm^3 min^{-1}$ process gas flow rate (0.25 $dm^3 min^{-1}$ CrO_2Cl_2 and 0.8 $dm^3 min^{-1}$ NH_3 at 550 °C).

Element	At. % at 6 $dm^3 min^{-1}$
Chromium	37.28
Oxygen	61.53
Nitrogen	0
Chlorine	1.19
Carbon	0

The resistance, crystallinity and heat-control mirror qualities of the films grown at high process gas flow rate were equivalent to those films of chromium oxide prepared in the earlier sections.

5.5 Effect of growth times

As has already been shown in this chapter, the films produced from the reaction of chromyl chloride and ammonia lead to chromium oxide films, which are not crystalline and do not possess heat mirror properties. The purpose of this study was to see how the deposition time affected the visual appearance of the film and the particle size as observed by SEM.

Three deposition times were selected for this study - 120, 240 and 600 seconds. All other factors were kept constant and are listed in table 5.5a.

Table 5.5a Conditions for deposition time study on films deposited from chromyl chloride and ammonia.

Variable	Level fixed at
Bubbler Temp.	77 °C
Coater Temp.	550 °C
Flow through Bubbler	0.25 $dm^3\ min^{-1}$
Process flow	6 $dm^3\ min^{-1}$
NH_3 Flow	0.8 $dm^3\ min^{-1}$
N_2/NH_3 flow	1.2 $dm^3\ min^{-1}$

XPS analysis was used to ensure that the composition of the material was the same over each of the deposition times. The results of this and the amount by which the atomic percentage varied between the samples is shown below in table 5.5b.

Table 5.5b Composition of films produced from variable growth time studies (0.25 dm^3 min^{-1} CrO_2Cl_2 and 0.8 dm^3 min^{-1} NH_3 at 550 °C).

Element	At. %
Chromium	37.15 (±0.13)
Oxygen	59.5 (±2)
Nitrogen	0
Carbon	1.8 (±1.5)
Chlorine	1.8 (±0.6)

All the films appeared bronze/yellow in colour and, as expected, the film deposited over 120 seconds was a lot lighter than the film deposited for 600 seconds.

5.6 Summary of chromium oxide and oxynitride films

The preparation of chromium oxide films from APCVD has proved to be quite disappointing in terms of preparing a film of potential use as a heat-control mirror. None of the films deposited under the conditions described in this chapter have shown anything to suggest that they may have useful optical properties.

The composition of the films seems to vary very little from Cr_2O_3 regardless of the preparation conditions. The exception to this was, of course, the film prepared in the absence of ammonia, which had almost 50 % carbon contamination and films prepared with high excesses of ammonia which contained up to 7 % nitrogen.

None of the chromium oxide films displayed any crystallinity (apart from the film prepared without ammonia) as measured by x-ray diffraction or conductivity as determined by four-probe resistance measurements.

Chromium oxide films have been prepared before by several methods in the literature. Maruyama *et al*[84] prepared Cr_2O_3 thin films by APCVD from $Cr(CO)_6$ and air at temperatures as low as 150 °C (or 60 °C with UV radiation). The films they describe have high IR reflectance coupled with significant solar absorptance (necessary for the conversion of solar energy to heat). This was not the case for the films deposited from CrO_2Cl_2 and NH_3 in this chapter. However, Maruyama *et al* state that the morphology of the chromium oxide films are strongly dependent on the source material and ratio of precursors[84]. Various other Cr_2O_3 films prepared by Erben *et al*[85], Poznyak *et al*[86] and Lee *et al*[88,89] have been extensively investigated for use as photothermal energy converters, due to their high solar absorptance (α >0.95) and high IR reflectance.

To conclude this chapter, chromium oxide films have been prepared from the APCVD reaction of chromyl chloride and ammonia. Chromium oxide films prepared by this method do not display heat-mirror properties.

Chapter 6

Mixed Metal coatings

6.1 Experimental details

Note: This chapter refers to any film deposited from the reaction of VCl_4 and NH_3 as vanadium nitride (VN) despite the variation in compositions noted in chapter 3. The films deposited from the reaction of $TiCl_4$ and NH_3 are referred to as titanium nitride (TiN) films. The films deposited from the reactions of VCl_4, $TiCl_4$ and NH_3 are referred to as vanadium / titanium nitride.

Mixed metal coatings were attempted using $TiCl_4$ in one bubbler and VCl_4 in the second bubbler, to form V_xTi_yN. The second set of mixed metal films was attempted using $TiCl_4$ from the first bubbler and CrO_2Cl_2 in the second bubbler to deposit films of $Cr_xTi_yO_zN$. Films of V_xTi_yN have been grown before by sputtering as was discussed in section 1.7 but $Cr_xTi_yO_zN$ films have never previously been grown. None of these mixed metal coatings have been deposited on glass before or investigated as heat-control coatings. $TiCl_4$ was purchased from Aldrich (99.9%) in Sure-seal bottles and used as supplied.

To attempt mixed metal coatings, firstly films of TiN, VN and Cr_2O_3 were laid down to provide a comparison for resistance measurements, XRD analysis and transmission and reflectance measurements.

The bubbler temperatures were set depending on the precursor (table 6.1a).

Table 6.1a Bubbler temperatures for some mixed metal coating precursors.

Precursor	Temperature
$TiCl_4$	95 °C
VCl_4	118 °C
CrO_2Cl_2	77 °C

The experimental details for mixed metal coatings is generally the same as those described in section 3.1 except that this time there are two bubblers in use. The changes from the experimental details in section 3.1 are described below.

For the first time in this work both precursor bubblers were used simultaneously. The main changes were in the moments immediately preceding and following the coating. In section 3.1 the flow was diverted through the bubbler by closing the bypass valve then opening the bubbler outlet valve and finally opening the inlet to the bubbler to allow the nitrogen flow to bubble through the precursor material. This procedure is followed for mixed metal coatings as well, except this time the corresponding valves must be closed or opened on the second bubbler at exactly the same time as those on the first bubbler. The reverse of this procedure is performed at the end of the deposition. As the metal halides precursors do not react with each other there was considered to be no problem with the early mixing of the precursor gases after their exit from the bubblers. As before, prereaction occurs when the precursor gases meet the ammonia line just before their entrance to the coater.

6.2 Effect of coater temperature

6.20 Reaction conditions for mixed metal films.

To begin this study, films of titanium nitride were deposited at several coater temperatures. It was found that below 500 °C, titanium nitride films had very poor adhesion to the glass substrate, so films were deposited at 500, 550, 600 and 650 °C. This has been noted in previous literature (discussed in section 1.5) and is due to the incomplete decomposition of the $TiCl_4$ / NH_3 complex. Films of vanadium nitride were also deposited at these four temperatures under identical conditions. Finally a mixed metal film was deposited with bubbler flow rates that together made up the same overall mass flow as had been used for the single metal coatings. The conditions used are summarised below in table 6.20a.

Table 6.20a Conditions for coater temperature study on mixed metal films

Variable	TiN films	VN films	Cr_2O_3 films	V_xTi_yN films	$Cr_xTi_yO_zN$ films
Bubbler 1 Temp	-	118 °C	77 °C	118 °C	77 °C
Bubbler 2 Temp	95 °C	-	-	95 °C	95 °C
Time of Run	30 secs	30 secs	4 mins	30 secs	1 min
Bubbler 1 flow	-	0.42 dm^3 min^{-1} (0.00735mols)	0.25 dm^3 min^{-1} (0.015mols)	0.33 dm^3 min^{-1} (0.0058mols VCl_4)	0.25 dm^3 min^{-1} (0.0037 mol CrO_2Cl_2)
Bubbler 2 flow	0.42 dm^3 min^{-1} (0.0036 mols)	-	-	0.1 dm^3 min^{-1} (0.00086 mols $TiCl_4$)	0.1 dm^3 min^{-1} (0.0017 mols $TiCl_4$)
Process flow	10 dm^3 min^{-1}	10 dm^3 min^{-1}	6 dm^3 min^{-1}	10 dm^3 min^{-1}	6 dm^3 min^{-1}
NH_3 Flow	0.5 dm^3 min^{-1} (0.00103mols)	0.5 dm^3 min^{-1} (0.00103mols)	0.5 dm^3 min^{-1} (0.082 mols)	0.5 dm^3 min^{-1} (0.00103 mols)	0.5 dm^3 min^{-1} (0.0021 mols)
N_2/NH_3 flow	1.2 dm^3 min^{-1}	1.2 dm^3 min^{-1}	1.2 dm^3 min^{-1}	1.2 dm^3 min^{-1}	1.2 dm^3 min^{-1}

The data in figure 6.20a shows that the bubbler flow rates are different in the mixed metal depositions. This was to see if one of the metals was more prominent in the final film. For example, for the mixed Ti/V film, six times more VCl_4 is reaching the deposition chamber than $TiCl_4$. If there is the same chance of each of the precursors reacting there should be six times as much vanadium as titanium in the final film.

In the same way, for the mixed Cr/Ti films, twice as much CrO_2Cl_2 should reach the reaction chamber as $TiCl_4$. The deposition times had to be altered from the individual depositions for chromium oxide and titanium nitride because a one minute coating of titanium nitride lead to a very thick film while a one minute coating of chromium oxide lead to a very thin film. A one-minute deposition time was chosen for the combined chromium / titanium oxynitride depositions.

6.21 Effect of coater temperature on titanium nitride films

As discussed in previous sections, titanium nitride films were deposited as amorphous, non-adhesive layers at substrate temperatures below 500 °C. The appearance of the films ranged from orange/brown with poor adhesion and uniformity at 500 °C to very dark brown/black films at 650 °C. Unlike the vanadium nitrides and oxynitrides the films were not visually metallic or reflective but were very dark and fairly uniform in thickness

Four probe resistance measurements changed as the substrate temperature was increased. The variation in 4-probe resistance measurement as a result of changing coater temperature is shown below in table 6.21a.

Table 6.21a Resistance measurements vs. coater temperature for titanium nitride films (0.42 dm^3 min^{-1} $TiCl_4$ and 0.5 dm^3 min^{-1} NH_3).

Temperature (°C)	Four-Probe Reading (Ω/□)
500	762
550	208
600	13
650	4

The four-probe reading obtained from the film deposited at 650 °C from the reaction of $TiCl_4$ and NH_3 is extremely low, however this film was thick and had no visual transmission (figure 6.21b).

Fig. 6.21b Transmission / reflectance spectra of TiN films deposited at variable coater temperatures (0.42 dm^3 min^{-1} $TiCl_4$ and 0.5 dm^3 min^{-1} NH_3).

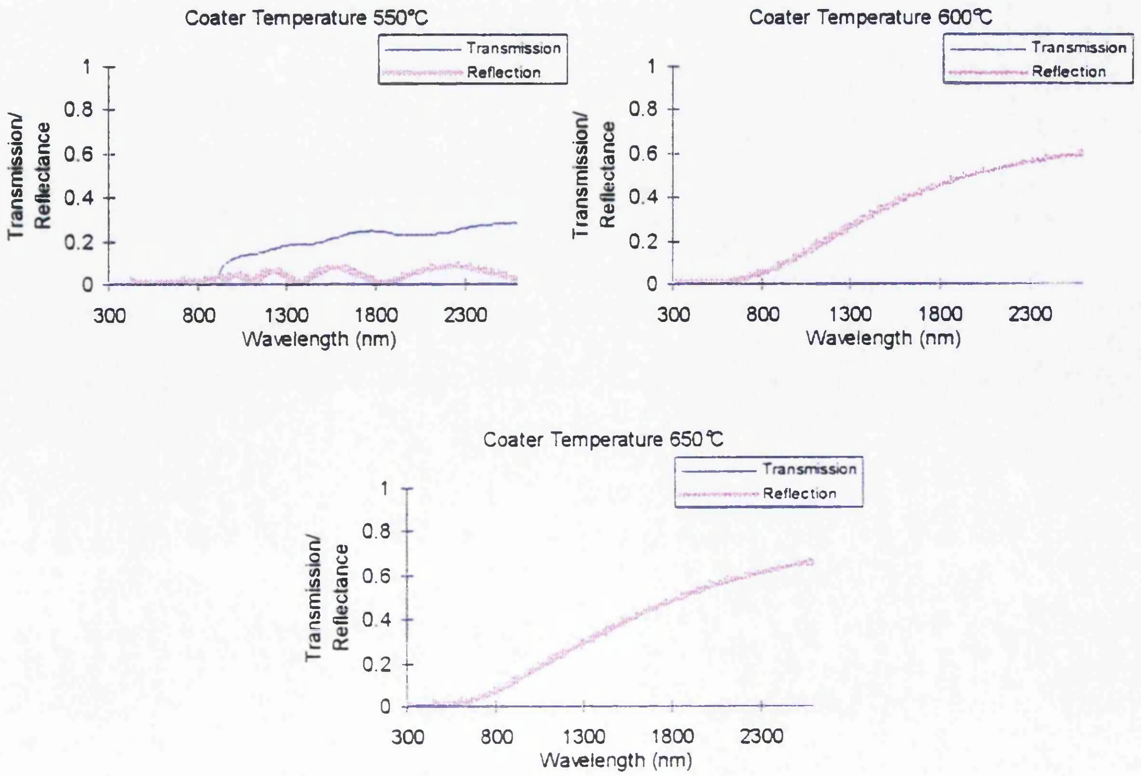

As can be seen from the spectra in fig 6.21b, at higher substrate temperatures, the films are too thick for any transmission in the visible or infrared regions. The reflectance properties of the films deposited at 600 and 650 °C are excellent and show why titanium nitride films have been extensively investigated as solar-control coatings.

6.22 Vanadium nitride films

The properties and composition of vanadium nitride films have been investigated as a function of coater temperature in chapter 3.2, however in this section, the conditions used to deposit TiN films were used. The films were deposited at 500, 550, 600 and 650 °C.

The visual appearance of the films did not change with rising deposition temperature. The films remained grey / black in colour with a metallic appearance. The composition of the films, as determined by XPS are shown in table 6.22a.

Table 6.22a Change in composition of vanadium nitride films with varying deposition temperature (0.42 $dm^3\ min^{-1}$ VCl_4 and 0.5 $dm^3\ min^{-1}$ NH_3).

Element	At. % at 500 °C	At. % at 550 °C	At. % at 650 °C
Vanadium	46.54	41.85	37.8
Nitrogen	31.17	30.3	26.92
Oxygen	19.50	24.41	27.74
Carbon	2.8	4.44	5.54
Chlorine	0	0	0

The four-probe resistance measurements for the VN films, increase with deposition temperature, as shown in table 6.22b.

Table 6.22b Resistance measurements vs. coater temperature for vanadium nitride films (0.42 dm^3 min^{-1} VCl_4 and 0.5 dm^3 min^{-1} NH_3).

Temperature (°C)	Four-Probe Reading (Ω/□)
500	116
550	149
600	282
650	222

These measurements show that four-probe resistance readings for vanadium nitride films are higher than those recorded for corresponding titanium nitride films deposited at equivalent temperatures. This is expected, as bulk titanium nitride has a lower resistance than bulk vanadium nitride[83]. However, the reason for the difference in resistance in the thin films is due to changes in thickness (as determined by SEM measurements). The VN films deposited at 500 °C were of the order of 300 nm thick. The titanium nitride films deposited at 500 °C were of the order of 600 nm

.

The transmission and reflectance data obtained from VN films is shown in fig. 6.22c.

Fig. 6.22c Transmission and reflectance spectra for VN films at varying substrate temperatures (0.42 dm^3 min^{-1} VCl_4 and 0.5 dm^3 min^{-1} NH_3)

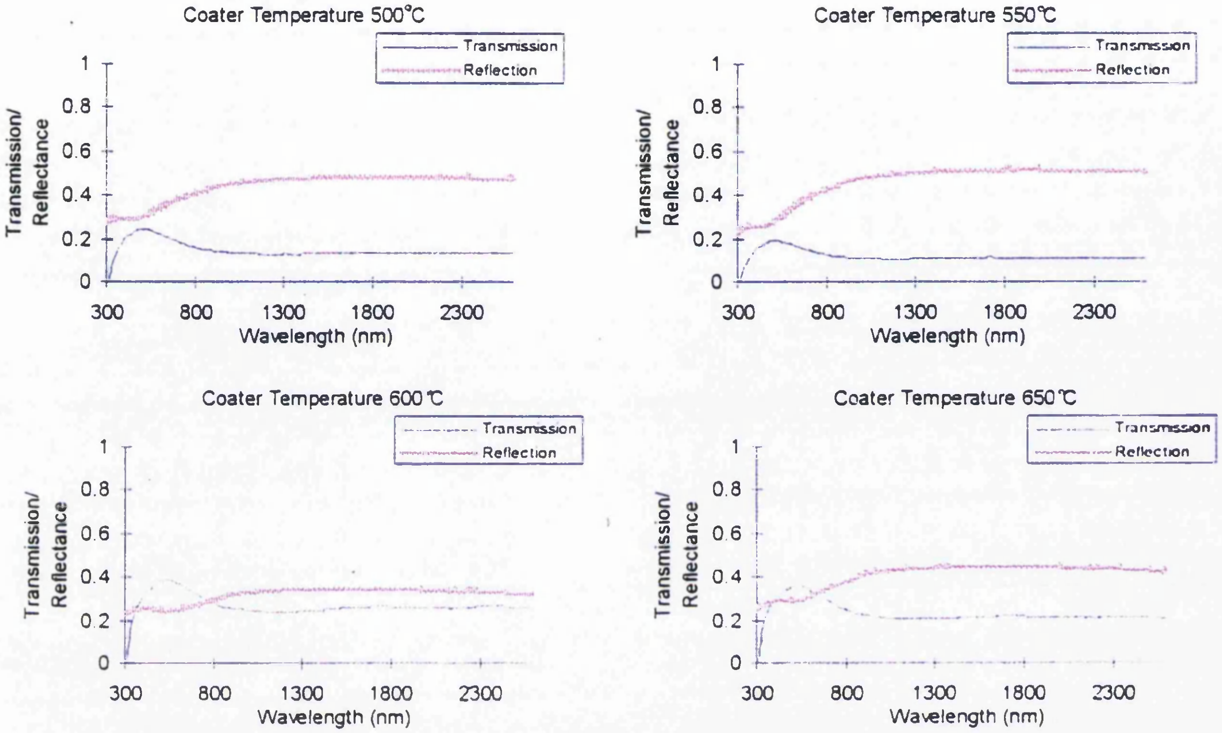

The spectra in fig. 6.22c show that for deposition temperatures from 350 °C to 550 °C the transmission and reflectance properties of vanadium nitride films are better than the corresponding titanium nitride films. At higher temperatures, assuming the films aren't too thick the optical properties are better in titanium nitride films. A full study of titanium nitride films on glass substrates of a similar type to that used in this thesis has been conducted[40].

6.23 Chromium oxide films

Chromium oxide films have been investigated with increasing coater temperature in section 5.2, but in this section they were investigated at 500, 550, 600 and 650 °C under similar conditions to those used to deposit mixed chromium / titanium oxynitride films. Four minute coatings were needed to produce a film of adequate thickness for analysis (~200 nm), even though a one minute coating was used for the mixed metal coating.

The films were light brown in colour with a metallic lustre. The only visible change with increasing coater temperature was the proportion of the substrate coated. At higher deposition temperatures the coating covered a smaller surface area of the substrate.

As has already been seen in chapter 5, chromium oxide films are non-conducting, amorphous and have poor optical properties. Fig. 6.23a shows the transmission / reflection spectra for chromium oxide films deposited with varying coater temperature.

Fig. 6.23a Transmission / reflectance data for chromium oxide films at varying coater temperature (0.25 dm^3 min^{-1} CrO_2Cl_2 and 0.5 dm^3 min^{-1} NH_3).

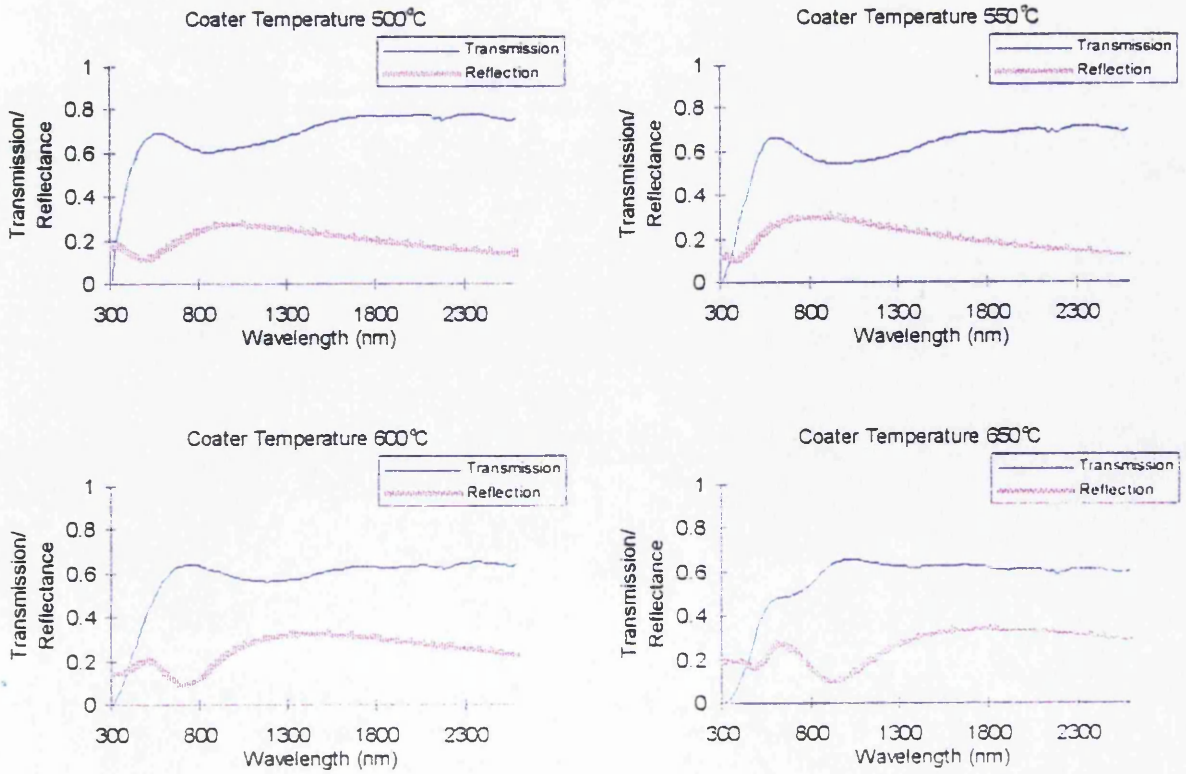

6.24 Vanadium / titanium nitride films

The conditions used for deposition of individual titanium nitride and vanadium nitride films were combined for the deposition of mixed vanadium / titanium nitride films. The conditions that were used for these depositions are shown in table 6.20a.

Mixed metal vanadium / titanium films inherited many of the characteristics of the individual metal nitrides films. At 500 °C the film was bronze in colour and not particularly adherrant to the surface of the glass and was akin to the titanium nitride films deposited at 500 °C. At higher deposition temperatures, the films took on the metallic appearance of vanadium nitride films, although they retained the bronze colour of titanium nitride films.

The composition of the mixed metal films at 550 and 650 °C, as determined by XPS, are displayed in table 6.24a.

Table 6.24a Change in the composition of titanium nitride films with variable deposition temperature (0.33 dm^3 min^{-1} VCl_4, 0.1 dm^3 min^{-1} $TiCl_4$ and 0.5 dm^3 min^{-1} NH_3).

Element	At. % at 550 °C	At. % at 650 °C
Titanium	36.8	34.1
Vanadium	4.5	1.01
Nitrogen	49.2	46.5
Oxygen	7.8	13.1
Carbon	0	5.4
Chlorine	1.7	0

These figures show that as the temperature of the coater is increased the level of carbon and oxygen contamination also increases. Interestingly, despite the high flow through the vanadium tetrachloride bubbler (six times more VCl_4 reaches the reaction chamber than $TiCl_4$), it is the titanium which is preferentially coated onto the substrate.

Glancing angle X-ray diffraction has been carried out on these films to show that the same cubic structure obtained for TiN and VN films is still present for the mixed vanadium / titanium nitride film. The spectra obtained from the mixed metal films are shown in figure 6.24b.

Figure 6.24b XRD spectra from mixed metal films prepared at variable coater temperatures (0.33 dm^3 min^{-1} VCl_4, 0.1 dm^3 min^{-1} $TiCl_4$ and 0.5 dm^3 min^{-1} NH_3).

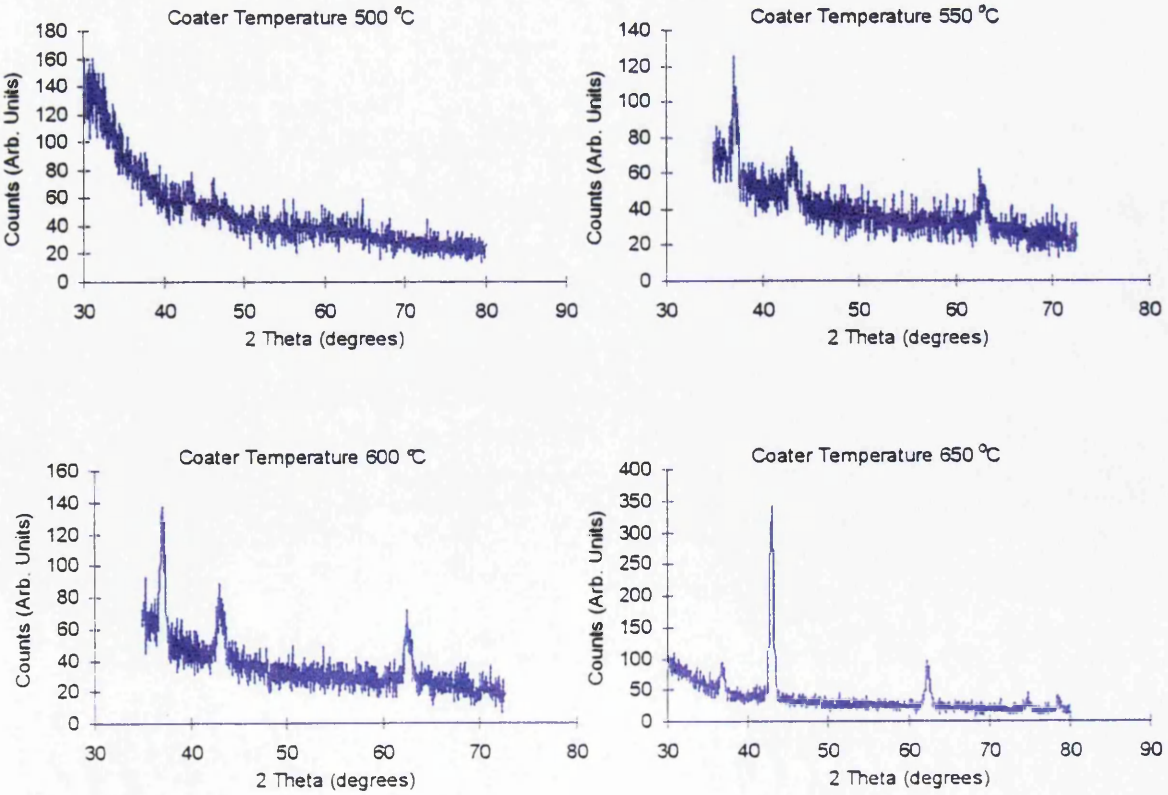

These films have been indexed and the lattice parameters have been calculated. The preferred orientation and the crystallite size have also been evaluated. The four compounds vanadium nitride, titanium nitride, $TiO_{1.04}$ and $VO_{0.9}$ all have the Fm3m (225) space groups with the following lattice parameters (ICPDS registry numbers in brackets).

(35-765) VN $a = 4.139$ Å
(10-313) $VO_{0.9}$ $a = 4.12$ Å
(43-1296) $TiO_{1.04}$ $a = 4.194$ Å
(38-1420) TiN $a = 4.241$ Å

Table 6.24c Lattice parameter and crystallite size information from XRD indexing of peaks in fig. 6.24b.

Deposition temperature	Lattice parameter a (Å)	Crystallite size Å
500	-	-
550	4.194	143
600	4.197	147
650	4.211	298

The lattice parameters observed from films obtained from the reaction of VCl_4 / $TiCl_4$ with NH_3 are intermediate between those for $TiO_{1.04}$ and TiN. There appears to be strong preferential growth in the (1 1 1) direction except in the film grown at 650 °C, which has preferential growth in the (2 0 0) direction. It can be concluded from the lattice parameters that the films have much more titanium content than vanadium and this has been confirmed by the XPS analysis shown in figure 6.24a.

It was hoped that the mixed metal nitrides would exhibit improved optical properties over those of the nitrides of vanadium or titanium alone. The transmission and reflectance spectra were obtained for these films and are displayed in figure 6.24d.

Fig.6.24d Transmission and reflectance spectra of mixed metal films deposited with varying coater temperature (0.33 dm^3 min^{-1} VCl_4, 0.1 dm^3 min^{-1} $TiCl_4$ and 0.5 dm^3 min^{-1} NH_3).

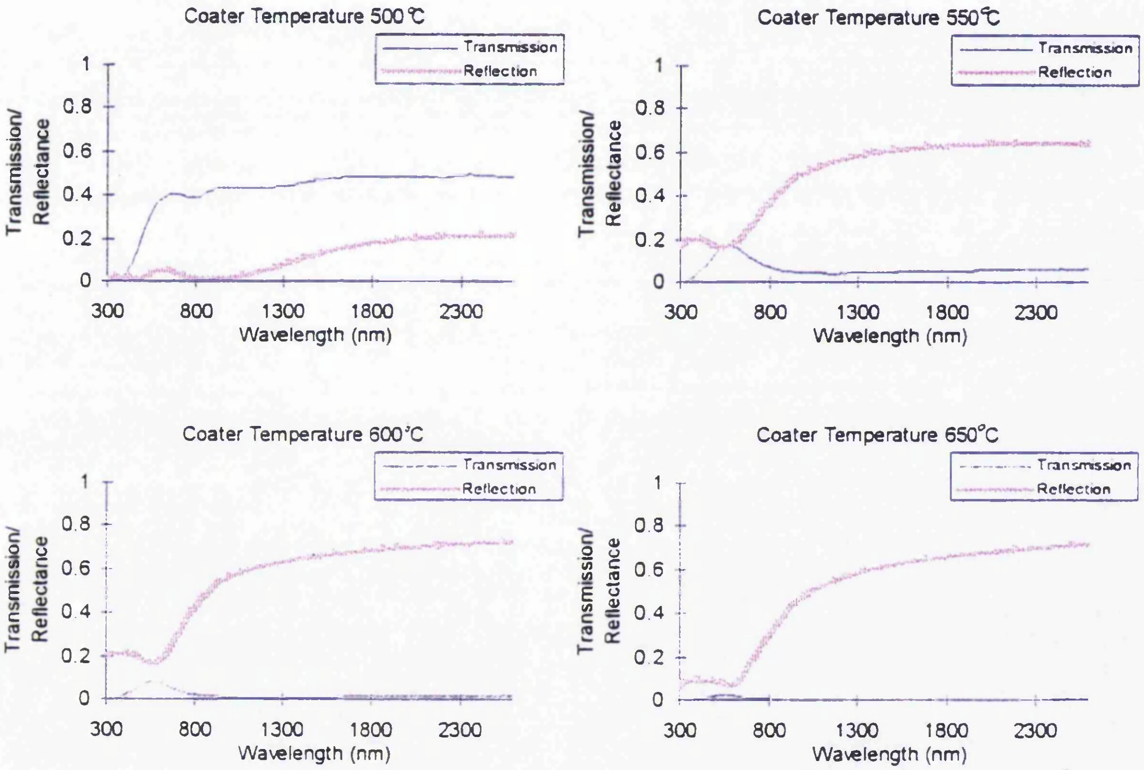
Coater Temperature 500°C

Coater Temperature 550°C

Coater Temperature 600°C

Coater Temperature 650°C

These films display some of the best heat mirror qualities ever reported. It appears that the addition of the second precursor has helped the overall optical qualities. These films are still very dark, and so their visual transmission is not very high. The use of both vanadium and titanium precursors seems to have obtained better heat mirror qualities in the film than the individual metal nitride films. VCl_4 has possibly aided removal of the contaminants in the process gas, by reacting with them before they are able to attack the growing film. Vanadium is very much less prominent in the final film than titanium.

6.25 Chromium / titanium oxynitride films.

The conditions used for deposition of individual titanium nitride and chromium oxide films were combined to deposited mixed chromium / titanium oxynitride films. The conditions that were used for this deposition are displayed in table 6.20a.

Chromium / titanium oxynitride films appeared green in colour. Films deposited at all temperatures (between 450 and 650 °C) had good adhesion and a metallic lustre. The composition of two of the films was calculated by XPS analysis and is displayed in table 6.25a.

Table 6.25a Composition of chromium / titanium oxynitrides at 600 and 650 °C (0.25 $dm^3\ min^{-1}$ CrO_2Cl_2, 0.1 $dm^3\ min^{-1}$ $TiCl_4$ and 0.5 $dm^3\ min^{-1}$ NH_3).

Element	At. % at 600 °C	At. % at 650 °C
Titanium	3.06	2.95
Chromium	40.85	18.18
Nitrogen	22.33	19.99
Oxygen	28.99	52.9
Carbon	1.67	0
Chlorine	3.10	0.88

It seems from this information that chromium is preferentially coated over the substrate rather than titanium. Although twice as much CrO_2Cl_2 reaches the reaction chamber than $TiCl_4$ (table 6.20a), chromium is much more prominent in the final film. This can be compared with vanadium / titanium coatings which lead preferentially to a coating of titanium. A further point of interest, is the high nitrogen content of the film (~20 %). This cannot be attributed to areas of TiN growth as the titanium atomic percentage is ~3 %. Nitrogen incorporation of this level was not present in films prepared from just CrO_2Cl_2 with NH_3. Even though it appears that $TiCl_4$ has had very little impact on the titanium content of the films, it does seem to encourage nitrogen incorporation.

Chromium / titanium oxynitrides are non-conducting and amorphous. No references to chromium / titanium oxynitrides could be found in the literature.

The transmission and reflectance spectra for chromium / titanium oxynitrides are shown in figure 6.25b.

Fig. 6.25b Transmission / reflectance spectra for chromium / titanium oxynitrides (0.25 $dm^3\ min^{-1}$ CrO_2Cl_2, 0.1 $dm^3\ min^{-1}$ $TiCl_4$ and 0.5 $dm^3\ min^{-1}$ NH_3).

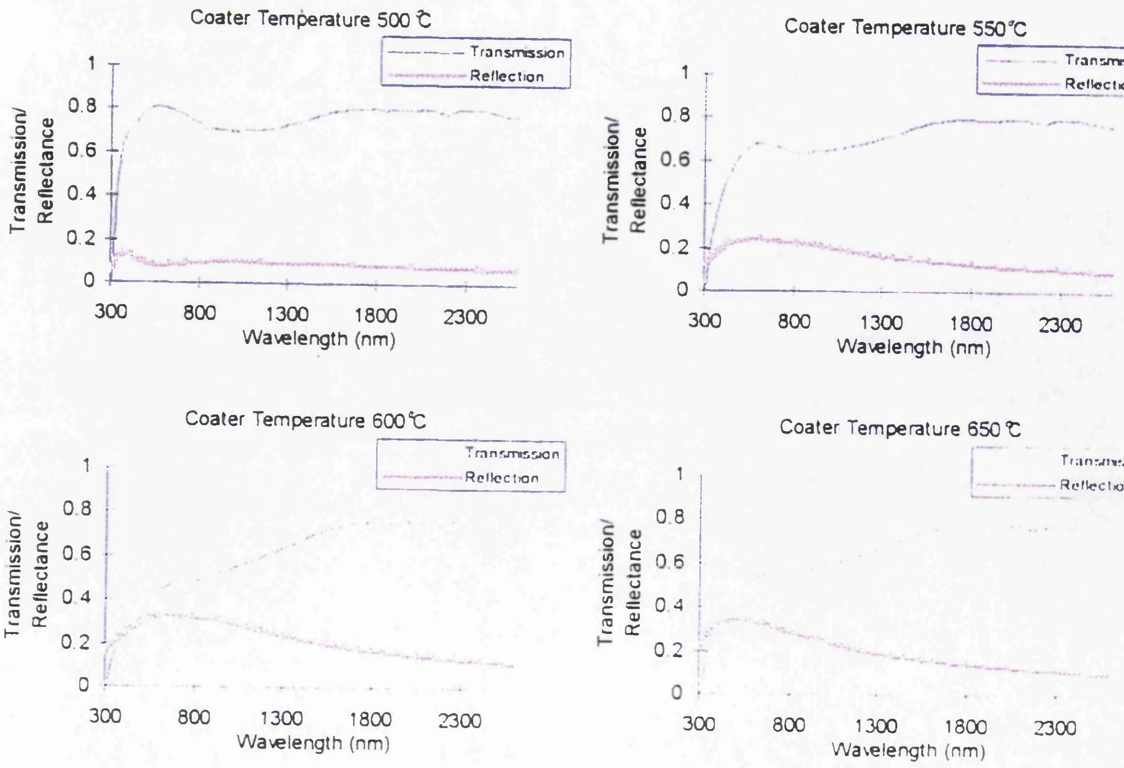

The spectra in figure 6.25b are interesting as at higher deposition temperatures the reflectance is high in the visible region and the transmission is high in the IR region, exactly the opposite from the properties required for a heat-control mirror. These properties may well be useful for other products such as UV filters.

6.3 Effect of ammonia gas flow concentration

In this study, the ammonia flow was altered between 0.2 $dm^3 min^{-1}$ and 1.0 $dm^3 min^{-1}$ to discover the effect this had on the composition of the mixed metal films. Vanadium / titanium nitride films and chromium / titanium oxynitride films will be dealt with separately.

6.31 Vanadium / titanium nitride films

For this study all conditions were kept constant except for the ammonia flow rate. Flows of 0.2, 0.4, 0.6, 0.8 and 1.0 $dm^3 min^{-1}$ ammonia were used. The conditions left unchanged throughout this study are shown in table 6.31a.

Table 6.31a Conditions for ammonia study of vanadium / titanium nitride films.

Variable	V_xTi_yN films
Coater Temp.	550 °C
Bubbler 1 Temp	118 °C
Bubbler 2 Temp	95 °C
Time of Run	30 secs
Bubbler 1 flow	0.33 $dm^3 min^{-1}$ (0.0058 mols VCl_4)
Bubbler 2 flow	0.1 $dm^3 min^{-1}$ (0.0009 mols $TiCl_4$)
Process flow	10 $dm^3 min^{-1}$
N_2/NH_3 flow	1.2 $dm^3 min^{-1}$

An ammonia flow of 0.2 $dm^3 min^{-1}$ (0.0041 moles) represents an excess of the metal chloride precursors, while 0.6 $dm^3 min^{-1}$ (0.012 moles NH_3) and 1.0 $dm^3 min^{-1}$ (0.0205 moles NH_3) represent an excess of ammonia.

An XPS study was carried out on the film prepared with a 0.6 $dm^3 min^{-1}$ flow of NH_3. The data collected from this analysis is displayed in table 6.31b.

Table 6.31b XPS composition analysis information for ammonia study (0.33 $dm^3 min^{-1}$ VCl_4, 0.1 $dm^3 min^{-1}$ $TiCl_4$ at 550 °C)

Element	At.% at 0.6 $dm^3 min^{-1}$ NH_3
Vanadium	4.5
Titanium	36.8
Nitrogen	49.2
Oxygen	7.7
Carbon	0
Chlorine	1.7

The XRD information for the vanadium / titanium nitrides from the ammonia study is shown in figure 6.31c.

Figure 6.31c XRD spectra for ammonia study (0.33 $dm^3\ min^{-1}$ VCl_4, 0.1 $dm^3\ min^{-1}$ $TiCl_4$ at 550 °C).

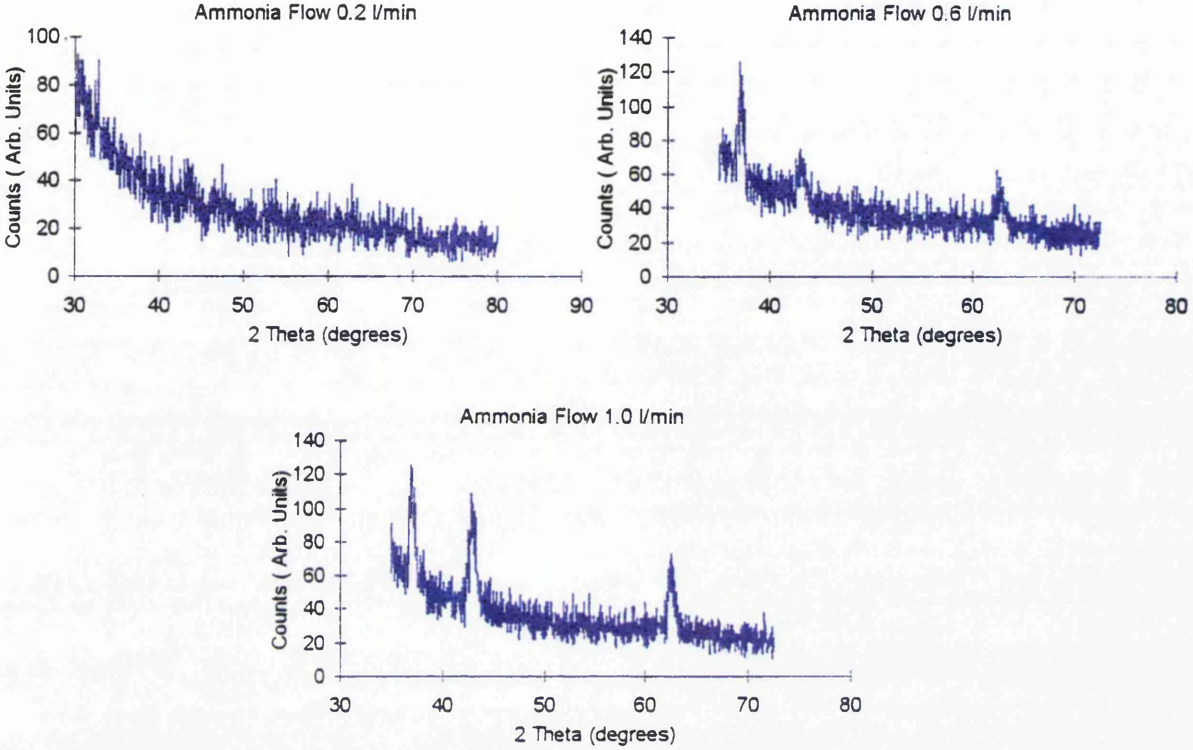

These spectra have been indexed to provide information on the lattice parameter. The crystal size has been evaluated using the Scherrer equation. This information obtained is displayed in table 6.31d.

Table 6.31d Lattice parameter from XRD indexing of peaks in 6.31c and crystallite size information.

Ammonia Flow ($dm^3\ min^{-1}$)	Lattice parameter a (Å)	Crystallite size Å
0.2	4.133	77
0.6	4.194	143
1.0	4.204	179

The spectra in figure 6.31c show that the films are more crystalline when deposited at higher ammonia flows. The preferred growth for both individual vanadium nitride and titanium nitride films prepared in this thesis is (2 0 0) but the preferred growth for the vanadium / titanium nitride films are (1 1 1).

The values shown in table 6.31d show how the lattice parameters of the mixed metal V/TiN films fall between those expected for $TiO_{1.04}$ and TiN.

An increase in the ammonia flow rate leads to an increase in the average crystallite size and grain size. An SEM photograph of the film deposited with 0.6 dm^3 min^{-1} NH_3 is shown in figure 6.31e.

Figure 6.31e SEM photograph of vanadium / titanium nitride deposited with ammonia flow rate of 0.6 dm^3 min^{-1} (0.33 dm^3 min^{-1} VCl_4, 0.1 dm^3 min^{-1} $TiCl_4$ at 550 °C).

The transmission and reflectance spectra for this study are shown in figure 6.31f.

Figure 6.31f Transmission / reflectance spectra for ammonia study (0.33 $dm^3\ min^{-1}$ VCl_4, 0.1 $dm^3\ min^{-1}$ $TiCl_4$ at 550 °C).

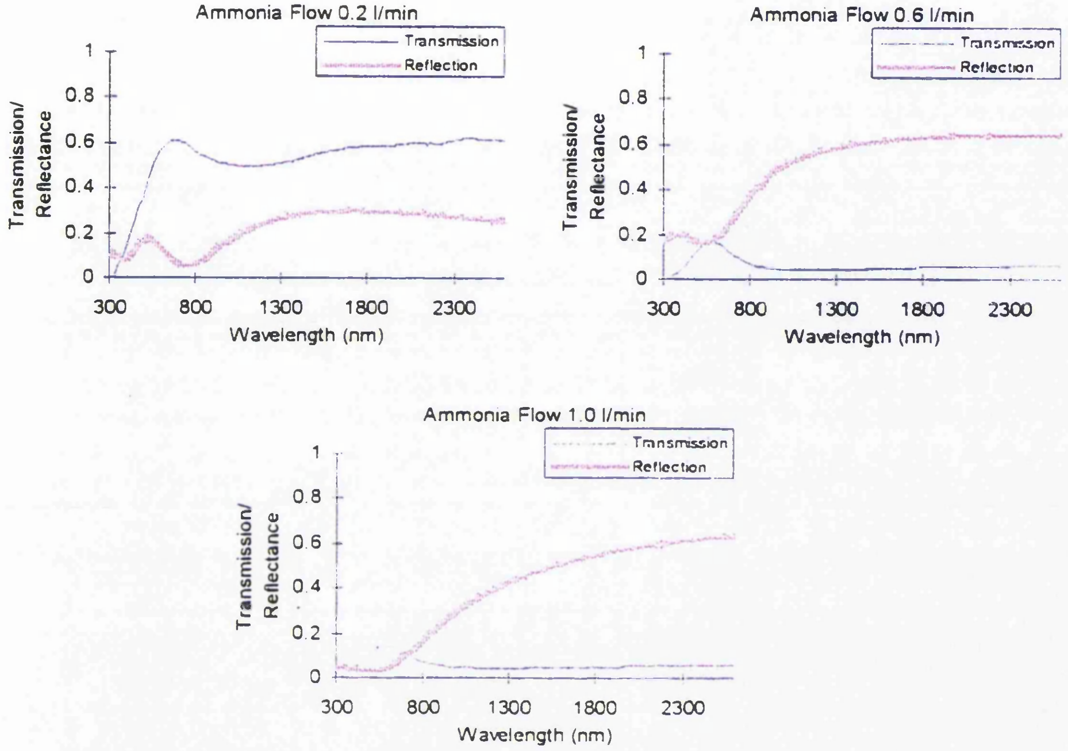

The extent to which the reflectance improves with higher ammonia flows can clearly be seen from the spectra in figure 6.31f. These spectra show how lower oxygen contamination in these films leads to better heat-control mirror qualities. The difference between the films deposited with 0.6 and 1.0 $dm^3\ min^{-1}$ flows of ammonia, are not that obvious, but on closer inspection the reflectance curve dips sharply as it reaches the visible region of the spectrum for the film deposited with a 0.6 $dm^3\ min^{-1}$ flow of ammonia. The reflectance curve for the film deposited with 1.0 $dm^3\ min^{-1}$ of ammonia, is less sharp, showing a gradual lowering of the reflectance properties at the edge of the infra-red region. The ideal heat-control mirror would have a very steep drop from high reflectance to low reflectance so as much infrared radiation is reflected as possible. So the film deposited with 0.6 $dm^3\ min^{-1}$ ammonia shows good heat-control mirror properties.

6.32 Chromium / titanium oxynitride films.

By now it has been realised that chromium / titanium oxynitride films do not display the properties required for heat-control mirrors, nor do they show conductivity or crystallinity. Therefore the purpose of this study was to discover the effect of ammonia flow rate on the composition of the deposited film.

The deposition conditions were kept constant for this study except the ammonia flows, which were 0.2, 0.6 or 1.0 $dm^3\ min^{-1}$. The conditions for the deposition are displayed in table 6.32a.

Table 6.32a Deposition conditions for chromium / titanium oxynitride films during ammonia flow rate study.

Variable	$Cr_xTi_yO_zN$ films
Coater Temp.	600 °C
Bubbler 1 Temp	75 °C
Bubbler 2 Temp	95 °C
Time of Run	60 secs
Bubbler 1 flow	0.25 $dm^3\ min^{-1}$ (0.0037 mols CrO_2Cl_2)
Bubbler 2 flow	0.1 $dm^3\ min^{-1}$ (0.0009 mols $TiCl_4$)
Process flow	6 $dm^3\ min^{-1}$
N_2/NH_3 flow	1.2 $dm^3\ min^{-1}$

An ammonia flow rate of 0.2 $dm^3 min^{-1}$ (0.0041 moles) represents a slight excess of the metal chloride precursors while 0.6 $dm^3 min^{-1}$ (0.012 moles NH_3) and 1.0 $dm^3 min^{-1}$ (0.0205 moles NH_3) represent an excess of ammonia.

XPS analysis has been used to acquire composition data for one of the films. This is shown in table 6.32b.

Table 6.32b XPS compositional analysis for a chromium / titanium oxynitride film deposited with 0.6 $dm^3 min^{-1}$ ammonia (0.25 $dm^3 min^{-1}$ CrO_2Cl_2, 0.1 $dm^3 min^{-1}$ $TiCl_4$ at 600 °C).

Element	At.% at 0.6 $dm^3 min^{-1}$ NH_3
Chromium	40.8
Titanium	3.1
Nitrogen	22.3
Oxygen	29.0
Carbon	1.7
Chlorine	3.1

XRD and four-probe measurements on chromium / titanium oxynitride films indicate the material is amorphous and non-conducting. In figure 6.32c the transmission and reflectance spectra are shown for chromium / titanium oxynitride films prepared using different ammonia flow rates.

Figure 6.32c Transmission / reflectance spectra for chromium / titanium oxynitride films at different ammonia flow rates (0.25 dm^3 min^{-1} CrO_2Cl_2, 0.1 dm^3 min^{-1} $TiCl_4$ at 600 °C).

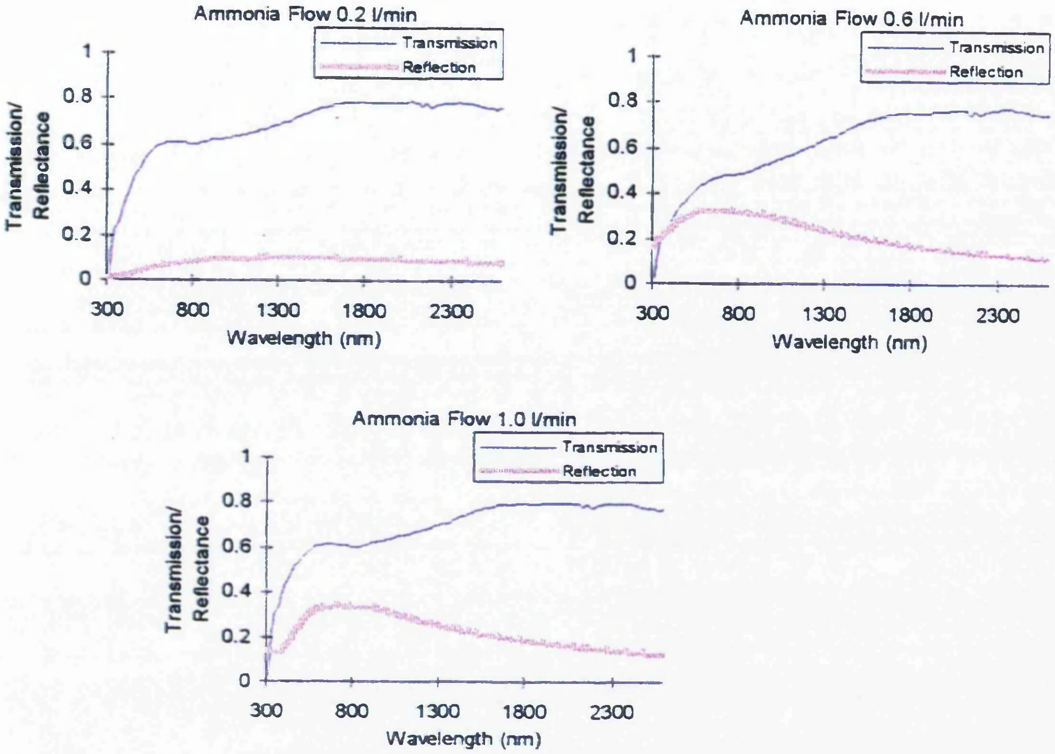

There is a definite difference in the reflectance in the visible region for the films prepared under increasing ammonia flows.

6.4 Effect of process gas flow

6.41 Vanadium / titanium nitride films

In this study, films were deposited with a process gas flow rate of 5 dm^3 min^{-1} or 10 dm^3 min^{-1}. The conditions used during this study are displayed in table 6.41a.

Table 6.41a Conditions for process gas study of vanadium / titanium nitride films.

Variable	V_xTi_yN films
Coater Temp.	600 °C
Bubbler 1 Temp	118 °C
Bubbler 2 Temp	95 °C
Time of Run	30 secs
Bubbler 1 flow	0.33 dm^3 min^{-1} (0.0058 mols VCl_4)
Bubbler 2 flow	0.1 dm^3 min^{-1} (0.0009 mols $TiCl_4$)
NH_3 flow	0.6 dm^3 min^{-1} (0.0123mols)
N_2/NH_3 flow	1.2 dm^3 min^{-1}

For this series of runs the ammonia was in excess (double what is required for a stoichiometric reaction). During the runs the film deposited under a process gas flow of 5 dm^3 min^{-1} experienced more blockages, and produced a thicker film. Both films were dark green / black in colour with metallic lustre. The film deposited with a process gas flow of 5 dm^3 min^{-1} had some pin-holes, due to particulates from prereaction being blown onto the substrate during deposition.

As with other films, a film formed at a lower process gas flow rates will be significantly thicker than a film formed when the process gas has a higher flow rate. This leads to a change in the XRD pattern, sheet-resistance and the optical properties of the film. The resistance measurements of these films show that the film deposited at low process gas flow rates have a lower four probe reading (29 Ω/□) compared with the film prepared with a higher process gas flow rate (31Ω/□). The XRD and transmission / reflectance spectra for these films are shown in figures 6.41b and 6.41c respectively.

Figure 6.41b XRD spectrum for vanadium / titanium nitride film deposited with a process gas flow rate of 10 dm^3 min^{-1} (0.33 dm^3 min^{-1} VCl_4, 0.1 dm^3 min^{-1} $TiCl_4$ and 0.6 dm^3 min^{-1} NH_3 at 600 °C)

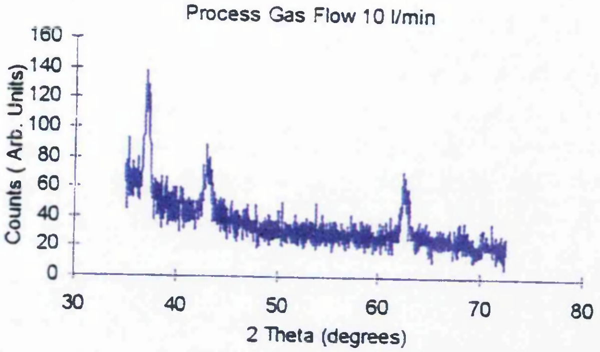

Indexing of the spectrum in fig. 6.41b shows preferred orientation in the (1 1 1) direction. The lattice parameter is a = 4.197 Å, again showing a structure intermediate between those of $TiO_{1.04}$ and TiN. The crystallite size was measured at 147 Å.

Figure 6.41c Transmission / reflectance spectra for vanadium / titanium nitride films deposited with varying process gas flow rates (0.33 dm^3 min^{-1} VCl_4, 0.1 dm^3 min^{-1} $TiCl_4$ and 0.6 dm^3 min^{-1} NH_3 at 600 °C).

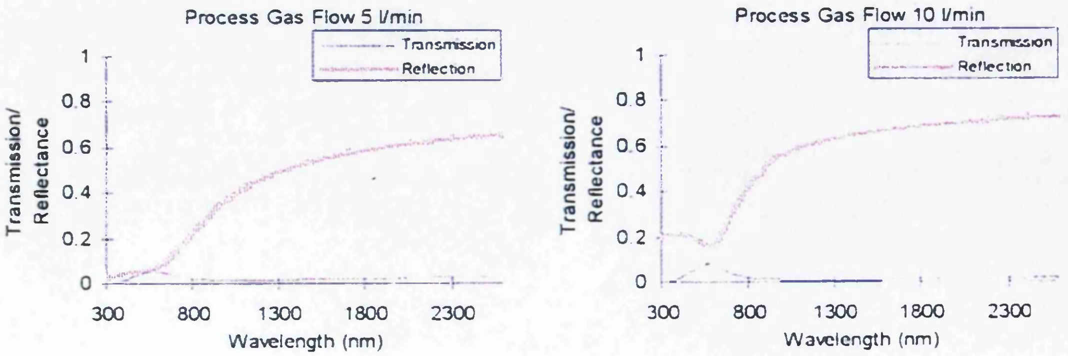

Both of these films are dark with poor visual transmission. The reflectance properties are excellent in both cases, but particularly in the film deposited at a process gas flow rate of 10 dm^3 min^{-1}, where the curve dips sharply just into the visible region. A thinner film would be required for use as a commercial heat-control mirror.

6.5 Effect of growth times

6.51 Vanadium / titanium nitride films

The purpose of this study was to see how growth time affected the deposited film. For vanadium / titanium nitride films growth times of 15, 30 and 60 seconds were used. Other conditions were kept constant and are displayed in table 6.51a.

Table 6.51a Conditions used for growth time study on vanadium / titanium nitride films.

Variable	V_xTi_yN films
Coater Temp.	600 °C
Bubbler 1 Temp	118 °C
Bubbler 2 Temp	95 °C
Process gas flow	10 dm^3 min^{-1}
Bubbler 1 flow	0.33 dm^3 min^{-1} (0.0058 mols VCl_4)
Bubbler 2 flow	0.1 dm^3 min^{-1} (0.0009 mols $TiCl_4$)
NH_3 flow	0.6 dm^3 min^{-1} (0.0123mols)
N_2/NH_3 flow	1.2 dm^3 min^{-1}

The compositions of the films obtained from XPS analysis are shown in table 6.51b.

Table 6.51b XPS composition analysis for growth time study (0.33 dm^3 min^{-1} VCl_4, 0.1 dm^3 min^{-1} $TiCl_4$ and 0.6 dm^3 min^{-1} NH_3 at 600 °C).

Element	At.% after 15 secs	At.% after 30 and 60 secs
Vanadium	0.00	4.5(±0.4)
Titanium	41.62	37.2(±1)
Nitrogen	52.89	48.8(±1.3)
Oxygen	5.5	7.7(±0.2)
Carbon	0	0
Chlorine	0	1.7(±0.4)

These results show that shorter growth times lead to no vanadium incorporation in the film. As growth time is increased some vanadium is incorporated into the film.

There was a lot of particulate build up during the 60 second run, almost completely stopping the process gas flow. The extra debris made the final film, pin-holed and non-uniform. The film was black and speckled due to the prereaction material landing on the substrate surface during deposition. The film deposited from the reaction of VCl_4 / $TiCl_4$ and NH_3 over 15 seconds, on the other hand, was very uniform and green/gold in colour. The pipework for the 15 second run showed minimal prereaction build up.

The four probe resistance readings of the three films of different thicknesses obtained from the reaction of $TiCl_4$ / VCl_4 and NH_3 are shown in table 6.51c.

Table 6.51c Four probe readings for vanadium / titanium nitride films obtained at different growth times (0.33 dm^3 min^{-1} VCl_4, 0.1 dm^3 min^{-1} $TiCl_4$ and 0.6 dm^3 min^{-1} NH_3 at 600 °C).

Deposition time (s)	Four probe reading (Ω/□)
15	46
30	31
60	34

As can be seen from table 6.51c, the resistance increases between the 30 and 60 second depositions. This is due to the loss of conductive properties, where the film is affected by prereaction (leaving amorphous debris incorporated in the film).

XRD spectra for these films are displayed in figure 6.51d.

Figure 6.51d XRD patterns for vanadium / titanium nitride films with varying growth times (0.33 dm^3 min^{-1} VCl_4, 0.1 dm^3 min^{-1} $TiCl_4$ and 0.6 dm^3 min^{-1} NH_3 at 600 °C).

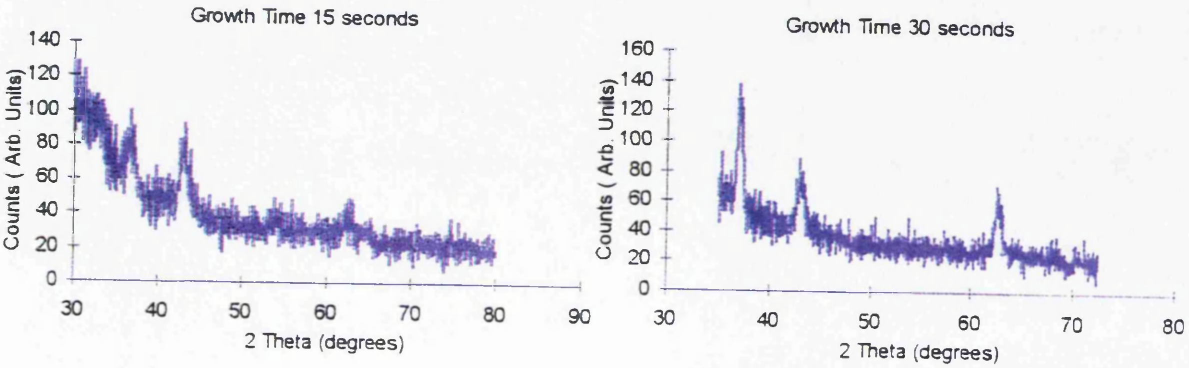

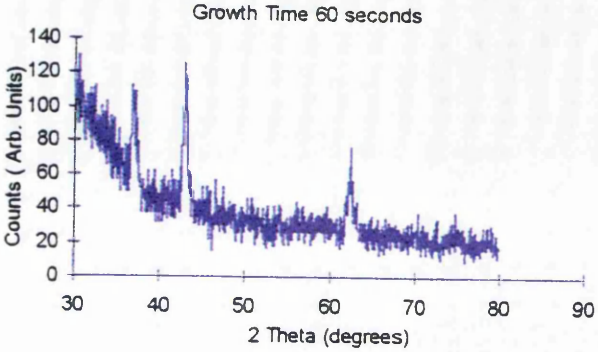

The spectra in figure 6.51d show that by increasing the growth time, the resultant increase in film thickness, leads to an increase in the intensity of the diffraction peaks (recorded over the same time period) by XRD. The thicknesses of the films can be estimated as between 200 nm (15 second run) and 800 nm (60 second deposition). The films deposited over 15 and 30 seconds show preferential growth in the (1 1 1) direction. Table 6.51e provides information on the lattice parameters and crystallite sizes of the films.

Table 6.51e Lattice parameter from XRD indexing of peaks in fig. 6.51d and crystallite size information.

Growth Time	Lattice parameter a (Å)	Crystallite size Å
15		-
30	4.197	147
60	4.21	93

These lattice parameters are intermediate between those of $TiO_{1.04}$ and TiN. The smaller average crystallite size for the film deposited over 60 seconds maybe due to the influence of the prereaction and amorphous materials interfering with crystallite growth.

Table 6.51f shows the effect that the increase in thickness has on the transmission and reflectance spectra.

Table 6.51f Transmission / reflectance spectra for vanadium / titanium nitride films with varying growth times (0.33 dm^3 min^{-1} VCl_4, 0.1 dm^3 min^{-1} $TiCl_4$ and 0.6 dm^3 min^{-1} NH_3 at 600 °C).

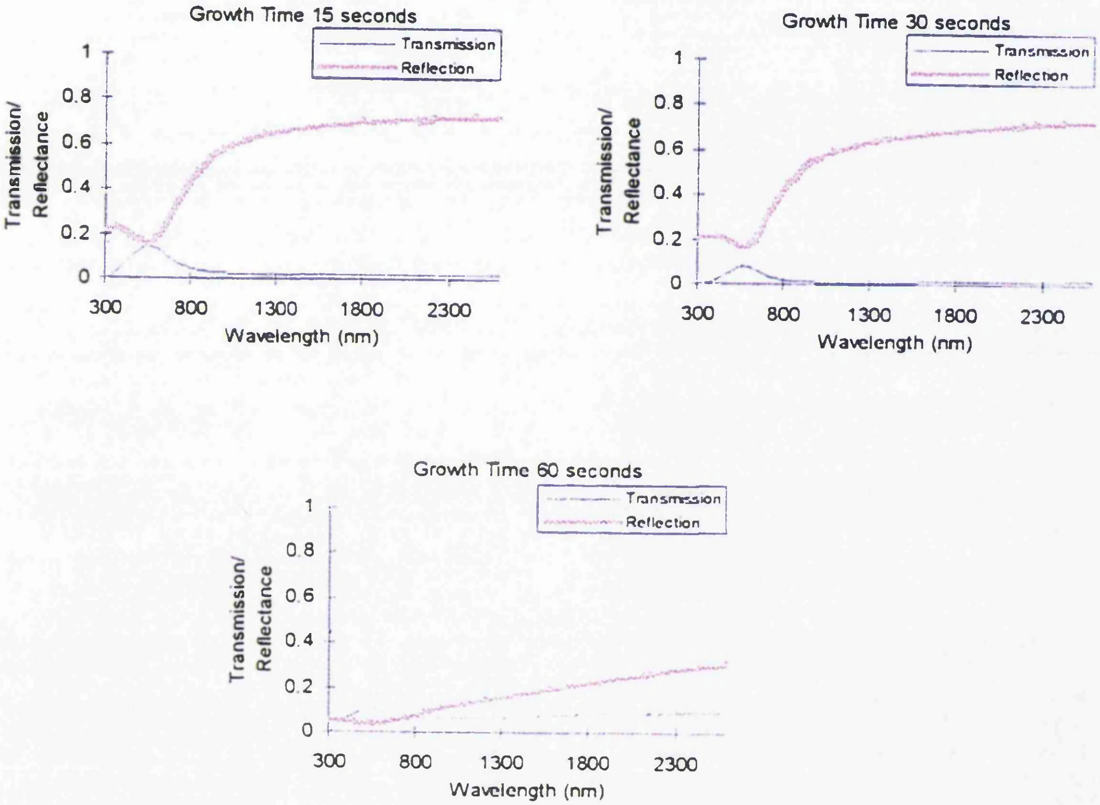

The thicker films show marked decreases in transmission. What is not expected is the loss of the reflectance properties in the 60 second deposition. The reason for this loss of heat mirror properties is probably due to the prereaction debris, which landed on the substrate during the deposition.

6.6 Summary of mixed metal films

The results observed in this section show that mixed metal films can be formed effectively by APCVD. Changing the deposition conditions of the films can affect the film composition.

Although mixed metal films have been prepared successfully, it appears that it is not easy to regulate the proportions of the metals in the film, simply by changing the flows through the bubblers. Despite 6 times as much VCl_4 reaching the reaction chamber than $TiCl_4$, the mixed metal films were found to be predominantly titanium as opposed to a mixed vanadium / titanium film. With mixed chromium / titanium oxynitride films, it is chromium that is preferentially deposited in the film.

Vanadium / titanium nitride films have properties which make them ideal for use as heat-control mirrors, if the thickness and colour of the films can be controlled. The properties of the vanadium / titanium nitride films seem to improve on those of the individual titanium nitride and vanadium nitride films. This could be due to obtaining the advantageous properties of each material, namely the IR reflectance of TiN films and the improved coloration and visual transmission of VN films. The improved properties could also be due to lower oxygen incorporation in the mixed V / Ti coating. VCl_4 is, therefore, possibly ferrying contaminants away from the reaction site, while $TiCl_4$ is reacting at the substrate surface.

Chromium / titanium oxynitride films have been formed, typically with high carbon and chlorine contamination. A large range of oxygen, nitrogen, carbon and chromium incorporation was observed depending on the conditions used. The chromium / titanium oxynitride films formed were non-crystalline, non-conductive and show no application as heat-control mirrors. These films, however, are interesting, due to high levels of nitrogen incorporation into essentially chromium oxide films which was not observed in the absence of $TiCl_4$. Despite this, titanium does not appear at significant concentrations in the resulting film.

Mixed metal films have been prepared previously in the literature although rarely by APCVD. The main method for the formation of mixed metal films appears to be through magnetron sputtering. J.R. Roos *et al* ((Ti,Al)N and (Ti,Nb)N))[59], Chu *et al* (TiN/NbN superlattices) [61], Burdis ($V_zTi_{1-z}O$)[66], Hirashita *et al* (TiN/VN superlattices)[60] and Shinn *et al* ($TiN/(V_{0.6}Nb_{0.4})N$) [64] have all prepared mixed metal films by PVD methods such as magnetron sputtering. Knotek *et al*[63] has also produced Ti-V-N coatings from magnetron sputtering. Their work shows ability to vary the amount of each metal in the mixed metal coating, although this was only possible because mixed metal alloys were prepared and ion sputtered in a nitrogen atmosphere. The films produced had lattice parameters between $a = 4.18$ Å and $a = 4.24$ Å which is the same as the range of lattice parameters for Ti/V N films deposited in this work. Hampden-Smith *et al*[27] have prepared mixed metal alloy films (Ag_xPd_{1-x}, Cu_xPd_{1-x}, and Ag_xCu_{1-x}) by aerosol assisted CVD from organometallic precursors, although it is not made clear in the literature whether this method could be used for deposition of nitrides. Funakubo *et al*[58] have prepared FeN_x-TiN films by APCVD, from $Fe(C_5H_5)_2$, $TiCl_4$, NH_3 and H_2. They comment on the difficulty of preparing ternary metal nitrides. Their method for the preparation was very similar to the method employed in this thesis with the mixing of the metal precursors $Fe(C_5H_5)_2$ and $TiCl_4$ occuring before the reaction chamber to ensure homogeneous elemental distributions throughout the product. Ammonia was added to the reactor at the last possible moment to cut down on pre-reaction. The deposition was carried out over 30 minutes with much lower partial pressures than used for the mixed metal film preparation described in this thesis. The composition, (whether preferential deposition of one of the metals occurs), is not commented on, although the degree of carbon contamination has been recorded as between 0 and 3 at. %[58].

No references to mixed chromium / titanium oxide, nitride or oxynitride films could be found in the literature.

In summary, mixed metal films of chromium / titanium oxynitride and vanadium / titanium nitride have been deposited on glass by APCVD. The routes for preparation and results compare well with mixed metal films prepared previously. Vanadium / titanium nitride has properties which make it a viable heat-control mirror.

Chapter 7

Conclusions and future work.

7.1 Conclusions

Films of vanadium nitride, vanadium oxynitride, chromium oxide, titanium / vanadium nitride and titanium / chromium oxynitride have all been successfully prepared by atmospheric pressure chemical vapour deposition on glass substrates. It has been shown that by varying the deposition conditions (e.g. coater temperature, amount of precursor, growth time, annealing conditions), the quality and composition of the films can be altered.

The work in this thesis has shown that carbon, oxygen and chlorine contamination can all be controlled in an atmospheric pressure preparation environment, although the loss of one contaminant may lead to another becoming more prominent. An example of this is in vanadium nitride films, where at lower deposition temperatures chlorine contamination is present, but at higher deposition temperatures carbon contamination becomes a problem. Another example is oxygen contamination, which becomes a problem at low ammonia flows. Higher ammonia flows lead to prereaction, which becomes a problem as it leads to blockages in the pipework and patchy films. For vanadium nitride films both chlorine and carbon contamination are minimised with a coater temperature between 450 and 550 °C. Annealing and cooling of the films under ammonia can lower the oxygen content of the films by exchanging oxygen for nitrogen.

Oxygen contamination is thought to have originated from impurities in the nitrogen process gas, but it has been found that by annealing, much of the oxygen can be removed. Carbon contamination in the films originates from the nitrogen process gas or reaction of the films in air. Less carbon is incorporated in the film if it is deposited at lower substrate temperatures. Chlorine contamination in the films originates from the incomplete breakdown of the precursors, but is only present for films deposited at 350 °C.

Prereaction of the precursors prior to entering the mixing chamber is a major problem for deposition experiments that use high ammonia flows. This problem could be limited by small changes in the rig design. By allowing the flow of precursors into the reaction chamber in a way that causes less disruption to the flow, less solid build up is observed. A diagram of a prereaction mixing chamber which has been designed, built and been shown to work effectively is shown in figure 7.1a.

Figure 7.1a Design for a new style mixing chamber that leads to less prereaction.

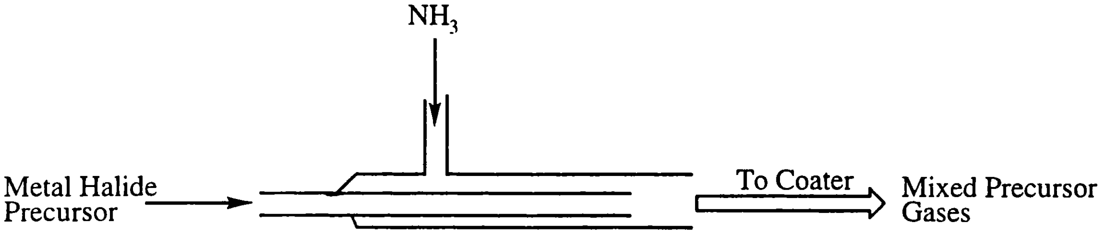

Vanadium oxynitride and vanadium nitride thin films on glass both show properties which make them ideal for heat-control mirrors. Chromium oxide prepared from chromyl chloride and ammonia does not show optical properties of any solar-control interest. Attempts at making titanium / vanadium nitride films resulted in very little vanadium incorporation, but did show solar-control optical properties which were better than those observed in either vanadium nitride or titanium nitride films prepared in this work. The mixed metal films also contain low levels of oxygen contamination. Attempts at forming chromium / titanium oxynitride films showed little titanium incorporation, however relatively large amounts of nitrogen were incorporated. Chromium / titanium oxynitride films do not show properties typical of heat-control mirrors.

7.2 Suggestions for future work

This thesis has given details of particular routes to vanadium nitride, vanadium oxynitride, chromium oxide, titanium / vanadium nitride and titanium / chromium oxynitride. An effort has been made to provide a complete account of these depositions. An improved understanding of the reactions could be undertaken from a number of approaches:

1 The suggested changes to the rig design in chapters 2 and 7 could be made and further depositions carried out.

2 Further annealing experiments could be carried out on deposited films that show excellent heat-control mirror properties to see if an improvement in their properties and compositions could be achieved.

3 Further mixed metal films could be prepared by varying the amounts of metal precursors, including an evaluation of the amount of each metal present in the resulting film.

4 *In situ* observation of the nucleation and growth of mixed metal films.

5 Comparison of the films prepared by APCVD in this thesis with films prepared by other CVD methods using the same precursors and glass substrates.

References

1 Hoffman, D. M.; *Polyhedron* , **1994**, 13, 1169.

2 G.H.J. Neville; "Titanium Compounds"; Encyclopaedia of Chemical Technology, 3rd Ed. , Vol 23, p131, Wily Interscience.

3 E.J. Markel, M.E. Leaphart II; "Nitrides"; Encyclopaedia of Chemical Technology, 3rd Ed. , Vol 17, p108, Wily Interscience.

4 CRC Handbook of Chemistry and Physics, 77th edition, CRC Press.

5 M. Woolery; "Vanadium and Vanadium alloys"; Encyclopaedia of Chemical Technology, 3rd Ed. , Vol 24, p782, Wily Interscience.

6 Benco, L.; *Journal of Structural Chemistry*, **1994**, 58.

7 D. M. Mattox; "Thin Films"; Encyclopaedia of Chemical Technology, 3rd Ed. , Vol 23, p1040, Wily Interscience.

8 Ohring, M; "The Materials Science of Thin Films", **1992**, Academic Press.

9 Hitchman, M. L.; Jensen, K. F.; "Chemical Vapour Deposition, Principals and Applications", **1993**, Academic Press.

10 Morancho, J. A.; Petit, J. A.; Dabosi, F.; Constant, G.; *J. Electrochem. Soc.*, **1982**, 4, 854.

11 Aylett, B. J.; Colquhoun, H. M.; *J. Chem. Soc. Dalton,* **1977**,2058.

12 Kouvetakis, J.; Bandari, A.; Todd, M.; Wilkens, B.; Cave, N.; *Chem. Mater.,* **1994**, 6, 811.

13 Jones, A. C.; Auld, J.; Rushmore, S. A.; *Adv. Mater.,* **1994**, 6, 229.

14 Kern, W.; Vossen, J. L.; "Thin Film Processes II", **1991**, Academic Press.

15 Kim, J.; Lee, E.J.; Baek, J. T.; Lee, W-J.; *Thin Solid Films*, **1997**, 305, 103.

16 Silvestre, A. J.; Parames, M. L.; Conde, O.; *Thin Solid Films,* **1994**, 241, 57.

17 Bernard, C.; Madar, R. ; *J. de Physique,* **1989**, 50, C5-479.

18 Aylett, B. J.; Tannahill, A. A.; *Vacuum* **1985**, 35, 435.

19 Gysling, H. J.; Wernberg, A. A.; *Chem. Mater.* **1992**, 4, 900.

20 Jagner, S. J.; Hakansson, M.; Daniele, S.; Papiernik, R.; Hubert-Pfalzgraf, L. G.; *Inorg. Chem.,* **1995**, 34, 628.

21 Gardiner, R. A.;Vaartstra, B. A.; Ostrander, R. L.; *Chem. Mater.,* **1994**, 6, 1967.

22 Desu, S. B.; Hendricks, W. C.; Peng, C. H.; *Chem. Mater.,* **1994**, 6, 1955.

23 Cowley, A. H.; Jones, R. A.; Nunn, C. M.; Westmoreland, D. L.; *Chem. Mater.,* **1990**, 2, 221.

24 Hoffman, D. M.; Fix, R.; Gordon, R. G.; *Chem. Mater.,* **1990**, 2, 235.

25 O'Brien, P.; "Precursors for Electronic Materials", **1990**, 491.

26 Chandler, C. D.; Powell, Q.; Hampden-Smith, M. J.; Kodas, T. T.; *J. Chem. Mater.,* **1993**, 3, 775.

27 Xu, C.; Hampden-Smith, M. J.; Kodas, T. T.; *Chem. Mater.,* **1995**, 7, 1539.

28 Dobkin, D.; Bartholomew, L.; McDaniel, G.; *J. Electrochem. Soc.,* **1990**, 137, 1623.

29 Blanquet, E.; *Thin Solid Films,***1990**, 474.

30 Hoffman, D. M.; Fix, R.; Gordon, R. G.; *Chem. Mater.,* **1991**,3,1138.

31 Neuman, G. A.: *Journal of Non-Crystalline Solids,* **1997**, 218, 92.

32 Ha, H. Y.; Nam, S. W.; Lim, T. H.; Oh, I-H.; Hong, S-A.; *Journal of Membrane Science,* **1996**, 111, 81.

33 Fix, R.; Gordon, R. G.; Hoffman, D. M.; *Chem. Mater.,* **1993**, 5, 614.

34 Auciello, O.; Gifford, K. D.; Kingon, A. I.; *Appl. Phys. Lett.,* **1994**, 64, 2873.

35 Thompson, J. R.; Ellis, J.T.; Christen, D. K.; Lewis, J.D.; Sekula, S.T.; *Physica B*, **1985**, 135, 157.

36 Scholl, M.; *Wear*, **1997**, 203-204, 57.

37 Eckertova, L.; Physics of Thin Films; **1977**, Plenum Press.

38 Sivaram, S.; "Chemical Vapour Deposition- Thermal and Plasma Deposition of Electronic Materials", **1995**, Van Nostram.

39 Chopra, K. L.; Thin Film Phenomena, **1969**, McGraw-Hill.

40 Johnson, S. E.; Doctor of Philosophy Thesis, University of Southampton, **1996**.

41 Dekker, J. P.; van der Put, P. J.; Veringa, H. J.; Schoonman, J; *J. Electrochem. Soc.*, **1994**, 141, 787.

42 Johnson, S. E.; Owen, J. R.; *Journal de Physique II,* **1995**, C5, 871.

43 Kurtz, S. R.; Gordon, R. G.; *Thin Solid Films*, **1986**, 140, 277.

44 Buiting, M. J.; Otterloo, A. F.; Montree, A. H.; *J. Electrochem. Soc.*, **1991**,138, 500.

45 Vogt, K. W.; Kohl, P. A.; Abys, J. A.; *Al.Ch.E. Journal,* **1995**, 41, 10.

46 Hegde, R. I.; Tobin, P. J.; Fiordalice, R. W.; Travis, E. O.; *J. Vac. Sci. Technol. A.,* **1993**, 11, 1692.

47 Hillman, J.; Foster, R.; Faguet, J.; Ameen, M.; Martin, F.; *Solid State Technology,* **1995**, 147.

48 Spee, C. I. M. A.; Linden, J. L.; Timmer, K.; *J. De Phys. IV,* **1993**, 3, 289.

49 Tripathy, P. K.; Arya, A.; Bose, D. K.; *Journal of Alloys and Compounds,* **1994**, 209, 175.

50 Tedrow, P. M.: Meservey, R.; *Physica,* **1981**, 107B, 527.

51 Soriano, L.; Abbate, M.; Pen, H.; Prieto, P.; Sanz, J. M.; *Solid State Communications*, **1997**, 102 (4), 291.

52 Chu, X.; Barnett, A.; Wong, M. S.; Sproul, W.D.; *J. Vac. Sci. Technol. A*, **1996**, 14 (6), 3124.

53 Kiuchi, M.; Chayahara, A; Kinomura, A; Ensinger, W.; *Surface and Coatings Technology*, **1994**, 65, 142.

54 Farges, G.; Beauprez, E.; Sainte Catherine, M. C.; *Surface and Coatings Tech.*, **1993**, 61, 238.

55 Raskolenko, L. G.; Maksimov, Y. M.; *Inorganic Materials*, **1983**, 19 (12), 1770.

56 Zaninulin, J. G.; *Zhural Neorganicheskoi Khimii*, **1984**, 29(5), 1145.

57 Cherkashenko, V. M; Kurmaev, E. Z.; Zainulin, Y.G.; *Journal of Structural Chemistry*, **1988**, 29(2), 311.

58 Funakubo, H.; Mizutani, N.; Tatsuno, T.; *J. Mat. Sci.,* **1993**, 28, 994.

59 Roos, J. R.; Veltrop, H.; Ebberink, J.; *Thin Solid Films*, **1990**, 193-194, 547.

60 Hirashita, N.; Greene, J. E.; Helmersson, U.; Birch, J.; Sundgren, J.E.; *J. Appl. Phys.* **1991**, 70 (9), 4963.

61 Chu, X.; Wong, M.S.; Barnett, S.A.; *J. Vac. Sci. Technol. A*, **1992**, 10 (4), 1604.

62 Sundgren, J.-E.; Birch, J.; Hakansson, G.; *Thin Solid Films*, **1990**, 193/194, 818.

63 Knotek, O.; Barimani, A.; Bosserhoff, B. Loffler, F.; *Thin Solid Films*, **1990**, 193/194, 557.

64 Shinn, M.; Mirkarimi, P. B.; Barnett, S. A; *Surface Science*, **1993**, 281, 1.

65 Mirkarimi, P. B.; Shinn, M.; Barnett, S.A.; *J. Vac. Sci. Technol. A*, **1992**, 10(1), 75.

66 Burdis, M. S.; *Thin Solid Films,* **1997**, 311, 286.

67 Lampert, C. M.; *Thin Solid Films*, **1993**, 236, 6.

68 Ma, H. L.; Zhang, D. H.; Win, S. Z.; Li, S. Y.; Chen, Y.P.; *Solar Energy Materials and Solar Cells*, **1996**, 40, 371-380.

69 Sokolov, A. V.; "Optical properties of Metals"; **1967**, Blackie & Son.

70 Drude, P.; "Theory of Optics", **1901**, Longmans, Green and Co.

71 Ward, L.; "The Optical Constants of Bulk Materials and Films", Second Edition, **1994**, IOP Publishing Ltd.

72 Weiller. B. H., Partido. V. B.; *Chem. Mater.* **1994**, 6, 260.

73 Cale, T. S.; Chaara, M. B.; Raupp, G. B.; Raaijmakers, I. J.; *Thin Solid Films,* **1993**, 236, 294.

74 Prybyla, J. A.; Chiang, C. M.; Dubois, L. H.; *J. Electrochem. Soc.*, **1993**, 140 (9), 2695.

75 Suni, I.;Nicolet, M. A.; Maenpaa, M.; *J. Electrochem. Soc.,* **1983**, 5, 1215.

76 Müller, G.; Sternitzke, M.; *J. Am. Ceram. Soc.,* **1994**, 77, 737.

77 Bull, S.J.; Evans, P.C.; Saleh, A.S.; *Surface and Coatings Technology*, **1996**, 78, 42.

78 Pischow, K. A; Eriksson, L.; Harju, E.; Korhonen, A. S.; Ristolainen, E. O.; *Surface and Coatings Technology*, **1993**, 58, 163.

79 Kuzel, R.; Cerny, R.; Valvoda, V.; Blomberg, M.; Merisalo, M.; *Thin Solid Films*, **1994**, 247, 64.

80 Berger, H.; *Solid State Technology* , **1991**, 79.

81 Dubois. L. H.; *Polyhedron*, **1994**, 13(8), 1329.

82 Sundgren, J.-E.; *Thin Solid Films*, **1985**, 128, 21.

83 W. H. Hartford; "Chromium Compounds"; Encyclopaedia of Chemical Technology, 3rd Ed. , Vol 6, p263, Wily Interscience.

84 Maruyama, T.; Akagi, H.; *J. Electrochem. Soc.*, **1996**, 143(6), 1955.

85 Erben, E.; Bertinger, R.; Muhlratzer, A.; Tihanyi, B.; Cornils, B.; *Solar Energy Materials*, **1985**, 12, 239.

86 Poznyak, S. K.; Makuta, I. D.; Kulak, A. I.; *Solar Energy Materials*, **1989**, 18, 357.

87 Contoux, G.; Cosset, F.; Celerier, A.; Machet, J.; *Thin Solid Films*, **1997**, 292, 75.

88 Lee, T. K; Kim, W. B.; Cho, S.H.; Chungmoo Auh, P.; *Solar Energy Materials*, **1991**, 23, 13.

89 Lee, T. K; Kim, D. H.; Chungmoo Auh, P.; *Solar Energy Materials*, **1993**, 29, 149.

90 Ohsaki, H.; Tachibana, Y.; Kadowaki, K.; Hayashi, Y.; Suzuki, K.; *Journal of Non-Crystalline Solids*, **1997**,218,223.

91 Freller, H.; Lorenz, H-P.; Schack, P.; *Surface and Coatings Technology*, **1992**, 54/55, 148.

92 Senzaki, Y.; Gladfelter, W. L.; *Polyhedron* , **1994**, 13, 1159.

93 Erola, M; Keinonen, J; Anttila, A; Kokinen, J; *J. Solar Energy Matter,* **1985**, 12, 353 .

94 Mayer, B.; *Thin Solid Films*, **1992**, 221, 166.

95 Hoffman, D. H.; Atagi, L. M.; *Chem. Mater.,* **1994**, 6, 360.

96 Goldschmidt, H. J.; "Interstitial Alloys", **1967**, London, Butterworth and co.